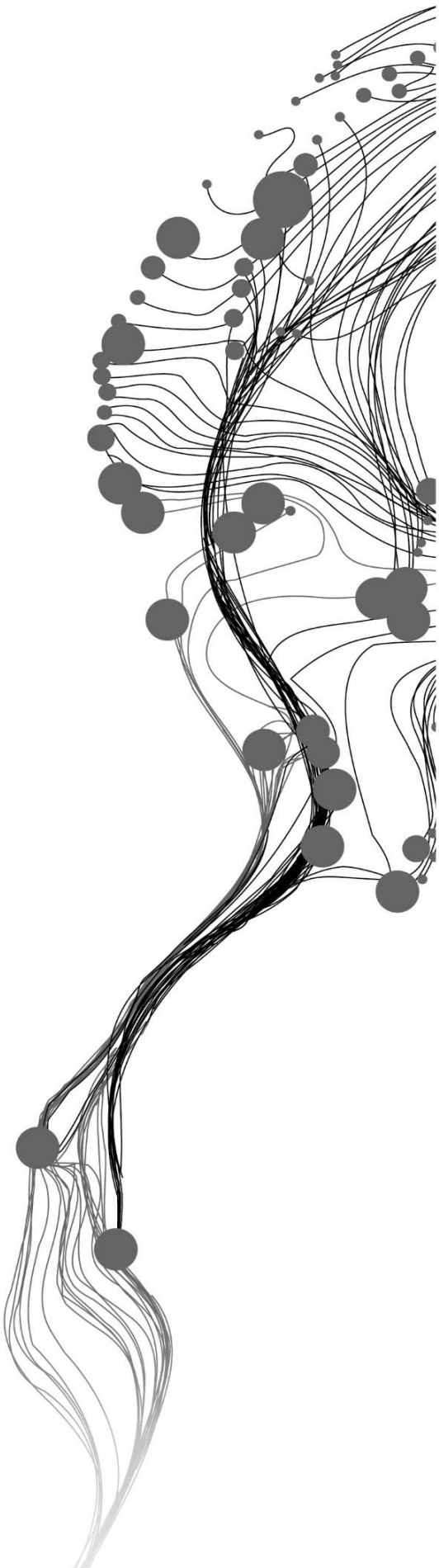

Estimating GERD Reservoirs Water Volume Variation over time with SWOT Satellite and Other Altimetry Products

MAHIR TAZWAR
Enschede, The Netherlands, July 2024

Thesis submitted to the Faculty of Geo-Information Science and Earth Observation of the University of Twente in partial fulfilment of the requirements for the degree of Master of Science in Geo-information Science and Earth Observation.
Specialization: Water Resources and Environmental Management

SUPERVISORS:
Dr. R. Rietbroek MSc
Dr. B.H.P. Maathuis

THESIS ASSESSMENT BOARD:
Dr.ir. C. van der Tol (Chair)
Dr. Eva Börgens (External Examiner, GFZ German Research Centre for Geosciences)
ir. G.N. Parodi (Procedural Advisor)

ABSTRACT

Monitoring inland water bodies is crucial for effective water resource management. Using a combination of satellite images and altimetry products, this study monitors at how the water level and extent changes during the different operational filling phases of the Grand Ethiopian Renaissance (GER) Dam. The primary aim was to utilize different remote sensing products to provide an accurate estimation of water volume changes over time. Sentinel-1 data were processed using an unsupervised edge Otsu algorithm to map reservoir extents. The output maps were validated against Planet and Sentinel-2 water masks, which showed good agreement with overall accuracy values raging from 0.97 to 0.99. Additionally, various SWOT satellite products were utilized to estimate reservoir extents, with the SWOT Lake Single Product performing poor with an IOU value close to 0.33, while the SWOT water mask raster and pixel cloud products showed moderate agreement with the validation sets with overall accuracy values ranging from 0.78 to 0.89. Volume variation across different dam operational phases was estimated using satellite-based observations and a DEM contouring method. Although both methods exhibited a high correlation (R^2 value of 0.98), significant differences in values were identified (RMSE value of 2736.35), likely due to an unnoticed scaling error and the inherent water slope in the GER Dam reservoir. A DEM slope correction method was applied, but the two-point correction approach was insufficient to accurately represent the complex terrain, leading to overestimations of volume variation. The SWOT satellite products were also utilized to estimate volume variation over time. However, due to the absence of temporally collocated in-situ data for validation, it was not possible to validate SWOT based volume estimations. The study findings identified SWOT satellite products demonstrating promising potential in estimating volume variations as the trends observed in SWOT-derived volume estimates closely aligned with those from other satellite observations, suggesting their reliability.

Keywords: Grand Ethiopian Renaissance Dam, edge Otsu algorithm, water extent detection, radar altimetry, water volume variation, SWOT satellite, water slope

ACKNOWLEDGEMENTS

I want to express my sincere gratitude to my supervisors, Dr. Roelof Rietbroek and Dr. Ben Maathuis, for their time, help, and advice through out the research period. Their comments, edits, and guidance helped me shape the study as better as possible. Special thanks to Amin Shakya for his assistance with ideation and understanding SWOT data products.

I deeply appreciate the ITC Faculty for awarding me the scholarship and providing me with the opportunity to pursue higher studies. This opportunity has been a significant milestone in my academic and professional life. I am grateful to Muna for being the best companion throughout this journey. Studying thousands of miles away from home in an unfamiliar place was initially overwhelming, but your presence made it a much more pleasant and manageable experience. Your support and companionship have been a source of strength and comfort. Lastly, I want to thank my family for their endless sacrifices and unwavering concern for my well-being. Their love, support, and encouragement have been the foundation of my success.

Above all, I extend my deepest thanks to Almighty Allah for His countless blessings and guiding me through this journey.

TABLE OF CONTENTS

LIST OF FIGURES

LIST OF TABLES

1. INTRODUCTION

1.1. Background

The interaction of inland water bodies with the regional and local hydrological cycle makes it a vital resource to monitor continuously (Nair et al., 2021). Accurate monitoring of its extent and elevation can provide vital information feeding into numerous hydrological variables such as water volume, balance, streamflow, discharge, water level fluctuation, sediment transport, etc. Consequently, accurate monitoring of water bodies can provide essential information for water resource management. It is so significant that water volume variations are linked to extreme consequences like flood events (Huang et al., 2018a). Studies by Nicholson & Yin (2002) and Tierney et al., (2013) have also reported the influence of ocean oscillations like El Niño–Southern Oscillation and Indian Ocean Dipole on temporal change in the water level of inland water bodies by resulting modification in ocean-land moisture transportation and precipitation.

Several factors have been found in the literature that affect inland water bodies. Climate change-induced temperature rise. Moreover, irregular precipitation directly influences inland water bodies by influencing evapotranspiration and surface runoff (Lei et al., 2014; Kang et al., 2010). Another study suggested that weather variations and climate change coupled with anthropogenic activities (e.g., hydropower and irrigation) increase stress on hydrological systems. For example, the Aral Sea of Central Asia started to shrink in the 1960s due to anthropogenic activities like irrigation coupled with climate warming (Cretaux et al., 2013; Aus der Beek et al., 2011). In another study conferred since 2000, Lake Mead, one of the major water reservoirs in the United States on which 40 million people are dependent, has lost 71% of its entire water content due to the ongoing drought (Hannoun & Tietjen, 2023). Up-to-date knowledge of the waterbody and variability in its physical dynamics (e.g., water volume, water level, and water extent variability) is essential for sustainable management of such hydrologic systems and strategic planning to mitigate effects of extreme climatic scenarios like droughts and floods (Awange, 2021). Therefore, to ensure informed planning and decisions by policymakers, it is crucial to monitor inland water bodies like lakes and rivers. When discussing monitoring, estimating the water volume in reservoirs comes first.

The water volume of reservoirs is approximated by utilizing the relationship between area, elevation, and volume (Gao, 2015a). The traditional way of water volume estimation involves field survey-based bathymetry data and, water extent approximates, and in situ gauge-based water height estimates. Recent developments in remote sensing have brought techniques using satellite gravimetry and satellite altimetry, which can be utilized here. Water volume variation can be determined using the satellite gravimetry of Gravity Recovery and Climate Experiment (GRACE), but only for areas larger than 200000 km2 (Singh et al., 2012). Therefore, most studies have used optical or Synthetic Aperture Radar (SAR) based water extent estimations and satellite altimetry-based height estimates for smaller- to medium-sized water reservoir volume estimation. (Crétaux et al., 2016; Duan & Bastiaanssen, 2013; Gao, 2015; Grippa et al., 2019; Musa et al., 2015; Zhang et al., 2011).

1.2. Research Gap and Problem Evaluation

The Grand Ethiopian Renaissance (GER) Dam region is the study area for this research. To date, no study has focused on estimating the volume variation of the GER Dam reservoir using remote sensing observations, particularly with newly available SWOT satellite products. Although some studies have utilized other satellite products to characterize the storage capacity of the GER dam reservoir, the effect of the water slope present in the reservoir was overlooked. Large reservoirs in mountainous regions exhibit different water levels in different reservoir parts due to their uneven terrain profile. To address this gap, this study

aims to assess the water volume variation of the GER Dam reservoir by considering both a single water level and the impact of the water slope. Moreover, another aim of this study is to assess the capability of newly available SWOT data products in water extent and volume derivation.

1.3. Aim and Objectives, Research Questions

This section outlines the study's aim and specific objectives. These objectives are complemented by associated research questions to provide a detailed exploration of water extent, level, and volume variations resulting from the Grand Ethiopian Renaissance (GER) Dam.

1.3.1. Aim

The primary objective of this study is to assess the variation in water volume caused by the Grand Ethiopian Renaissance (GER) Dam. This has been achieved by employing (SWOT) altimetry-based water height estimation and machine learning techniques to determine changes in reservoir water extent over time.

1.3.2. Specific objectives and research questions

I. To map the water extent and level variation over time
   - How much has the extent and level of the Water changed upstream and downstream over time due to the GER Dam?

II. To estimate the water volume dynamics over time.
   - To what degree has the water volume of the GER Dam reservoir changed throughout time?

III. Compare SWOT with other satellite products.
   - How accurately can SWOT satellite products estimate the reservoir's water extent?
   - How effective are SWOT satellite products in estimating GER Dam reservoir volume variation?

1.4. Thesis Structure

Following this introduction, the subsequent chapters and their brief outline are listed below-

Chapter 2- Literature Review: This chapter provides a comprehensive overview of the related literature to establish a clear understanding of the topic, and it also covers the state of the art in water extent and water level detection and discusses the SWOT mission in detail.
Chapter 3- Study Area and Datasets: This Chapter provides a description of the study area and dataset used for this study.
Chapter 4- Water Extent & Water Level Timeseries Development: This chapter describes the methodological framework and steps followed for water extent detection and presents the detailed analysis and findings obtained for this objective.
Chapter 5- Water Volume Estimation: This chapter describes the methodological framework and steps followed for water volume estimation with satellite-based observation and digital elevation model (DEM). It also presents the details of the analysis and findings obtained for this objective.
Chapter 6- SWOT Satellite Based Water Extent and Volume Estimation: This Chapter the methodological framework and steps followed for water extent and volume estimation with SWOT satellite based products
Chapter 7- Discussion and Conclusion: This Chapter provides an interpretation to the study findings presented in chapters 4 to 6 and discusses the limitations of the study.

2. LITERATURE REVIEW

2.1. Water Extent Detection

Water extent monitoring, taking advantage of orbital platforms, emerged as a viable solution for tracking the temporal variation in the extent of water bodies (Alsdorf et al., 2007). Utilizing a variety of available band combinations from existing optical satellites (Sentinel 2, MODIS, Landsat, SPOT), the extent of water bodies can be derived successfully (Musa et al., 2015; Pickens et al., 2020; Sheng et al., 2016). The fundamental principle of satellite water detection is utilizing water's distinctive spectral features, which differ significantly from other ground features. Water has unique reflectance properties, particularly in the near-infrared regions, where it absorbs most of the incident radiation and makes it easily distinguishable from other landcover types - vegetation, soil, and urban areas (Huang et al., 2018b).

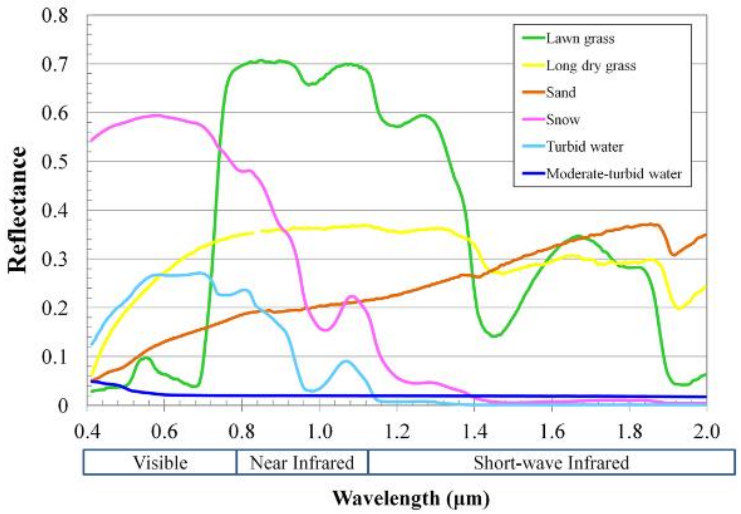

Figure 2-1 Spectral Characteristics of different land cover type. Source: (Huang et al., 2018b).

Surface water can be measured using two main types of sensors: optical sensors and microwave sensors. Due to the high data availability and suitable spatial and temporal resolutions, optical sensors are widely used in this field (Huang et al., 2018b). There are two global water extent dynamics mapping initiatives based on optical remote sensing already exist: Global Surface Water Dynamics (GSWD) and Global Surface Water Explorer (GSWE), which provides observations from 1972 (Pekel et al., 2016; Pickens et al., 2020). Despite this, optical remote sensing is susceptible to cloud cover and atmospheric pollutants and incapable of identifying waterbodies beneath forested regions, making it a less effective standalone solution (Huang et al., 2018a). On the other hand, active remote sensing techniques based on microwave sensors utilize long-wave radiation and can penetrate clouds to detect water bodies under forested areas (Martinis et al., 2015).

Many studies have demonstrated the suitability of SAR-based water extent derivation (Bartsch et al., 2008; Binh & Son, 2021; Rosenqvist & Birkett, 2002). Water bodies, having smoothed surfaces, contribute almost no backscattering to radar satellite receivers and appear as distinctively black regions in radar images. Estimating these backscattering values can determine areas with water bodies(Shen et al., 2019). However, other landcover types with similar backscattering values result in false positives in water extent detection, leading to overestimating the areal extent of water bodies (Y. Li et al., 2020). Few studies also utilize a combination of SAR and optical images to delineate water extents. Using a combination of Landsat 8, Sentinel 2, and Sentinel 1, Druce et al. (2021) applied multivariate logistic regression to identify monthly

water extents. Another study improved water extents by minimizing differences between SAR, LiDAR, and WorldView-2-based water extent outputs using a multilevel decision tree (Irwin et al., 2017). In a nutshell, having many methods for water extent detection utilizing remote sensing helps us minimize the gap of water extent detection using field surveillance and in situ monitoring stations.

However, the accuracy of techniques for detecting water extent heavily relies on the detection algorithm employed. Various methods exist for this purpose. One approach involves threshold-based techniques where the radiative property from a single band is used to establish a stable threshold value. This method is advantageous due to its efficiency in computational time(Huang et al., 2018b). Machine learning is another widely used method for classifying images. There are two types of image categorization algorithms: supervised and unsupervised. The first stage in supervised classification is to choose training sites, such as areas that are known to contain water. After analyzing the training data's statistical parameters, each remaining pixel is categorized into a training class according to statistical similarity(Gao, 2015b).

2.2. Water Height Detection

Water surface elevation is as essential as water extent when assessing reservoir volume (Zhang et al., 2014)]. In situ gauges are commonly used to monitor the surface height of waterbodies for the last few decades. It can give more precise estimates of water levels over a wide range of periods. However, these gauge networks have limited spatial coverage, leaving many lakes and rivers ungauged. The number is even higher in developing countries where monitoring station networks are still poorly distributed (Nair et al., 2021). Satellite altimetry missions emerged with a higher potential to bridge this gap by providing higher spatial coverage. Currently, only a few satellite missions are active, and they can estimate water surface height by using radar and laser nadir altimetry.

The satellite altimetry missions were first launched with the Topography Experiment/Poseidon in 1992 and were later followed by the Jason series and ICESat missions (Zhang et al., 2011; Elmer et al., 2020). In principle, all satellite altimetry missions emit a short energy pulse reflected to the sensor by the surface. The water surface elevation products are estimated by leveraging the relationship between the altimeter's distance to the surface and the time difference between transmitted and received reflected energy (O'Loughlin et al., 2016). Most of the current satellite altimetry missions are onboard with nadir altimeters working on C-band and Ku-band, which results in a coarser resolution in the along-track direction, ideally for ocean surface topography estimation (Elmer et al., 2020). Despite low spatial resolution not being ideal for inland water body monitoring, few studies have reflected the capability of these products for monitoring inland water bodies. A study by Da Silva et al. (2014) estimated water levels in the Amazon basin with radar altimetry products of Topography Experiment/Poseidon, ERS-2, ENVISAT, and JASON-2. Another study explored the possible methods to analyze the spatiotemporal fluctuations of water level and volume of one of the world's largest freshwater lakes, Lake Victoria, with remotely sensed products (Awange, 2021). Duan & Bastiaanssen (2013) analyzed different lake volumes in various countries around the globe using a variety of altimetry databases and laser altimeters.

Apart from altimetry missions, water-level databases provide water-level time series data over extended periods and contribute significantly to hydrological research and water resource management. Two well-established databases in this domain are the Database for Hydrological Time Series over Inland Waters (DAHITI) and Hydroweb. Hydroweb offers time series data from missions such as Jason-2 and Envisat, covering a variety of inland water bodies. Similarly, the DAHITI database provides 250 time series for rivers, reservoirs, and lakes (Kostianoy et al., 2022; Schwatke et al., 2015).

2.3. SWOT Instrument and Available Products

Most studies reported the low spatial resolution and spatial coverage caused by narrow swaths as a significant barrier in routinely estimating small and medium-sized inland water bodies with current altimetry products (Grippa et al., 2019). To fill this gap, the Surface Water Ocean Topography (SWOT) satellite was launched

in December 2022 with the capability of nadir radar altimetry and side-looking SAR interferometry. This mission is pioneering in its use of wide-swath altimeter radar interferometry and aims to generate precise, two-dimensional maps of ocean surface topography and land surface water elevation, presented as water masks (Hamoudzadeh et al., 2024a).

The main principle of swot measurement involves determining the geocentric height of the water surface by calculating the difference between the satellite's geocentric position and the distance from the satellite to the water surface. This distance is measured by two separate radar instruments, KaRIn and NAlt. Each instrument provides complementary spatial coverage along the satellite's ground track. Both KaRIn and NAlt utilize the distinct spectral characteristics of water, which has a higher average reflectivity compared to land, to measure water height (JPL D-109532, 2024). The KaRIn synthetic aperture radar interferometer is the key driving factor for the SWOT mission. It effectively captures range measurements across two 50 km swaths, spanning from 10 to 60 km on either side of the nadir ground track. Meanwhile, the NAlt instrument complements KaRIn by providing range measurements along the nadir ground track and focuses mainly on sea surface height over the ocean. This setup bridges the gap between KaRIn's measurements on either side of the nadir. (Biancamaria et al., 2016).

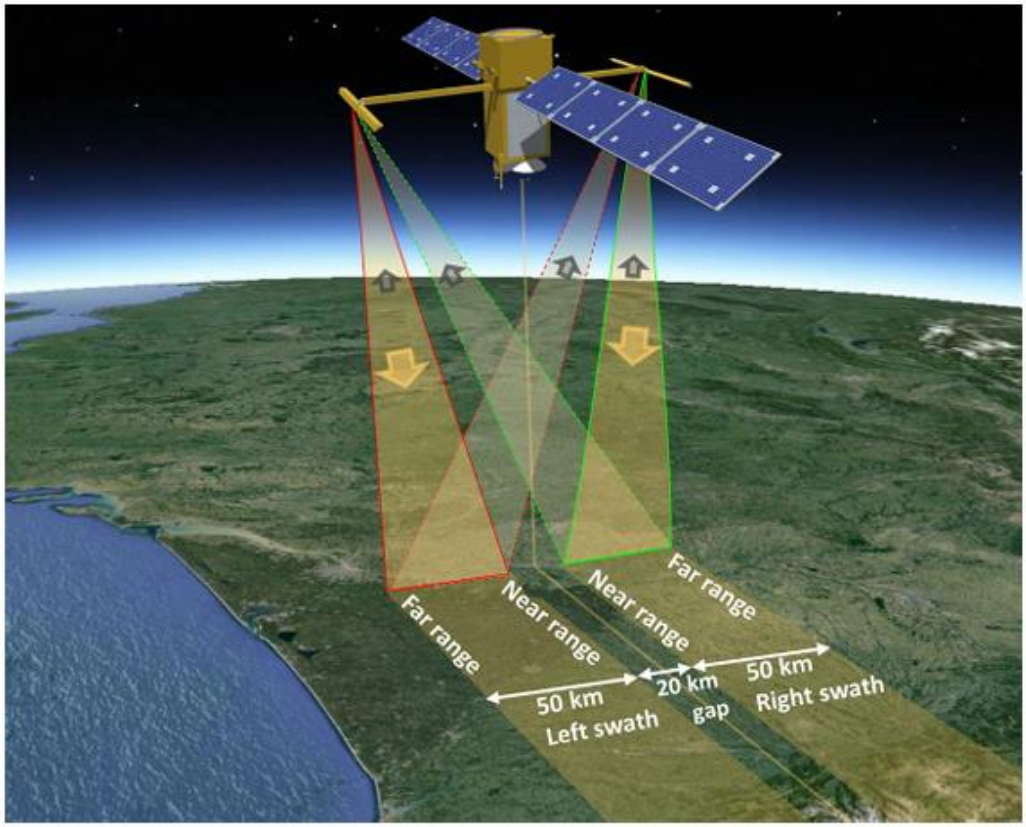

Figure 2-2. Conceptual view of the SWOT mission with its principal payloads: the Ka-band radar interferometer (KaRIn, with the observed swaths shown by the yellow polygons) and a Ku-band nadir altimeter (yellow line). Source:(Biancamaria et al., 2016)

SWOT produces detailed water masks capable of resolving features as narrow as 100 meters for rivers and 250 x 250 meters for lakes and reservoirs. Each mask includes water level elevations with an accuracy of 10 cm and a slope accuracy of 1.7 cm per kilometer for areas larger than one square kilometer. The mission's orbit ranges from 78° S to 78° N, covering at least 86% of the globe over its three-year mission. SWOT revisits the same paths on Earth every 21 days, completing 292 unique orbits. The water surface elevation (WSE) data collected by SWOT is referenced to the Earth Gravitational Model (EGM2008) and corrected

for delays caused by the atmosphere (wet and dry troposphere, ionosphere) and tidal effects (solid tide, load tide, and pole tide) (Hamoudzadeh et al., 2024b).

Table 2-1. SWOT Mission Characteristics

Swot Mission Characteristics	
Orbit altitude	890.5 km
Orbit Inclination	77.6 degree
Repeat Period	20.86 days

SWOT data products include various products in oceanographic, hydrology, and other fields. The products that have been used for this study are- L2_HR_LakeSP, L2_HR_PIXCVec, and L2_HR_Raster. The details about these products can be found in the Dataset chapter.

2.4. Water Volume Variation

When bathymetry data is available, any reservoir storage can be approximated using the water extent and water surface height derived from remote sensing techniques(Musa et al., 2015). This method relies on accurate topographic or bathymetric data to precisely measure volume variations in water bodies. However, without precise topographic or bathymetry data, the estimation of volume variations in water bodies can be achieved by applying the elevation-area relationship (Duan & Bastiaanssen, 2013; Gao, 2015a). Water level data time-series, either from in situ measurements or satellite altimetry products, are utilized to estimate the volume variations. The lowest water level in a reservoir is first identified and used as a reference level. Water level variations over time are then simultaneously estimated and matched with the water extent. By analyzing the relationship between the water surface elevation above the reference level and its corresponding water extent, temporal variations in volume can be deduced. However, when bathymetry data of a reservoir is known, it is possible to measure the whole volume utilizing reservoir water extent and underwater topographic information (Bose et al., 2021; Y. Li et al., 2021). This study, therefore, utilizes this method to measure the volume of the reservoir. Additionally, there is a new satellite altimetry mission, the Surface Water Ocean Topography (SWOT) satellite, which was launched in December 2022 with the capability of nadir radar altimetry and side-looking SAR interferometry. However, this dataset has not been tested against other measured volume results in the GER region. Therefore, the measured data is tested with SWOT data to evaluate its performance.

3. STUDY AREA AND DATASETS

3.1. Study Area

The Grand Ethiopian Renaissance (GER) Dam was selected as the study area to assess its impact on reservoir volume variance. It is one of the second largest hydropower dams in that region, making it a significant project on one of the main tributaries of the Blue Nile River, which is a vital lifeline for the downstream nations, including Egypt and Sudan. By utilizing the river's yearly discharge of 1,541 m3/s, GER Dam seeks to produce six thousand MWh of energy, estimated at 15,000 GWh annually. According to BBC, it has started filling up in different phases since July 2020. This 1,780-meter-long and 155-meter-tall dam is intended to build a reservoir that, at full supply, can hold roughly 74 billion cubic meters of water. Even though hydropower is the intended use of the Grand Ethiopian Renaissance (GER) Dam, the downstream countries are expected to experience several adverse consequences. It substantially alters the river's water consumption, profoundly affecting the water supplies of downstream nations, such as Egypt and Sudan.

The reason for choosing this as the study area is its recent construction and filling. Since it has been started to fill recently, the underwater topography of this dam is already known, facilitating the estimation of its volume through the utilization of such data. The underwater topography-based volume estimation also enables the validation of volume calculations based on satellite and altimetry products. Another significant reason for selecting this as the study area is the availability of numerous satellite altimetry tracks over it.

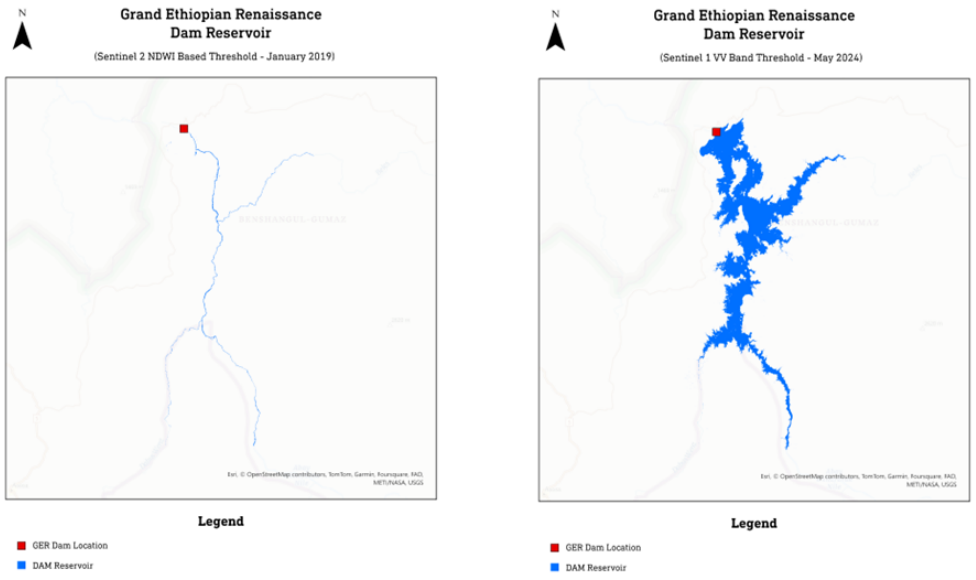

(a) Before Dam became Operational *(b) Recent State of the Dam Reservoir*

Figure 3-1. Study area Map

3.2. Datasets

This study used a wide range of data products to extract water extent and estimate water volume variations. The dataset includes various optical, radar satellite, and altimetry products to ensure an accurate dataset for estimation and validation. For the optical dataset, Sentinel-2 and Planet data were used, which offered high-resolution images essential for identifying and delineating water bodies. The radar dataset provided by Sentinel-1 offered images in all weather conditions and at any time of the day or night. Additionally, multiple altimetry products were collected, including the Surface Water and Ocean Topography (SWOT) mission and other altimetry datasets sourced from DAHITI and Hydroweb. A detailed description of the datasets and the rationale behind their selection is provided in the following sections.

Table 3-1. Table of datasets used for each objective

Datasets	Source
Sentinel 2 Band 3	European Space Agency (ESA)
Sentinel 2 Band 11	European Space Agency (ESA)
Sentinel 1 Band VV	European Space Agency (ESA)
Planet Green	Planet
Planet NIR	Planet
Copernicus Digital Elevation Model (DEM)	European Space Agency (ESA)
Multi-Error-Removed Improved Terrain (MERIT) DEM	University of Tokyo and Japan Agency for Marine-Earth Science and Technology (JAMSTEC)
ICEsat2 (ATL13)	National Aeronautics and Space Administration (NASA)
DAHITI	German Research Centre for Geosciences (GFZ)
Hydroweb	Laboratoire d'Etude en Géophysique et Océanographie Spatiale (LEGOS)
Global Reservoirs and Lakes Monitor (G-REALM)	National Aeronautics and Space Administration (NASA)
SWOT Level 2 Lake Single-Pass Vector Data Product	National Aeronautics and Space Administration (NASA)
SWOT Level 2 Water Mask Raster Image Data Product	National Aeronautics and Space Administration (NASA)
SWOT Level 2 Water Mask Pixel Cloud Data Product	National Aeronautics and Space Administration (NASA)

3.2.1. Sentinel-1 Synthetic Aperture Radar

This study uses the Sentinel-1 dual-polarization C-band Synthetic Aperture Radar dataset from the European Space Agency's Sentinel-1 mission. Sentinel-1 provides continuous and reliable data in different polarizations every 6 days. The dataset used for this study spans from January 2019 to May 2024, with a specific focus on the VV (vertical transmit/vertical received) single polarization band as it is highly sensitive to water, providing low backscattering value and making it suitable for detecting water bodies. SAR VV polarisation was also employed in recent studies focusing on monitoring water or flood(Bhatt et al., 2020; Nagai et al., 2021). The dataset is collected from the Google Earth engine data catalog as it offers processed

sentinel-1 GRD data, including the processing of thermal noise removal, radiometric calibration, and terrain correction. The usual revisit period of the Sentinel 1 mission, which included both Sentinel 1A and 1B satellites, was close to 6 to 12 days. However, as of December 2021, due to an anomaly in the instrument's power supply, the operation of the Sentinel 1B satellite has ended. Therefore, the revisit period of Sentinel 1 has increased, which resulted in fewer available imageries after 2022 than usual.
Sentinel-1 data is chosen to study the Grand Renaissance Dam reservoir because of its ability to penetrate cloud cover and provide consistent, all-weather imagery. The objective of the study is to monitor the water extent dynamics of the reservoir over time. The changes in water extent dynamics are mostly visible in the wet season, as heavy precipitation during the wet season facilitates the filling of the reservoir. Heavy rainfall is also associated with cloud cover, reducing the visibility of optical images. Therefore, optical imagery cannot provide accurate data that can be used to monitor data all over the year. As a result, Sentinel-1 data has been used.

3.2.2. Sentinel 2 Optical Imaging

In addition to the Sentinel-1 SAR data, this study uses optical imagery from the Sentinel-2 mission. Sentinel-2 provides high-resolution (10-meter) optical images essential for detailed land cover and water body monitoring. However, one significant challenge of using optical imagery is its cloud cover, which poses a significant challenge for the study area around the Grand Ethiopian Renaissance (GER) Dam. To address this, a cloud filter was applied to identify images with less than 5% cloud cover from January 2019 to May 2024, and then 3 images were randomly selected from them as validation products. Subsequently, a cloud masking process was performed to remove both cirrus and normal clouds using the quality band (Band 60). Monthly median composites were then computed to get a clear, cloud-free overview of the monthly data. The study uses Bands 3 (Green) and 11 (Short-wave infrared) from Sentinel-2 to calculate MNDWI, a modified version of NDWI that is more accurate for detecting water. These bands are particularly suitable for detecting water bodies, as water typically reflects the green band and absorbs more shortwave radiation.

3.2.3. Planet Satellite Data

As a Validation dataset for the water class, this study uses another high-resolution (5 meters) and open-source data from the NICFI (Norwegian International Climate and Forest Initiative) satellite data program of Planet. The NICFI program provides high spatial and temporal resolution monthly composite imagery, with monthly base maps available. Besides, this high temporal resolution offers a monthly composite of the best possible cloud-free images. However, during visual inspection, it was seen that some images were cloud contaminated. Therefore, to obtain cloud-free images, a thorough manual review was conducted. Through this process, two cloud-free months, December 2022 and January 2024, were randomly selected. Only the green and Near-Infrared (NIR) bands were collected for this study to calculate NDWI. Typically, water reflects the green band more and absorbs a great amount of the NIR band.

3.2.4. Copernicus Digital Elevation Model (DEM)

This study uses the Copernicus Digital Elevation Model (DEM) dataset from the Copernicus program as bathymetry data. The DEM dataset was generated to ensure harmonization with the other Copernicus products regarding spatial resolution. This product provides data in several different resolutions. In this study, one European Environmental Agency dataset with a 10 m resolution and one global 30 m resolution were used. It is important to mention that the vertical unit for measurement of elevation height is meters, and it used EGM2008 geoid as the reference for all Copernicus data. Another reason for using this dataset is that it was generated before the construction of the Grand Ethiopian Renaissance (GER) Dam, providing topographic information about the regions currently inundated. This historical topographic data is important for understanding the pre-construction landscape and accurately modeling the water extent, level, and volume in the reservoir area.

3.2.5. SWOT Satellite Products

Several products from the Surface Water and Ocean Topography (SWOT) satellite program have been used for this study to obtain the water surface elevation dataset.

SWOT Level 2 Lake Single-Pass Vector Data Product (L2_HR_LakeSP):

The L2_HR_LakeSP product delivers high-resolution measurements from KaRIn of water surface elevation, storage, and extent for lakes and similar features. Each lake object is represented as a polygon linked to its measured water surface elevation and area. These measurements are derived using an algorithm that identifies which pixels from the L2_HR_PIXC product should be grouped together as a lake object and then aggregates those pixel measurements. The product also includes quality flags, uncertainty estimates, and details on the processing parameters used to compute the main measurements (JPL D-109532, 2024).

SWOT Level 2 Water Mask Raster Image Data Product (L2_Water_mask_Raster):

The L2_HR_Raster product provides data on water surface height, inundation extent, and backscatter (σ°) on a 2-D global grid. It is simplified for user convenience and is based on the L2_HR_PIXC product. Even though it is simpler, it is versatile enough to investigate complex situations like flood events, where the assumptions used for the L2_HR_RiverSP and L2_HR_LakeSP products may not apply. Compared to the L2_HR_PIXC product, the L2_HR_Raster typically has a coarser resolution. It is produced operationally at two different resolutions, 100 and 250 meters, with each resolution provided in separate files but otherwise identical in format (JPL D-109532, 2024).

SWOT Level 2 Water Mask Pixel Cloud Data Product (L2_HR_PIXC):

The L2_HR_PIXC product is designed to provide detailed, low-level information on KaRIn HR measurements of inland water features. This allows users to process SWOT data using their specialized methods without dealing with the complexities of the KaRIn implementation or the large data volumes of the L1B_HR_SLC product. This product offers geolocated KaRIn height measurements from the HR data stream after pixel-level processing of the 2-D KaRIn SLC images, optimized specifically for terrestrial hydrology. It includes pixel 3-D geolocation information, surface classification data derived from KaRIn, and prior external information. The classification algorithm automatically detects water based on the surface reflectivity observed by KaRIn, assuming water is more reflective of radar signals than land at the wavelength and incidence angles used by KaRIn. Along with pixel 3-D geolocation and classification information, the L2_HR_PIXC product includes backscatter (σ°) data, quality flags, and uncertainty estimates, providing comprehensive information for further analysis (JPL D-109532, 2024).

Table 3-2. Definitions of numeric surface classification values for the L2_HR_PIXC product.

Class Number	Class Name
1	Land
2	Land near water
3	Water near land
4	Open water
5	Dark water
6	Low-coherence water near land
7	Open low-coherence water

3.2.6. Multi-Error-Removed Improved Terrain (MERIT) DEM

The MERIT DEM was generated by correcting errors such as absolute bias, stripe noise, speckle noise, and tree height bias from existing spaceborne DEMs like SRTM3 v2.1 and AW3D-30m v1. This improved DEM provides high-resolution terrain elevation data at approximately 90 meters at the equator and covers land areas between 90°N and 60°S with a reference to the EGM96 geoid (Yamazaki et al., 2017). By removing these errors, the accuracy of land area mapping with a vertical precision of 2 meters or better increased from 39% to 58%. Significant improvements are evident in flat regions where previous height errors were greater than the actual topographic variations. Features such as river networks and hill-valley structures are now distinctly represented. The previously distorted slopes in major floodplains, including the Ganges, Nile, Niger, and Mekong, as well as swamp forests like the Amazon, Congo, and Vasyugan, have been accurately depicted. This new DEM has the ability to enhance various geoscience applications that rely on accurate terrain data. This hydrologically adjusted DEM is now available as part of the MERIT Hydro datasets. For this study, MERIT hydrologically adjusted DEM was used.

3.2.7. Radar Altimetry Water Height Databases

Water height data has been collected from both the DAHITI and Hydroweb global databases. The DAHITI (Database for Hydrological Time Series of Inland Waters) database, accessible at DAHITI, hosts water level time series data for inland water bodies derived from satellite altimetry observations. It is developed by the Deutsches Geodätisches Forschungsinstitut at the Technical University Munich (DGFI-TUM. The estimation of water level time series in DAHITI is based on an extended outlier rejection and a Kalman filter approach (Schwatke et al., 2015). All measurements are subjected to the same retracker and geophysical corrections by DAHITI. This is done in order to reduce the impact of any potential sources of bias (Tourian et al., 2021). Similarly, the Hydroweb database, accessible through the Hydroweb website, was the early platform that offered altimetric water level time series data contributed by the efforts of the Laboratoire d'Etude en Géophysique et Océanographie Spatiale (LEGOS) (J.-F. Crétaux et al., 2011). Likewise, G-REALM is also a water height database generated from radar altimetry data. G-REALM uses data from radar altimeters provided by NASA, CNES, ESA, and ISRO over inland water bodies and produces surface elevation products through a semi-automated process to monitor these water bodies. These products are available on a website for the USDA and the public. Initially, these databases offered water height time series for various inland water bodies derived from altimetry flights from both current and historical sources. Besides, many lake and river water level time series are available in Near Real Time (NRT). Virtual stations that coincide with the study area around the Grand Ethiopian Renaissance (GER) Dam were selected for this study. Specifically, two stations from the DAHITI database, one from the G-REALM database, and three from the Hydroweb database were chosen.

3.2.8. ICEsat 2 Along Track Science Data (ATL13 Product)

The Advanced Topographic Laser Altimeter System (ATLAS) is a feature of the ICESat-2 satellite that enables monitoring shallow water depths. Because of this feature, it becomes a suitable tool for mapping and monitoring water levels on a large scale in lake and river applications. The lidar on ICESat-2, which counts photons at 532 nm, can capture a high density of photons from both the water surface and shallow underwater regions. With a 91-day repeat orbit and a 92° inclination, the satellite covers up to 88° north and south latitudes, creating 1,387 ground tracks. The 26 data packages of ATL13 include aggregated data on lakes, reservoirs, rivers, bays, estuaries, and a 7 km near-shore buffer. ATL13 contains data on water surface height along the track, significant wave height, wind speed at 10 meters, and estimated bottom depth for minor parts. Both strong beams (gt1r, gt2r, and gt3r) and weak beams (gt1l, gt2l, and gt3l) can be used to derive the height of water surface with minimal reported error (Dandabathula et al., 2020). ATL13 along track data from January 2019 to May 2024, which intersected the study region, were extracted for this study.

4. WATER EXTENT & WATER LEVEL TIMESERIES DEVELOPMENT

This chapter describes the methodological framework and steps followed for water extent detection and presents the detailed analysis and findings obtained for this objective.

4.1. Methodology

4.1.1. Sentinel 1-based water extent map development

To monitor the reservoir filling curve of the GER dam, the study used the Sentinel-1 "VV" band as the primary dataset. The "VV" band effectively differentiates between water and non-water areas, making it ideal for this purpose. Around 150 sentinel 1 imageries based on water extent need to be derived for the time series development. The study adopted an unsupervised method to map surface water using Otsu's thresholding on Sentinel 1 VV band images described in the section below.

4.1.1.1. Data acquisition and Speckle Filtering

This study acquired Sentinel-1 GRD data from the Google Earth Engine Data Catalogue; therefore, the data was already radiometric calibrated. Additional preprocessing, speckle filtering, and terrain correction were done using the Sigma Lee filtering technique and the Copernicus Digital Elevation Model (DEM).

4.1.1.2. Radiometric slope correction

Although GEE provides basic processing steps, it is necessary to perform additional radiometric slope correction to mask out areas affected by layover and shadow. These radiometric distortions result from the side-looking SAR imaging geometry. One such distortion is a layover, which occurs when the radar signal reaches the top of a slope before the bottom. It is common in rugged terrain where the top of a mountain may be at a greater distance in ground range but a shorter distance in slant range. This effect appears when the slope steepness in range (αr) exceeds the incidence angle (θi) on a slope facing towards the sensor (foreslope) and causes the sequence of pixels to be distorted and terrain features to appear out of order in the SAR image. Radar shadow, on the other hand, occurs when a slope facing away from the sensor (backslope) exceeds the radar's look angle, defined as $\theta = 90° - \theta i$. In this case, the emitted radar beam does not reach the ground at all, resulting in shadowed areas with no returned radar signal (Vollrath et al., 2020). Both layover and radar shadow regions exhibit similar characteristics in the radar VV band received signal, leading to the possibility that a thresholding-based approach might misclassify these zones as water pixels. To address these issues, an algorithm based on Earth Engine was employed to identify and mask potential radar layover and shadow areas, minimizing the risk of misclassification.

4.1.1.3. Thresholding using Edge Otsu Algorithm

Otsu's method is an automated technique that identifies an optimal threshold to split pixels into two distinct classes: foreground (representing water) and background (representing land). It identifies the value for which the highest inter-class variance is the optimal threshold. The pixels are split into binary classes based on that optimal thresholding value. This method works best with images that clearly separate two classes. Nevertheless, the effectiveness of the method could decrease when the image contains more than two classes. The study used the “Edge Otsu” technique to ensure the bimodality in the input imageries. This

technique selects specific areas in the image that are more likely to show a clear water/no water separation, making the histogram more likely to be bimodal. This helps in getting a more accurate threshold for surface water mapping. This algorithm was first introduced by Donchyts et al. (2016) for unsupervised water detection, and it was later successfully used in different studies and applications (Markert et al., 2020a).
The Edge Otsu algorithm takes a raster as input in which water bodies have been highlighted. It then identifies the edges of these water features with the canny edge filter method (Xi & Zhang, 2012) and creates a buffer around them. Afterward, it samples histogram values from these buffered areas to find the best threshold using Otsu's method. This threshold is then used to classify the entire image into two parts: water and non-water regions.

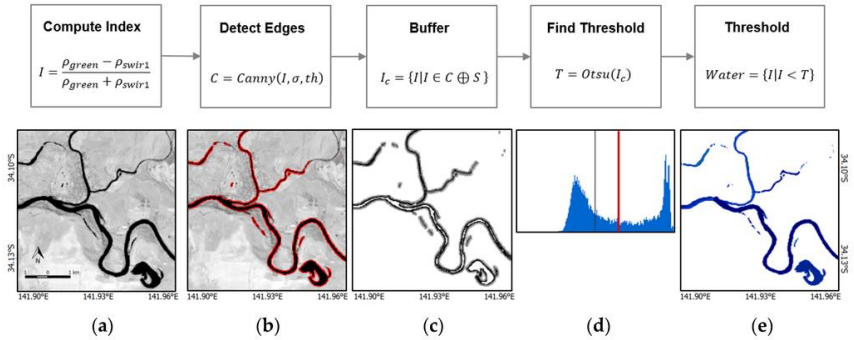

Figure 4-1 Image Source: Donchyts et al. (2016) Here (a) the raster where water had been highlighted (for this study Sentinel1 VV Band. (b) Detected edges with canny edge detector filter. (c) Developed buffer region around the detected edges (d) Finding out optimal threshold value with Otsu method (e) Detected threshold based binary classification of input raster.

After the preprocessing steps, the imageries were ready for the thresholding approach. The study used the Hydrologic Remote Sensing Analysis for Floods (HYDRAFloods) python module developed by NASA SERVIR to implement the edge otsu algorithm. The pre-processed sentinel 1 VV bands were supplied as input as a raster for the Edge Otsu algorithm. As for initialization, the algorithm requires to be provided with an initial thresholding value. Thus, different initial thresholding values were investigated. For the imageries with a greater amount of water region (images after July 2020), the initial threshold value of -18 dB performed best. Imageries with fewer water regions (images from January 2020 to July 2020) had a higher initial threshold value was required, which was -22 dB. Edges detected by the canny edge filter were buffered 300 meters on each side for histogram sampling. Otsu threshold was applied for the sample histogram to find the optimal threshold. Later, with the optimal threshold value, the entire imagery was classified into water and non-water regions.

4.1.1.4. Masking out dam reservoir outside the region

After classifying water and non-water regions, some areas outside the dam reservoir region were also classified as water. This occurred because the initial rectangular area of interest used in the processing covered both the dam reservoir region and downstream regions beyond the dam location. To eliminate this external water region, a rough polygon representing the actual dam reservoir boundaries was generated by closely examining the highest water extent using the latest high-resolution Planet satellite data. Then, using this polygon, downstream regions beyond the dam were masked out. This step ensured that only the water within the reservoir was considered in the final analysis.

4.1.1.5. Detecting disconnected water pixels

After masking out downstream regions beyond the dam, some water pixels were still not a part of the main GERD reservoir area. This happened because some areas close to the main reservoir might have a presence of water that is not a part of the reservoir. These are mostly very small water pixel collections. To disregard

these non-connected water pixels, a filtering operation was performed to find out all the present connected water pixel clusters. By examining the size of these water clusters, the main reservoir was easily identified because of its greater size than other water clusters. Then, all other smaller clusters were disregarded with a size-based filter, and the main reservoir cluster was taken as the final water map. This process was performed to eliminate disconnected water pixels and to ensure that the mapped water pixel accurately corresponded to the connectivity and layout of the reservoir in reality.

However, when the reservoir water extent was insignificant for pre-dam operation and initial dam operation periods, the Sentinel 1 thresholding approach could not classify the whole reservoir as one connected water region. Rather, it developed several segmented water regions along the reservoir area. Therefore, identified water cluster size-based filtering was not possible. As a solution, a range of size-based filters were selected manually by examining such water maps.

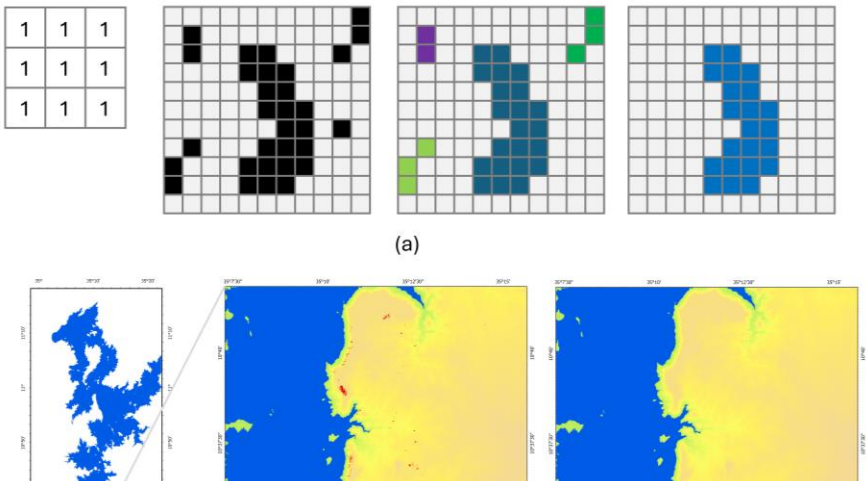

Figure 4-2. (a) shows a conceptual representation of the filter operation. A 3x3 filter was used to consider spatial neighbors in all 8 directions. Implementation of this filter will identify all the water pixel clusters present in the raster. After that area base area based filtering of identified clusters will result final map of desired water body. (b) illustrates the operation in the study region. After filter operation few disconnected water pixels were detected (in red), which were disregarded at the final processing step to result GERD reservoir water extent map.

4.1.2. Development of validation datasets

Two validation datasets were developed to validate the Sentinel-1 based water extent maps: one using Sentinel-2 MNDWI with edge Otsu thresholding and the other using Planet green and near-infrared bands with Support Vector Machine (SVM) classification. More information about these two validation datasets can be found in the following sections.

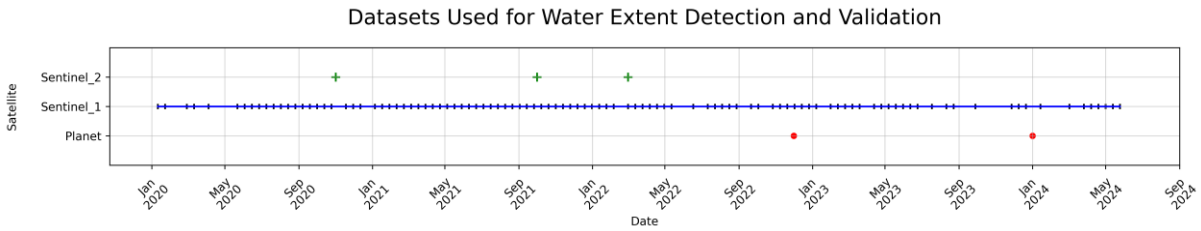

Figure 4-3. Dataset Used for Water Extent Detection and Validation To validate the Sentinel-1 water extent detection algorithm, 5 validation datasets (green + and red dots for Sentinel 2 and Planet respectively) have been compared against.

4.1.2.1. Sentinel 2-based water map development using MNDWI Edge Ostu thresholding

Using the spectral characteristics of water, thresholding-based water body detection has been a practiced method for a long time in scientific studies. Water reflects very little in the infrared wavelengths. Combining water's reflectance in the green and infrared bands makes distinguishing water from other landforms possible. Leveraging this principle, different water indexes like normalized difference water index (NDWI) (McFeeters, 1996), modified normalized difference water index (MNDWI) (Xu, 2006), High-Resolution Water Index (HRWI) (Pekel et al., 2016), Two-Step Urban Water Index (TSUWI) (Wu et al., 2018) have been coined for water detection. This study used sentinel 2-based MNDWI to develop a validation set. After experimenting with Sentinel 2-based NDWI and MNDWI for the study region, MNDWI edge otsu thresholding proved to be the most effective for water extraction. Therefore, MNDWI-based waterbody extent extraction was used in this study.

For Sentinel 2 MNDWI edge Otsu thresholding, the same *HYDRAFloods* python module was used. After performing the cloud masking process (detailed in the dataset chapter), MNDWI was calculated for each time step. Then, the MNDWI band was supplied to the edge Otsu algorithm as input. 0 was given as the initial threshold value for initialization, which was derived from several experiments. The canny edge filter detected edges that were buffered 300 meters inside and outside the direction of the sample histogram. The optimal threshold was identified from the sample histogram with the Otsu algorithm. It was later used to classify water and non-water regions.

4.1.2.2. Planet based water maps development using the SVM Model

Water extent maps from Planet Satellites were prepared by using the Support Vector Machine (SVM) algorithm. Recent studies on water extent detection report higher accuracy of SVM than other machine learning algorithms (Duan & Bastiaanssen, 2013; J. Li et al., 2022) and spectral indices-based extractions, especially in mountainous regions (Liu et al., 2020). SVM is a type of machine learning algorithm that is used to solve classification and regression issues. It falls under the category of supervised learning, meaning that it requires labeled training data to make predictions. It classifies data by finding an optimal hyperplane that separates different classes by maximizing the margin (Vapnik, 1995). In lament words, the model is trained by using information extracted from the provided features by the labeled training samples. Based on that information, a decision function is developed to distinguish between different classes.

In the context of this study, SVM was employed as a supervised classification method, requiring input features and labeled training data for model learning. Planet Green and NIR bands were chosen as input features because of the distinct reflectivity of water in these bands. As for labeled data, around 200 water and non-water sample points were carefully selected from the manual interpretation of a planet image (2024 January) and labeled as either "water" or "non-water." regions. The labeled datasets were then divided into training and testing sets. One recent study discussed models' exposure to overfitting if spatial data are divided into train–test sets randomly like non-spatial data (Roberts et al., 2017). This is because in spatial data, nearby points tend to be similar, and this similarity decreases as the distance between points increases. When randomly splitting data into training and testing sets, nearby points could end up in different sets, leading to overfitting because the model learns too much from similar points. Thus, this study adopted the grid split technique to split the whole labeled dataset into training and testing sets. The ratio was maintained at 67% for training data and 33% for testing data.

20% of the training dataset was set aside as a validation dataset to evaluate the model's performance and tune hyperparameters. As linear SVM was used for classifying Planet Images, the only hyperparameter that needed to be tuned was the regularization parameter (C). The study utilized a grid search approach to determine the optimal regularization parameter (C). The grid search approach specifies a range of values for each hyperparameter. These values are used to construct every possible combination. Through iterative evaluation on the training and validation sets, the model identifies the combination that yields the best performance. Subsequently, the final model is trained using the optimal hyperparameter values, and its performance is assessed using the testing set. This study experimented with 50 values ranging from 0.001 to

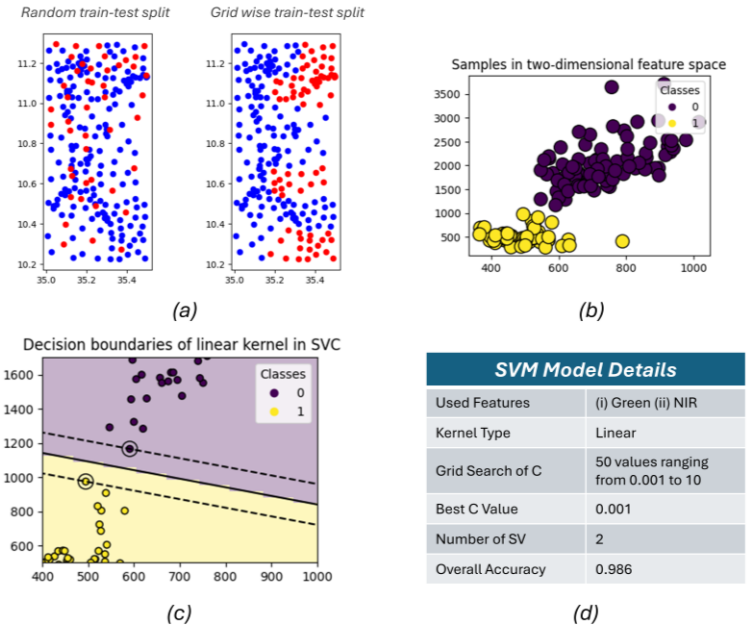

Figure 4-4. (a) illustrates the spatial distribution of training and testing set with different train-test splitting techniques. (b) shows the distribution of training points Planet Green and NIR bands values in 2D feature space (c) illustrates SVM linear kernel d detected optimal hyperplane separating training points in the 2D feature space. (d) shows the range of hyperparameters used for SVM model tuning and the final hyperparameters for which the best accuracy was resulted. Grid wise train test splitting technique based trained model produced desired results and better output than the random splitting technique.

10 as regularization values (C) with a linear kernel. With the grid search approach, 0.001 was identified as the best possible value for the regularization parameter (C). With this hyperparameter value, the SVM was trained using a training set. The model was evaluated using the testing set, where it reported 98.6% overall accuracy. Then, with this trained model, the whole Planet image of January 2024 and December 2022 was classified into water and non-water regions. By employing these methods, the study successfully extracted the required validation dataset to evaluate water extent time series derived from Sentinel 1 data.

4.1.3. Accuracy assessment with validation datasets

The study compared Sentinel-1-based water extent maps with the validation datasets. This evaluation estimated various accuracy assessment metrics – Confusion Metrics, Precision, recall, and F1-score. These criteria were selected based on their widespread usage in evaluating classification methods (Markert et al., 2020b; Ngo et al., 2017).

Confusion Matrix

Sentinel 1-based water maps were evaluated in five different timesteps with Sentinel 2 and Planet-based water maps. For each time step, confusion matrices were developed using a random sampling points-based approach. A confusion matrix is a table used for evaluating actual values with the model-predicted values by reporting the number of correct positive predictions (True positive), correct negative predictions (True negative), incorrect positive predictions (false positive), and incorrect negative predictions (false negative). From these instances, the models' overall accuracy can be calculated by dividing the total positive predictions (sum of true positive and true negative) by the total population (sum of true positive, true negative, false positive, and false negative).

	Predicted Positive	**Predicted Negative**
Actual Positive	True positive (TP)	False negative (FN)
Actual Negative	False Positive (FP)	True Negative (TN)

(a)

Overall Accuracy = $\frac{TP + TN}{TP + TN + FN + FP}$

(b)

Formula:
$\text{Precision} = \frac{TP}{TP+FP}$

(c)

Formula:
$\text{Recall} = \frac{TP}{TP+FN}$

(d)

Formula:
$\text{F1-Score} = 2 \times \frac{\text{Precision} \times \text{Recall}}{\text{Precision} + \text{Recall}}$

(e)

Figure 4-5. (a) A sample confusion matrix (b) The formula for overall accuracy calculation (c) The formula for Precision calculation (d) Formula for Recall calculation (d) Formula for F-1 score calculation.

For comparison, 10,000 points were randomly generated and used to extract classification values from both the Sentinel-1 water map and the validation dataset water map. These extracted values populated the confusion matrix. This process was repeated 50 times for each Sentinel-1 and validation set water map pair to mitigate the effects of randomness. The accuracy metrics were then reported as a range of values for each pair. The following metrics were generated to better understand the model's performance with the derived true positive, true negative, false positive, and false negative values from the confusion matrix.

- **Precision**

The precision of a model refers to the degree of accuracy of its positive predictions. It is the ratio of true positive (TP) predictions to the total predicted positives (TP + FP). The formula is given above (Figure 4-5-c). High precision indicates a low false positive rate, meaning that most of the positive predictions made by the model are accurate. For this study, the precision rate is crucial as the focus would be on how accurately the model can detect water pixels.

- **Recall**

Recall measures the error of omission rate. It is the ratio of true positive (TP) predictions to the total actual positives (TP + FN). The formula is given above (Figure 4-5-d). High recall indicates a low false negative rate, meaning the model is good at detecting true positives.

- **F1- Score**

The F-1 score measures the model accuracy by taking the ratio of precision and recall. The formula is given above (Figure 4-5-e). It denotes how the model identifies true positives and minimizes false positives and false negatives.

4.1.4. Altimetry Based Water Level Timeseries Development

4.1.4.1. From altimetry-based water level databases

- **Data Acquisition**

The altimetry dataset used to calculate water level time series was collected from two primary sources. The first source includes established databases such as DAHITI, HydroWeb, and G-REALM. These databases provide water height time series for various inland water bodies derived from current and historical altimetry flights. The second source of data came from the ICESat-2 satellite. It provides aggregated data on lakes, reservoirs, rivers, bays, estuaries, and a 7 km near-shore buffer.

- **Virtual water station finalization**

GERD reservoir had a few virtual station points from which water height observations were available from DAHITI, hydroweb, and G-REALM databases. However, during the virtual station selection, it was identified that DAHITI and Hydroweb provided virtual stations almost at the same geographical points. By examining the reported error values of the observations per virtual station, the stations with the minimum error values were selected to ensure data accuracy. It was found that DAHITI stations 17706 and 17705 had a lower reported error value range than hydroweb-based stations. Figure – XX depicts the error distribution of both DAHITI and hydroweb stations. Therefore, DAHITI based stations were selected for those two locations.

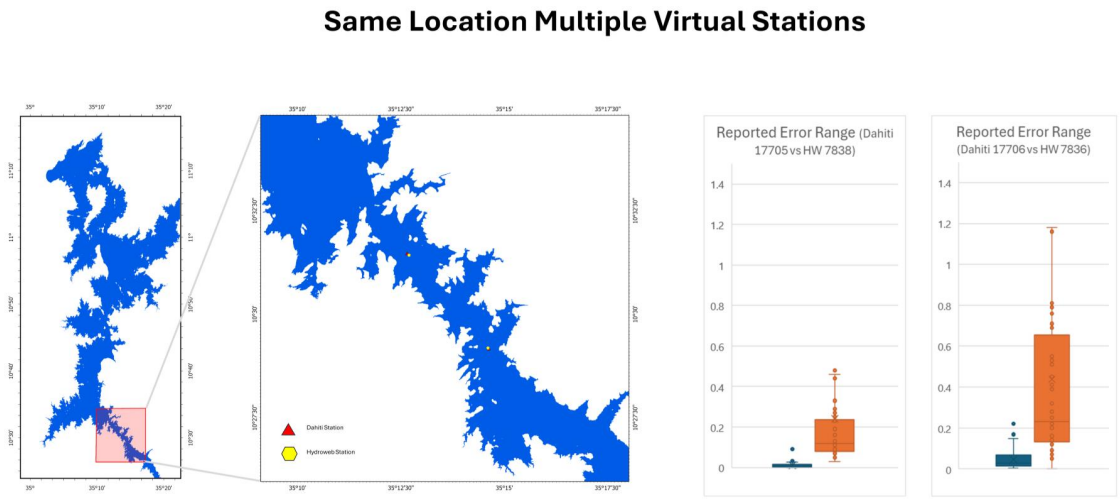

Figure 4-6. (left) Same location had multiple Virtual Station from DAHITI and Hydroweb, (right) boxplot showing reported error distribution for the station sharing same location.

Furthermore, observations from all selected virtual stations with an error value greater than 0.50 meters were filtered out. After finalizing the virtual stations, a water database was developed based on the observations from these stations.

4.1.4.2. From ICEsat-2 ATL13 product

Unlike altimetry water height databases like DAHITI, hydroweb, and G-REALM, ICEsat2 data is available for every available water body along its ground track. It has different data products, but the ATL13 product is dedicated to land-based water bodies. Though ICEsat2 has better precision than other altimetry missions,

but its higher revisit period makes it less appropriate for continuous monitoring. From NASA Poodac API, the ICEsat2 data were availed. For preprocessing ICEsat2-based height estimate data, quality flags mentioned in the ICEsat2 ATL13 product handbook were used (Jasinski et al., 2020). The dataset was specifically improved by eliminating data points where "qf_bckgrd" equaled 6. These segments, which are usually taken during midday and have the maximum density of background photons, have the lowest signal-to-noise ratio and a higher likelihood of outliers.

Furthermore, data with "qf_bias_em" values of 3 or -3 were removed due to considerable electromagnetic bias, which often implies a high water surface slope and causes potential elevation problems in water level estimates. Similarly, data with "qf_bias_fit" values of 3 or -3 were deleted, as stated in the official document of ATL13 (). This was done since these data displayed the greatest elevation bias between the fitted Gaussian centroids of the observed and integrated surface water histograms. Lastly, records where the "stdev_water_surf" was more than 2 were also deleted. This was done because it indicates a standard deviation in water surface elevation greater than two meters. This corresponds to a significantly high wave height (SWH) on lake surfaces. The outliers were eliminated from the dataset using these quality filters.

Table 4-1. The list of quality filters used to eliminate outliers from the ICEsat-2 observations and the final number of valid ICEsat2 observations after the outlier removal operation.

	Quality Flags	Percentage of Valid ICEsat2 Observations	Percentage of Valid ICEsat2 Observations after combining All flags
qc_bg	x>=6	93.76	93.72
qc_bias_em	-3 < x < 3	94.39	
qf_bias_fit	-3 < x < 3	95.78	
std_ws	x>2 & x==nan	97.37	
swh	x==nan	96.79	

The mean elevation was then determined based on all the along track points from the same datetime. This was done by taking the middle point of each available track and assigning the measured mean elevation to that point. The ICESat-2 observation points were visually inspected for each date with a corresponding Sentinel 1-based water map to ensure the points fell within the water body mask for that specific date. With such steps, ICEsat2 observations were preceded for further analysis.

After gathering all the valid observations from virtual stations and ICEsat2, a time series was developed to analyze the overall trend of water levels in the GERD reservoir.

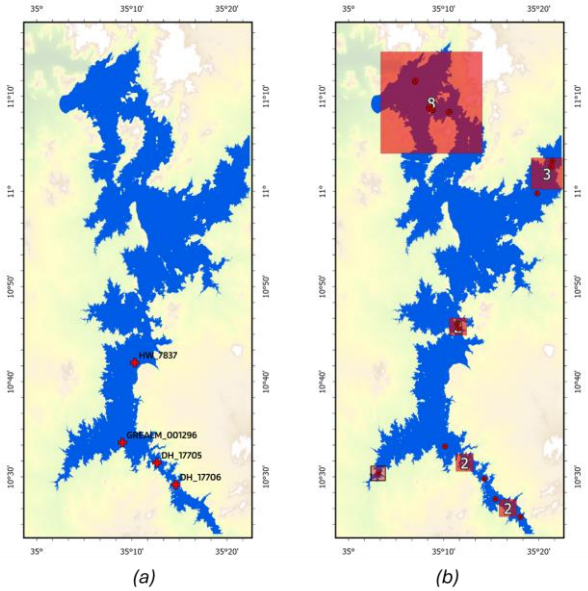

Figure 4-7. (a) Showcasing all the available virtual station in the GERD reservoir (b) Showing all the available observations of ICEsat2 in the GERD reservoir throughout the study period (2020 – 2024)

4.2. Result

4.2.1. Sentinel-1 based water extent timeseries

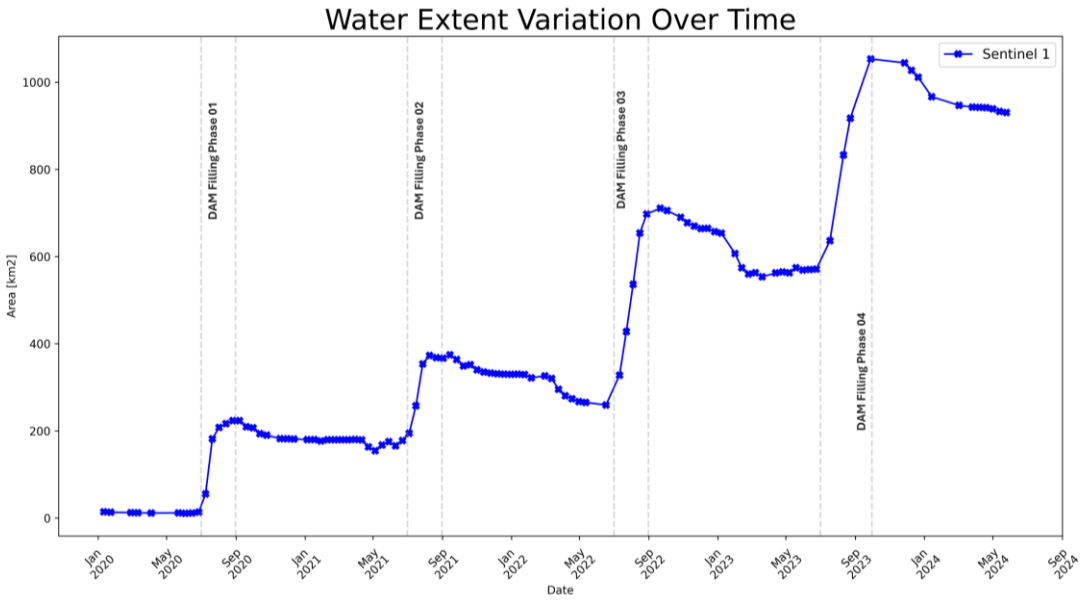

Figure 4-8. Water Extent Variation Over Time

Figure 4-8 illustrates the temporal variation in water extent derived from Sentinel-1 satellite observations. The graph shows distinct operational phases of the dam, which correspond to the observed increase in water extent. The first operational phase started in June 2020. Before that, the dam water level was in a steady position. Therefore, over the study period, a general upward trend in water extent is evident, indicating the continuous operational phases. Specifically, there is a marked decline in water extent values from January to June. Conversely, an increase is observed from July to September, and a peak water extent is observed between September and October 2023.

Figure 4-9 further details the variation in water extent over time for each operational phase. Notably, there is a significant difference in water extent from phase 1 to phase 4.

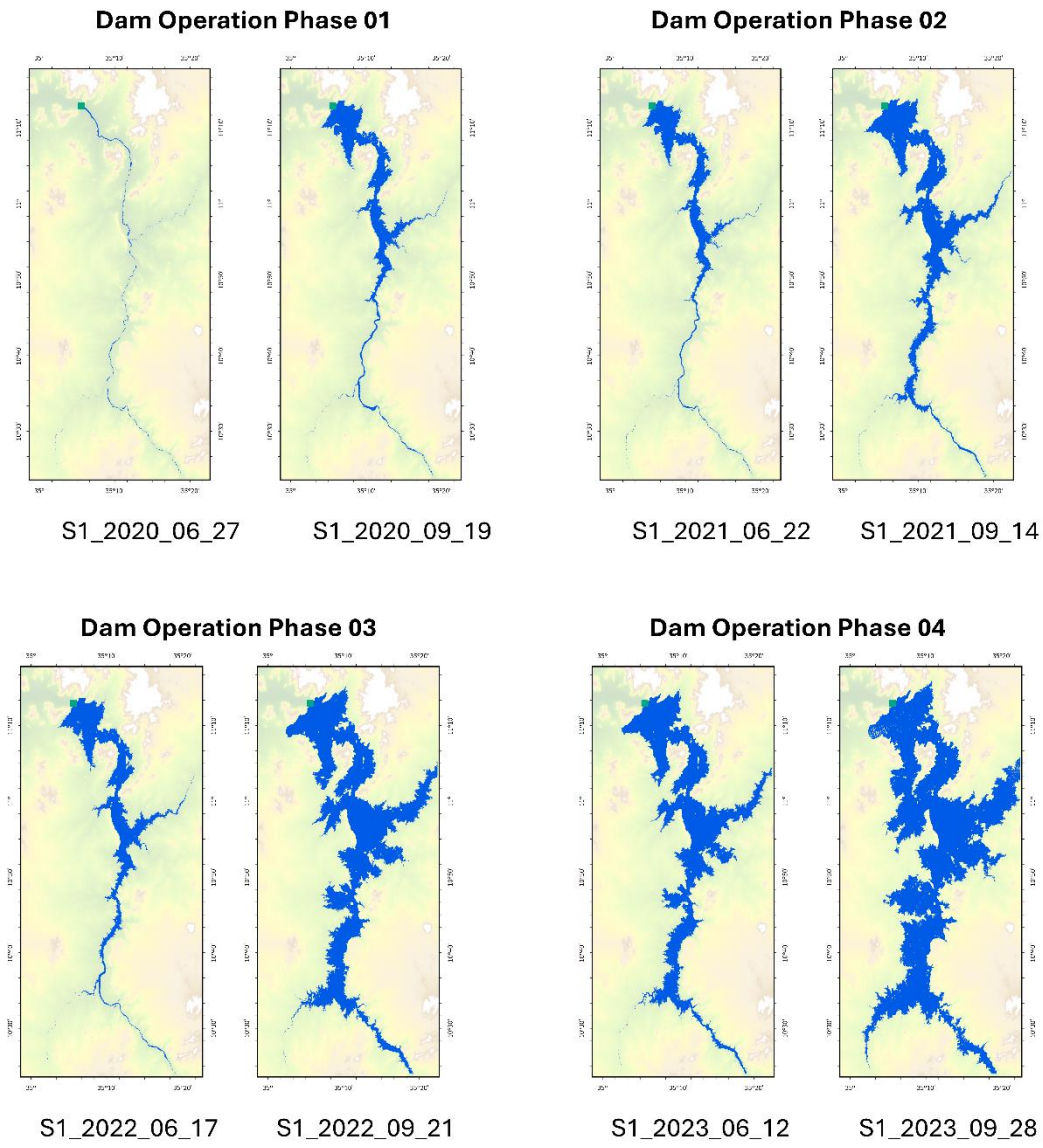

Figure 4-9. Water Extent Variation during different dam operational phases

Table 4-2. Table of mean accuracy assessment values

Dates	Validation Set	Overall Accuracy	Precision	Recall	F1 Score
Sentinel1_2024-01-14	**Planet 2024_01**	0.972872	0.996471	0.897583	0.944436
Sentinel1_2022-12-02	**Planet 2022_12**	0.971688	0.969889	0.85141	0.913392
Sentinel1_2022-03-01	**Sentinel 2 2022_03**	0.990412	0.975275	0.909116	0.941001
Sentinel1_2021-10-20	**Sentinel 2 2021_10**	0.982902	0.993859	0.831382	0.907246
Sentinel1_2020-11-18	**Sentinel 2 2020_11**	0.993702	0.992901	0.877454	0.931542

When comparing Sentinel-1 datasets from different acquisition dates, there are noticeable differences in the counts of true positives, true negatives, false positives, and false negatives. However, these differences

become less significant when analyzed using statistical metrics such as overall accuracy, precision, recall, and F1 score (Table 4-2). Precision, which is the ratio of true positives to the sum of true positives and false positives, is particularly important for classifying water and non-water pixels. All Sentinel-1 datasets performed well in detecting water pixels, with precision values ranging from 0.96 to 0.99. This high precision indicates a low false classification rate for water and non-water pixels and signifies accurate model results. Recall, or sensitivity, which measures the model's ability to identify actual positives, ranges from 0.83 to 0.90. This high recall value also indicates the model's accuracy in classifying water and non-water classes. The F1 score, the harmonic mean of precision and recall, ranges from 0.90 to 0.94. This high F1 score reflects the model's ability to identify true positives while minimizing false positives and negatives. Overall accuracy, which measures the ratio of accurate classifications (both true positives and true negatives) among the total number of cases identified, ranges from 0.97 to 0.99.

Although it has a high overall accuracy of the model in classifying water and non-water pixels while visually comparing the Sentinel-1 product with the validation product, the result shows that the model cannot perform well near the land-water edge areas of the reservoir in every time step. Besides, the result also shows poor performance before the dam operation time. The classification results were very fragmented (Figure 4-10).

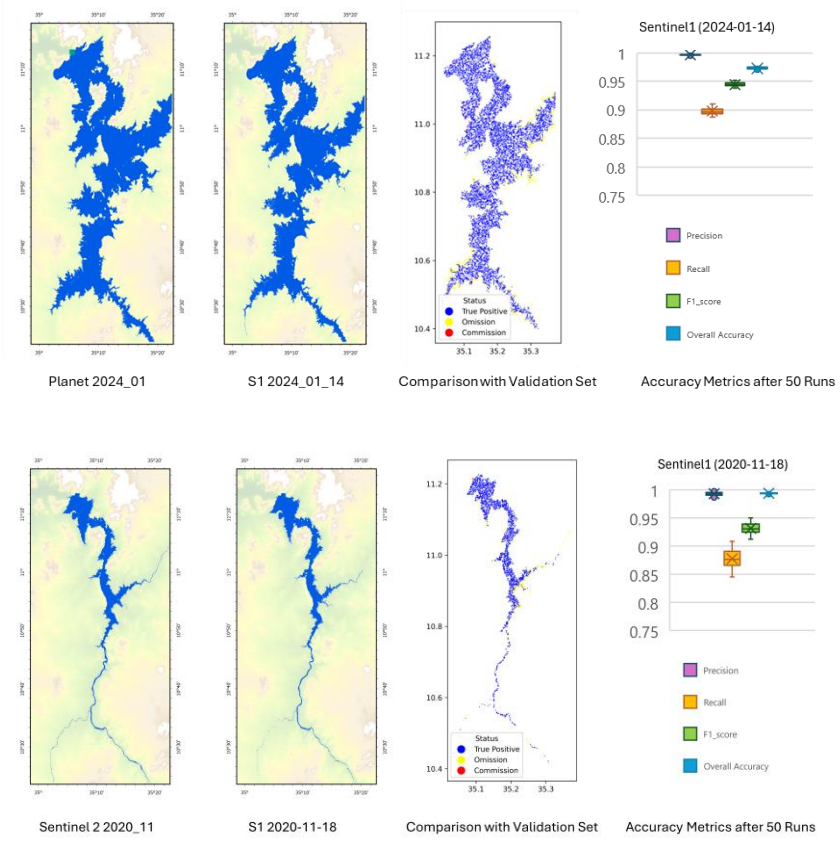

Figure 4-10. Visual Comparison of Sentinel-1 based classification result with Validation Product.

4.2.2. Radar altimetry-based water level timeseries

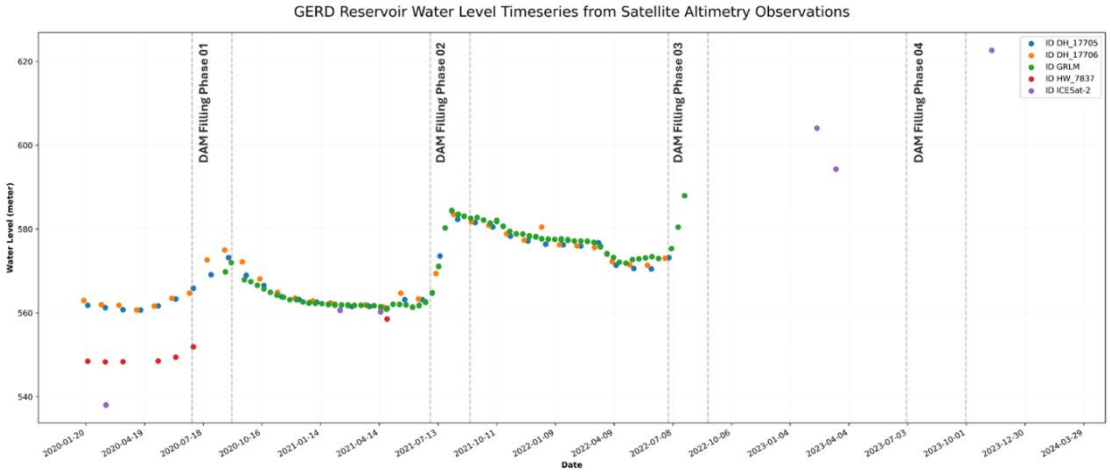

Figure 4-11. GERD Reservoir Water Level Timeseries from satellite Altimetry Observation

Figure 4-11 shows a time series of water levels derived from altimetry data, incorporating observations from two DAHITI stations, one Hydroweb station, and one G-REALM virtual station. Additionally, 12 ICESat-2 observations were collected from various locations within the reservoir at different times. The water level increases observed in different dam operation phases can be seen in this figure. Since the G-REALM and DAHITI stations are located upstream of the dam, the first operation period did not significantly affect their water levels. In contrast, the Hydroweb 7837 station, which is situated slightly downstream from the other stations, shows a rise in water level after the first operation period. All stations displayed increased water levels during the second and third operation periods. ICESat-2 observations were taken from various regions within the reservoir. Those taken before the dam operation period showed lower water levels compared to others because they were closer to the dam location, further downstream from the virtual stations. ICESat-2 observations located near the virtual stations during the first and second dam operation periods showed similar water heights to those stations. Three ICESat-2 observations collected after 2023 indicate higher water levels than all other time series observations. Since no other height observations were available for this time range, these observations could not be validated.

5. WATER VOLUME ESTIMATION

This chapter describes the methodological framework and steps followed for water volume estimation with satellite-based observation and digital elevation model (DEM) and presents the analysis and findings obtained for this objective.

5.1. Methodology

The water surface of big lakes and reservoirs can exhibit different water heights in different parts of the water body. In mountainous places, the difference in elevation between the areas upstream and downstream of the water body makes this gradient much stronger. Considering this slope in water volume estimation is challenging because, in most cases, only a limited number of water level observations are available for water bodies. Therefore, most studies did not consider the water slope phenomena while estimating reservoir water volume. In volume estimations, only a single water level was considered for the whole reservoir.
Being a mountain reservoir, the presence of a water slope is noticeable in the GERD reservoir. Despite having few radar altimetry-based virtual stations in the reservoir, it was not possible to estimate the water slope because of the absence of concurrent observations in these virtual stations. Thus, for volume estimation, this study deployed two different approaches. (i) Water volume estimation considers a single water level, and (ii) water volume estimation considers the water slope.

5.1.1. Volume estimation considering a single water level

5.1.1.1. Mean water level timeseries

For the GERD reservoir, water height estimates are available from altimetry data for different reservoir points. With these water height observations, a water height database was developed in the previous chapter. To have a single water level for the whole reservoir, with a 21-day window, mean water level timeseries were calculated from the water height database. This resulted in a timeseries of the mean water level for the GERD reservoir.

5.1.1.2. Lowest water level determination

The GER Dam began filling in different phases, and the first phase started in July 2020. Therefore, topographic information on river bed surrounding regions is available in digital elevation models developed before 2020. However, the Blue Nile River has flowed for decades in this region. Thus, underwater topography of this permanent water region is not available. Without proper underwater topographic information, volume estimation is challenging. Hence, the method of Duan & Bastiaanssen (2013) for estimating water volume fluctuation above a reference level was applied in this study. This reference water level is the lowest elevation of the water body, found by studying a series of water elevation measurements over time. From the developed 21-day mean water level time series, the lowest possible water level was detected before the dam operational period in February 2020. This was regarded as the reference water level, above which the water level variation was calculated.
The difference between the mean water level time series and this reference water level was considered as Water Level Above Lowest Level (WLALL). The Operational Dam resulted in a severe rise of water elevation in the reservoir. Therefore, the dam operational period's lowest possible water elevation must be lower water height estimates after the dam operation phases.

Water Level Above Lowest Level (WLALL) = Reference Water Level – Altimetry Based Water Level

This determined the time series of altimeter-based Water Level Above the Lowest Level (WLALL).

5.1.1.3. Volume variation above the lowest level

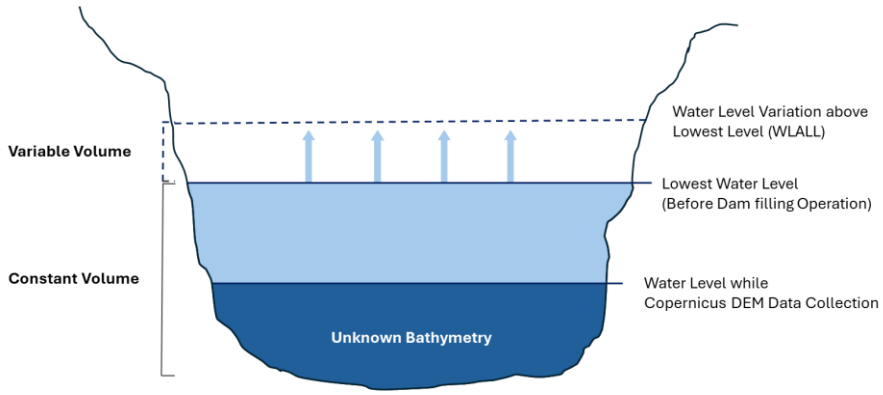

Figure 5-1. Conceptual representation of GERD reservoirs water volume and water level variation scenarios.

As the bathymetry information for the permanent water regions of the Blue Nile River is not available, water volume estimation for the whole reservoir is difficult. However, this study aims to assess only the changes in water volume that appeared after the GER dam became operational. The entire volume of the reservoir can be regarded as this equation:

$$Total\ Volume = Constant\ Volume + Variable\ Volume$$

Here, the variable volume represents the additional water volume produced by varying water levels after the dam was operational. The constant volume can be regarded as the corresponding water volume for the dam operation period's lowest water level. Thus, calculating the variable volume is enough to estimate the volume variation resulting from the dam construction.

5.1.1.4. Satellite observation-based water volume variation estimation

Water volume can be estimated from satellite-based observations by developing a relationship between satellite-based water height and water extent estimates. Through previous steps, the study had already developed water levels above the lowest level (WLALL) time series and sentinel 1-based water extent maps over time. A relationship can be established between these by aligning these water extent and water height estimates based on the nearest timestamps. The relationship between WLALL and subsequent water extent will be determined with regression analysis considering second-order polynomial function.

$$WaterExtent(A) = \int WaterElevation(L)$$

$$\Rightarrow WaterExtent(A) = aL^2 + bL + c$$

Here, L is the WLALL, and Water Extent is the corresponding water extent from Sentinel 1-based satellite observations. a, b, and c are the coefficients of the equation. These coefficient values were determined from the regression analysis.
After that, by analytically integrating this Water Extent - WLALL equation against dL, the volume variation of the reservoir could be derived. Because water volume is the integration of the functional relationship between water level and extent.

$$V(L)= \int_0^H (aL^2 + bL + c)dL$$
$$V(L)=\int aL^2dL+\int bLdL+\int cdL$$
$$Volume\ Variation = aL^3/3+bL^2/2+cL+d$$

Here, the integral starts from L=0 and sums until L=H (maximum height variation). V is the WVALL, volume variation above the reference level. As at the reference water level, L=0, the corresponding volume will also be 0. Taking this as a condition, the coefficient d's value can be calculated as 0. Thus, the final equation of WVALL – WLALL would be this:

$$Volume\ Variation = aL^3/3+bL^2/2+cL$$

This equation calculated volume variation for all the available water height estimates and Satellite based water volume above the lowest level (WVALL) timeseries was developed. This WVALL was later compared to volume variation estimates from other sources.

5.1.1.5. Digital Elevation Model (DEM) based variation

The Digital Elevation Model (DEM) represents elevation estimates of the earth's surface and establishes a 3D representation of the earth's terrain. For this study, Copernicus DEM was used to calculate water volume. At first, several pre-processing of the DEM data were done, including clipping with the GERD reservoir region and modifying the dam and its saddle dam location with respective elevations. After that, elevation bands were developed for terrains with the same elevation values. The associated area with that band was calculated by integrating DEM grid cells enclosed by that elevation band. With this, the water extent and water elevation curve from DEM was determined. Then, the corresponding volume was estimated by combining the area under the extent–elevation curve. As a result, the cumulative volume for each elevation band was developed.
Using this extent – elevation – volume relationship, the corresponding volume for all the water levels from the mean water level timeseries, was computed. The cumulative volume determined by the lowest water level was determined as the *constant water volume*. This constant water volume was subtracted from all other volume estimates to determine volume variation over the lowest water level.

$$WVALL = Water\ volume\ at\ (i\text{-}th\ elevation) – Water\ volume\ at\ lowest\ water\ level$$

This DEM-based WVALL timeseries was developed and evaluated with satellite-based WVALL. Volume variation time series estimated from both approaches were compared using different goodness of fit measurements like R^2, percent error, and root mean square error (RMSE).
Percent error is a measure used to quantify the accuracy of a measurement or estimate compared to a true or accepted value. Percentage error ranges from 0% to potentially very large values. A low percentage error, close to 0%, means the measured value is very close to the true value and indicates high accuracy. On the other hand, a high percentage error suggests a big gap between the measured value and the true value, which indicates the potential error in the measurement process.

5.1.2. Volume estimation considering the water slopes

Large lakes and reservoirs generally exhibit a slope due to topographic variation across their whole area. However, there is a limited availability of data that describes this slope. Consequently, many studies that measure water volume do not account for this water slope; instead, they use a single water level measurement to perform their analyses. This study utilizes a method using the overall gradient along the longitudinal profile of the mainstream extracted from the DEM as a correction factor to adjust the elevation model (personal communication B.H.P Maathuis). For further details, readers are referred to Removing elevation trend over sloped surfaces.

The methodology for considering this slope is based on the assumption that a reservoir or any large water body maintains a stable longitudinal profile over a certain distance. This assumption is used to determine the gradient correction factor, which is then applied to the entire upstream region. In order to determine the distance for this correction, two points in the downstream and upstream directions are taken into consideration, and their distance is calculated based on the direction of the stream flow instead of relying on Cartesian distance. Two points were selected to calculate this gradient correction factor: one downstream (A) and one upstream (B). The gradient between these points (A-B) is calculated as the *Elevation Distance (ED)* divided by the *Horizontal Distance (HD)*. Here, HD represents the distance along the stream network, and ED is the elevation difference between the outlet locations.

This part of the analysis was done using the ILWIS 3.8 application. As this process required some hydrological processing, preprocessed MERIT hydrological DEM was used in this process for the terrain elevation profile. This product was referenced to the EGM96 vertical datum. It was first converted into an EGM2008 vertical datum to make all the data homogenous. Subsequently, various tools from the ILWIS

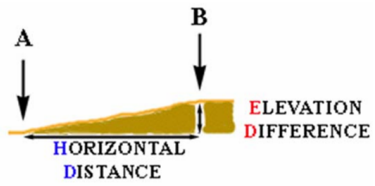

	At the Dam Pixel	At Upstream Pixel
Elevation from MERIT DEM	501	600
Distance from Dam	0	163800

$$\text{Correction Coefficient} = \frac{\text{Elevation Difference}}{\text{Distance along the River}}$$

Correction Coefficient = 0.000604

Figure 5-2. (right) Representation of table and equation required for calculating correction coefficient. (left) Conceptual representation of upstream and downstream points. Figure collected from a training material developed by B.H.P Maathuis

DEM - Hydro Processing utilities are utilized for drainage network extraction. Then, "Flow length to Outlets" was calculated for the region of interest, which resulted in the distance along the stream network from the downstream designated pixel. After that, along stream network distance for selected upstream pixels was noted for calculating the gradient correction factor. Then, with this correction factor, a modified DEM was developed with a few map calculations.

$$DEM\_slope\_correction = gradient\ correction\ factor * Along\ Stream\ Distance\ Map$$

$$Final\_Modified\_DEM = Original\ DEM - DEM\_slope\_correction$$

Then, following the similar DEM-based WVALL estimation process, volume variation timeseries were calculated from this modified DEM. Volume variation and area estimations from this modified DEM were then compared with satellite-based area estimations and WVALL timeseries with different goodness of fit metrics like R-square value and RMSE value to understand the effectiveness of these modification methods.

R-squared (R^2) is a metric that shows how much of the variance in the dependent variable can be accounted for by the model's independent variables. Its values range from 0 to 1. A high R-squared value, close to 1, indicates that a large proportion of the variance in the dependent variable is explained by the model, suggesting a good fit. Conversely, a low R-squared value, closer to 0, implies that the model does not explain much of the variance, indicating a poor fit.

RMSE measures the differences between values predicted by the model and the actual values observed. It is calculated as the square root of the average of the squared differences between predicted and observed values. RMSE values range from 0 to ∞. A lower RMSE value indicates a better fit, meaning the model's predictions are close to the actual data. Higher RMSE values suggest larger discrepancies between the predicted and observed values, indicating poorer model performance.

$$\text{RMSE} = \sqrt{\frac{1}{n}\sum_{i=1}^{n}(R_{rf} - R_{rt})^2}$$

$$R^2 = 1 - \frac{\sum_{i=1}^{n}(R_{rf} - R_{rt})^2}{\sum_{i=1}^{n}(R_{rf} - R_{rt})^2}$$

Volume estimation considering the water slope was also carried out with the SWOT water mask raster product, which is discussed in the following chapter.

5.2. Result

5.2.1. Volume estimation considering a single water level

5.2.1.1. Satellite-based volume estimation

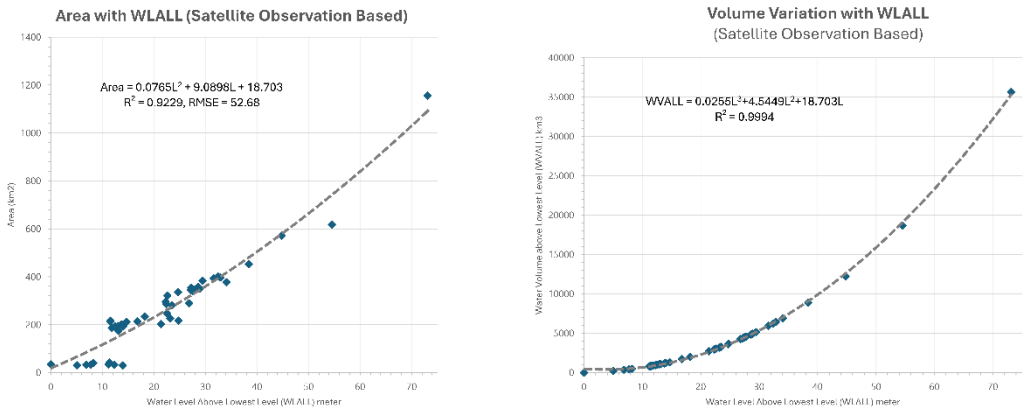

Figure 5-3. (a) Area with WLALL (Satellite observation Based), (b) Volume Variation with WLALL (Satellite Observation Based)

To estimate the hypsometric curve (a), the water level and surface area timeseries from satellite observations were utilized to generate a polynomial function. The water level above the lowest level was calculated for the entire time series. Subsequently, the water extent data from sentinel 1 were joined with the time series of water levels above the lowest level based on the closest neighbor approach. After that, a regression analysis was performed on these matched observations of water level above the lowest level and water extent. During this analysis, a polynomial function ($Area = 0.0765L^2 + 9.0898L + 18.703$) was fitted to the data, which resulted in the hypsometric curve. This curve demonstrated a strong correlation, with an R^2 value of 0.922 and an RMSE of 52.68 km², indicating high accuracy in representing the relationship between water level above the lowest level and corresponding water extent estimates.

After deriving the polynomial function, it was integrated with respect to the variation of water levels above the lowest level. This process resulted in a function representing the volume variation (b) of the reservoir. The obtained function for volume variation is given by $Volume\ Variation=0.0255L^3+4.5449L^2+18.703L$. This function showed a high correlation coefficient of 0.9994, indicating a nearly perfect fit.

$$Area = 0.0765L^2 + 9.0898L + 18.703$$

$$Volume\ Variation = 0.0255L^3 + 4.5449L^2 + 18.703L$$

5.2.1.2. DEM-based volume estimation

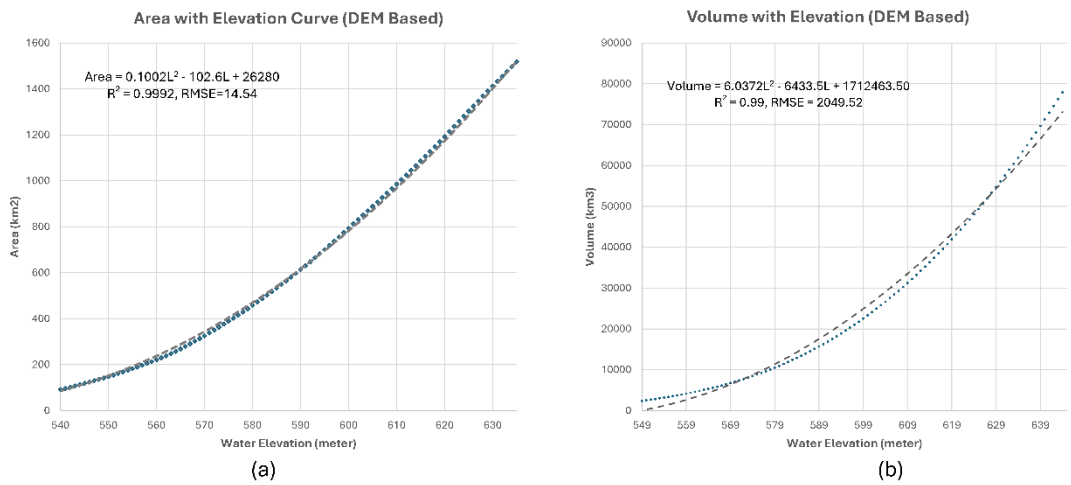

Figure 5-4. (a) Area with Elevation curve (DEM Based), (b) Volume with Elevation (DEM Based)

Here in the graph (a), a hypsometric curve has been generated from DEM-based water elevation and area time series. The DEM was first modified to include dam locations and elevations. Simulated water levels were used to compute the area. The volume above the reference water level was retrieved by integrating this derived area for each elevation band. The generated polynomial curve is $Area = 0.1002L^2 - 102.6L + 26280$. The resulting curve showed a higher correlation value of 0.922 and RMSE with 14.54 km². Then, this polynomial function is again integrated against the water elevation, and the volume with elevation function was obtained: $Volume = 6.0372L^2 - 6433.5L + 1712463.50$. The correlation is 0.99, and RMSE is 2049.52 km².

For a water level of 549.50 meters, the volume was estimated using the V-E relationship-based equation. This resulting volume was regarded as the volume at the lowest water level. This volume estimate was then subtracted from all other volume estimates to estimate volume variation above the lowest water level. Volume above the lowest water level over time was calculated with both satellite observations based volume estimates and DEM based volume estimates to compare with one another. Table 5-1 shows the volume variation timeseries based on two sources and their comparison.

Table 5-1. Water Level variation above Lowest Level over time from Satellite and DEM based observation.

Date	Water_Level (m)	Water Level Above Lowest Level (m) (WLALL)	Area (km2) (Satellite Based)	Area (km2) (DEM Based)	Area Percent Error (%)	WVALL (Satellite Based)	Volume (DEM Based)	WVALL (DEM Based)	WVALL Percent Error (%)
				$(0.1002L^2 - 102.6L + 26280)$		$(0.0255L^3+4.5449L^2+18.703L)$	$(6.0372L^2 - 6433.5L + 1712463.50)$	(i-th volume – volume at lowest water level)	
1/11/2020	557.729	8.219078	40.8635	216.8672133	81.15736381	474.9023978	3754.922821	1443.875632	67.10918952
1/23/2020	549.509922	0	34.8095	148.5007258	76.55937382	0	2311.047189	0	0
2/28/2020	561.798	12.288078	32.0608	255.7221128	87.46264074	963.4038168	4688.16117	2377.113981	59.47170289
3/11/2020	554.5575	5.047578	30.9722	188.8829303	83.60243568	213.4793735	3131.960846	820.9136573	73.99490536
4/4/2020	560.6865	11.176578	33.871	244.7790868	86.16262507	812.3671656	4417.569388	2106.522199	61.43562284
4/4/2020	557.26	7.750078	33.871	212.6019387	84.06834848	429.8034699	3657.239673	1346.192484	68.07265862
5/22/2020	563.477	13.967078	30.2409	272.7216872	88.9114429	1217.321552	5120.194135	2809.146946	56.66579303
6/3/2020	556.382	6.872078	32.6131	204.7355293	84.07062022	351.4391439	3479.63463	1168.587441	69.92615771
6/27/2020	560.8493333	11.33941133	41.9852	246.3667514	82.95825238	833.6546743	4456.457452	2145.410263	61.14241231
7/21/2020	570.8755	21.365578	203.1724	354.3580388	42.66465615	2722.99714	7382.030475	5070.983286	46.30238384
8/2/2020	572.6566667	23.14674467	227.409	375.6496882	39.46248136	3184.177774	8020.048005	5709.000816	44.22530533
8/26/2020	572.0735	22.563578	248.1717	368.6086634	32.67339468	3028.813758	7806.948539	5495.90135	44.88959017
9/19/2020	567.73075	18.220828	235.1646	318.3182502	26.12280324	2003.941327	6346.487514	4035.440325	50.34144564
10/13/2020	566.30475	16.794828	215.0479	302.6287993	28.94004122	1716.876536	5913.697591	3602.650402	52.34407048
10/25/2020	564.181	14.671078	210.8387	280.017621	24.70520274	1333.164025	5309.890167	2998.842978	55.54405364
11/18/2020	563.2646667	13.75474467	201.2874	270.5406529	25.59809484	1183.476945	5063.98121	2752.934021	57.01034111
12/12/2020	562.6478	13.137878	195.1463	264.2555956	26.15244361	1088.009945	4903.276901	2592.229712	58.02802736
1/5/2021	562.3845	12.874578	191.5317	261.5961319	26.78343573	1048.549611	4835.853725	2524.806536	58.47010076
1/17/2021	562.0568333	12.54691133	192.1037	258.3059303	25.62938846	1000.513224	4752.918303	2441.871114	59.02677998
2/10/2021	561.3436815	11.8337595	187.5061	251.2193113	25.36158983	900.0428388	4576.097312	2265.050123	60.26388866
3/6/2021	561.836	12.326078	191.7651	256.1006092	25.12118553	968.8058549	4697.62671	2386.579521	59.40609369
3/30/2021	561.1065841	11.59666209	216.5654	248.8858346	12.98604828	867.870709	4518.418736	2207.371547	60.68307077
4/11/2021	561.0134286	11.50350657	213.4024	247.9720941	13.94096147	855.3975154	4495.907001	2184.859812	60.84886038
5/5/2021	562.6263333	13.11641133	174.6687	264.0382513	33.8471986	1084.763998	4897.753822	2586.706633	58.06389547

5/29/2021	561.926	12.416078	190.0558	256.998202	26.04780946	981.6633907	4720.102183	2409.054994	59.25110082
6/22/2021	563.5682	14.058278	193.4326	273.6612436	29.31677228	1232.013567	5144.48019	2833.433001	56.51869774
7/4/2021	574.2755	24.765578	216.4413	395.5522195	45.28123233	3638.065605	8633.499681	6322.452492	42.45800012
7/28/2021	583.5891667	34.07924467	377.167	520.2580273	27.50385767	6925.084141	12830.13613	10519.08894	34.16650265
8/21/2021	582.4265	32.916578	397.5413	503.7410782	21.08221521	6449.504233	12240.85781	9929.810623	35.04907115
9/14/2021	581.9192857	32.40936371	401.7916	496.6203941	19.09482478	6248.028553	11989.85918	9678.811987	35.4463279
9/26/2021	581.1302	31.620278	393.3515	485.6450412	19.00432073	5941.765553	11606.62115	9295.573961	36.07962694
10/20/2021	578.971	29.461078	383.0525	456.2505581	16.04339038	5147.837534	10602.27296	8291.225774	37.91222583
11/13/2021	578.1101667	28.60024467	356.9926	444.7919526	19.73942021	4849.073924	10219.60471	7908.55752	38.68573489
12/7/2021	578.427	28.917078	350.2846	448.9920744	21.98423536	4957.869502	10359.28735	8048.240157	38.39809194
12/19/2021	577.313	27.803078	347.3781	434.3132218	20.01668782	4581.307601	9874.081539	7563.03435	39.42500604
1/12/2022	577.0498333	27.53991133	341.314	430.881858	20.78710354	4494.776103	9761.862796	7450.815607	39.67403919
2/5/2022	576.7528333	27.24291133	353.9019	427.0260163	17.12404244	4398.226406	9636.310704	7325.263515	39.95811349
3/1/2022	576.6674	27.157478	344.553	425.9201398	19.10384887	4370.670231	9600.409152	7289.361963	40.04042805
3/13/2022	574.2155	24.705578	335.0467	394.8051879	15.13619621	3620.644551	8610.18111	6299.133921	42.52154986
4/6/2022	571.772	22.262078	296.1924	364.9951393	18.85031659	2950.164372	7698.390115	5387.342926	45.23897193
4/30/2022	571.919	22.409078	286.8793	366.7546819	21.7789672	2988.368679	7751.182175	5440.134986	45.06811529
5/12/2022	572.0955	22.585578	321.6851	368.8730498	12.79246338	3034.597265	7814.912835	5503.865646	44.86425614
6/17/2022	573.001	23.491078	280.8902	379.8390857	26.05021163	3277.928214	8147.821252	5836.774063	43.84007024
6/29/2022	576.3266667	26.81674467	289.139	421.5241248	31.40629848	4261.728771	9458.170751	7147.123562	40.37141329
7/23/2022	587.94	38.430078	452.5227	584.4694376	22.57547257	8878.273004	15212.45772	12901.41053	31.18370288
1/31/2023	604.06183	54.551908	618.8528	855.4661607	27.65899711	18685.21165	26731.53337	24420.48619	23.48550514
3/8/2023	594.3008	44.790878	571.2719	685.1702766	16.62336801	12247.24778	19227.32591	16916.27872	27.60081585
9/28/2023	622.638065	73.128143	1156.5509	1232.289635	6.146179693	35644.85749	46154.75413	43843.70694	18.70017392

5.2.1.3. Comparison of volume estimations between satellite based products and DEM based product

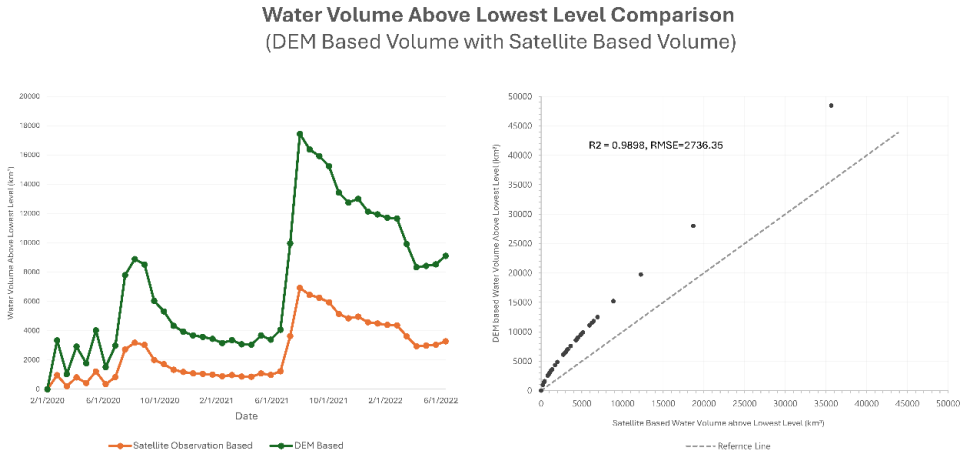

Figure 5-5. Water Level above lowest water level

Figure 5-5 compares water volume variations above the lowest level using DEM- and satellite-based measurements. Both curves exhibit similar increase and decrease trends and capture variations across different dam operation phases, indicating a high correlation between the two methods, as shown in Figure 6-6. Despite this high correlation, their value ranges have a significant difference. The satellite-based observations range from 0 to 35644.85, while the DEM-based volumes range from 0 to 43843.70. This higher level of difference results in a high RMSE value of 2736.35. The potential causes of this high RMSE are discussed in the discussion section of this study. Furthermore, the results indicate that DEM-based volume tends to overestimate compared to satellite-based observations, especially at lower water levels. Additionally, the percentage error decreases with increasing elevation.

5.2.2. Volume estimation considering the water slopes

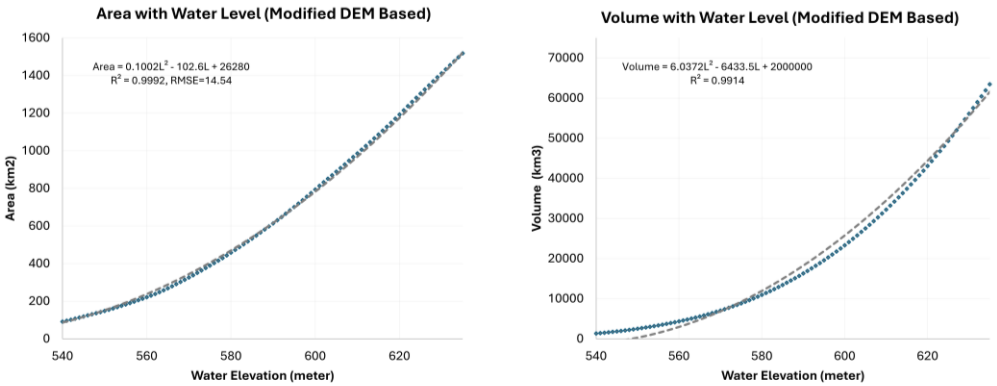

Figure 5-6. Area with water level (Modified DEM Based) (left), Volume with water level (Modified DEM Based) (right)

Here in graph 5-6 hypsometric curve has been generated from Modified DEM based water elevation and area time series. After performing the preprocessing task Modified DEM was obtained. Then simulated

water level was calculated for this modified DEM to calculate the area. Subsequently, the process involved integrating the area calculated for each elevation band, which allowed us to determine the volume above the reference water level. The polynomial curve generated here is represented by the equation Area = $0.1002L^2$ - 102.6L + 26280. This curve exhibits a strong correlation of 0.9992 and an RMSE of 14.54 km^2. Subsequently, this polynomial function was integrated with respect to water elevation to derive a volume-elevation function, expressed as Volume = $6.0372L^2$ - 6433.5L + 2000000. This volume-elevation function also shows an even higher correlation of 0.9914.

After obtaining this volume equation, the 21-day mean water level was applied to derive the mean water volume. The corresponding water level value for the lowest water volume value was taken as the reference lowest level and subtracted from all volume estimates to determine volume variation over time.

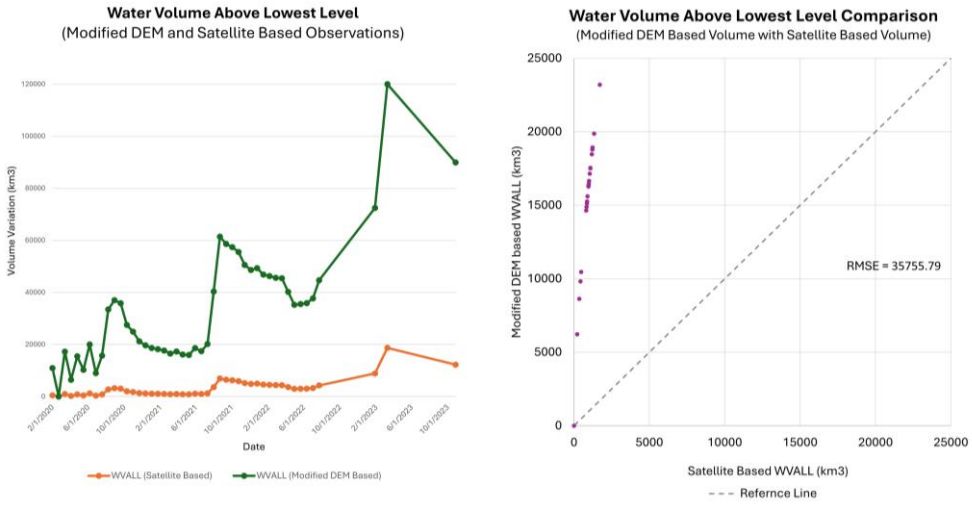

Figure 5-7. Water Volume above lowest level (left) and Water Volume above lowest level comparison (right)

Figure 5-7 compares water volume variations above the lowest level using modified DEM- and satellite-based measurements. The two curves show distinctly different patterns and indicate no significant correlation between the methods. Additionally, the RMSE value is notably high at 35755.79, highlighting substantial differences between the DEM-based and satellite-based volume estimates.

6. SWOT SATELLITE-BASED WATER EXTENT AND VOLUME ESTIMATES

This chapter describes the methodological framework and steps followed for water extent and volume estimation with SWOT satellite based products.

6.1. Methodology

6.1.1. SWOT product based water extent maps development

This study utilized three different SWOT satellite products for GER dam reservoir extent detection. These are: (i) SWOT Lake Single Pass product is a vector product, (ii) SWOT Water Mask Raster is a raster product, and (iii) SWOT pixel cloud product is a vector product of point clouds. A sequence of quality filtering procedures was performed before determining the reservoir area using such data to ensure product quality.

Quality Flag Based Filtering

All three data products were filtered using the quality flags described in respective product handbooks (JPL D-56411, 2023; JPL D-56416, 2023; JPL D-109532, 2024). A list of quality filters and criteria used for filtering is described in the following table 6-1.

Table 6-1. This table showcases listed quality flag values and meanings collected from the designated product description document (PDD). A detailed description and list of quality flags for SWOT L2 Water Mask Pixel Cloud Data is given in the annex section.

SWOT Product	Quality Flag Identifier	Values and Meanings	Filtering Criteria
SWOT Level 2 Lake Single Pass Version 2.0	'quality_f'	0 = good	Considered all the available observations
		1 = bad	
SWOT Level 2 Water Mask Raster Version 2.0	Ex: 'wse_qual'	0 = good	• For reservoir extent detection, considered all the available observations • For volume estimation, only considered "wse_qual" values with 0 and 1
		1 = suspect - may have large errors	
		2 = degraded - likely to have large errors	
		3 = bad - may be nonsensical and should be ignored	
SWOT Level 2 Water Mask Pixel Cloud Data Version 2.0	Classification_qual	x < 32768: Good	• For reservoir extent detection, consider all the available observations
		32768 < x < 134217728 : Suspected	
		x > 134217728: bad	

For all three data products, data with quality flag 0 and good quality was unavailable. Thus, data with all the quality flags were used for water extent detection for the SWOT Lake Single Pass product and SWOT Water Mask Raster. SWOT Water Mask Raster was also used for volume estimation in the next step. To have a precise volume close to reality, "wse_qual" with values 2 and 3 were disregarded. SWOT Pixel Cloud Data product was used only for extent detection. All the available observations were used for this product. After that, the filtered data products were masked out only for the area of interest. SWOT Lake Single Pass product was supposed to have one single polygon for the whole reservoir area but had detected few segmented polygons at reservoir extent. Thus, all the polygons were accumulated using a union operation to determine the whole reservoir's extent.
SWOT pixel cloud data product has a "class" variable denoting the detected landcover type. This product mostly classifies and detects water regions and land features in the water–land transitioning zone. The classes are 1: Land, 2: Land_near_water, 3: water near land, 4: open water, 5: dark water, 6: low_coh_water_near_land, and 7: open_low_coh_water. As only water extent was required, classes 1: Land and 2: Land_near_water were reclassified into non-water. The rest of the classes were designated as water classes. SWOT Water Mask Raster product provides detected water pixels as a raster image where each pixel has a water level value. For reservoir water area mapping, all the pixels with water level were reclassified as water pixels, and the rest were classified as non-water pixels. After the quality filtering and preprocessing steps, SWOT product based water maps were ready for the reservoir area.

6.1.1.1. Water Extent Comparison Method

This study evaluated SWOT product-based water maps against Planet water masks detected with Support Vector Machine (SVM) classification, as produced in the earlier objective. The evaluation process utilized several accuracy metrics to assess the performance of the SWOT-based water maps. The detailed description and equations for the confusion matrix, recall, and precision are provided in the previous chapter. Since the SWOT Lake Single Product is available in vector format, the Intersection over Union (IOU) metric was additionally employed to quantify the overlap between the SWOT LakeSP-based water maps and the SVM-based water masks. IOU is calculated as the ratio of the intersection of the predicted and actual water areas to their union. This metric measures the spatial accuracy and agreement between the two sets of water maps. By considering both the areas correctly identified as water and the areas of discrepancy, IOU offers a comprehensive assessment of the effectiveness of the SWOT-derived water maps in capturing the true extent of water bodies. An IOU value close to 1 denotes better accuracy.

6.1.2. SWOT product based water volume estimation

6.1.2.1. Volume estimation considering single water level

SWOT Lake SP product was used for single water level based volume variation estimation. For all the available timestamps of this product, had detected more than one polygon as the GER dam reservoir. Each polygon had a distinct water surface elevation, uncertainty, and total area estimation. One polygon shares most of the GER dam reservoir area among those polygons. Others share the very small area of the reservoir. Therefore, to develop a single water level timeseries from SWOT Lake SP Product, the study opted for an area-based weightage average of water surface elevation calculation. A similar method was applied in a recent study by Hamoudzadeh et al., (2024), where they evaluated the performance of SWOT LakeSP products for different water bodies. After developing one single water surface elevation estimation for each timestep of the SWOT LakeSP product, the water level above the lowest level (WLALL) was calculated. This lowest water level estimate came from *Chapter 5, in which the lowest water level was detected from the mean water level time* series. 549.50 was the lowest water level from there. This was subtracted from all the

SWOT LakeSP-based single water levels to determine the WLALL. After having WLALL estimation from SWOT Lake SP, these estimates were supplied as input in the satellite observation based WVALL – WLALL relationship based function, which was $Volume\ Variation = 0.0255L^3 + 4.5449L^2 + 18.703L$ (section 5.2.1.1). WVALL has derived from SWOT LakeSP product based water height estimates as an output of the function. These volume variation estimates were later plotted with satellite observation based volume variation timeseries to evaluate the performance of SWOT LakeSP products performance.

Table 6-2. The attribute table of SWOT Lake Single Product for 2024-02-11, where three distinct polygons represent the GER dam reservoir.

Time	We	Wse_u	Wse_r_u	Wse_std	Area_total	Quality_Flag
2024-02-11T19:49:05	596.839	0.027	0.001	5.036	475.355617	1
2024-02-11T19:49:06	597.725	0.082	0.080	0.094	0.014230	1
2024-02-11T19:49:08	604.573	0.048	0.030	0.090	0.066042	1

6.1.2.2. Volume estimation considering the water slope

Unlike other radar altimetry products, SWOT water mask raster delivers water mask rasters with only water pixels, each with an elevation value. This product is ideal for understanding and estimating the slope considered volume variation.

Issues

The first quality flag-based filtering was carried out as part of the data preparation. As height estimates need to be accurate, quality flags with only 0 and 1 were selected. Because of this filtering, a part of the reservoir was lost for every timestep. Even though quality-based filtering was utilized, the data showed different discrepancies.

- **Offset in North Western Region**

While availing the data, the SWOT water mask raster product was already transformed into a UTM36N projection. However, while plotting it alongside other data products, it was found that the SWOT data showed a slight spatial offset in the northwestern region. Therefore, the SWOT water mask raster was georeferenced using ArcGIS Pro software with respect to designated high-resolution Plant Imageries.

Figure 6-1. SWOT Water Mask Raster Product visual comparison with Planet based reservoir boundary. (left) SWOT Water Mask Raster only, (middle) SWOT Water Mask Raster with planet reservoir boundary shoing offset (right) Final Georeferenced SWOT Water Mask Raster.

- **Water Elevation Outliers**

With the georeferenced SWOT water mask raster product, water level variation above the Copernicus DEM was computed. As the DEM was developed many years before the dam became operational, each water elevation recorded in the SWOT water mask raster had to be higher than DEM pixel elevations. Because the SWOT water mask raster was acquired recently, after the 4th dam operation period, by this time, the reservoir was almost flooded. Therefore, the water height had to be higher than the DEM height.
However, while calculating the difference between SWOT water mask raster and DEM, it was found that many water pixels show negative values. This means the SWOT water mask raster had lower values than the DEM. Practically, it was not possible. Thus, outlier detection and removal were necessary.
For the outlier removal operation, the first difference between SWOT water mask raster and DEM was calculated using a map calculator for every water pixel. The bottom 15th percentile value was identified for every raster. After that, pixels with less than the bottom 15th percentile value were disregarded. This reduced the negative value range for each raster. The pixels proximity to land water transitional zones was mostly filtered out through this step.

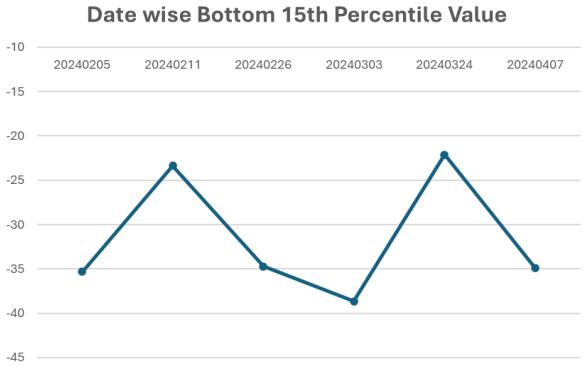

Date	Added Int	Bottom 15th Percentile
20240205	35.33447266	-35.3347168
20240211	23.36737060546875	-23.36844482
20240226	34.71105957	-34.71118774
20240303	38.65325927734375	-38.65345764
20240324	22.10644531	-22.10655518
20240407	34.890625	-34.8918335

Figure 6-2. (left) SWOT Raster Master Date wise bottom 15th percentile values (right) Final list of assumed height offset and 15th percentile values.

- **Height Offset Selection**

Even after removing detected outliers, the SWOT water mask and Copernicus DEM difference based raster showed negative values. Therefore, the lowest value of each calculated raster was identified, and then, using the map calculator, this value was added as an offset with each pixel. After this step, the final raster was ready for volume calculation. Table XX shows each timestep's designated height offset values and bottom 15th percentile values.

Volume Estimation with the Processed Raster

In the processed raster, only positive water height estimations were for each pixel. The pixel size of the SWOT water mask raster was 100 meters. Therefore, the map calculator multiplied the pixel area by each pixel value. This resulted in a raster with volume estimates at each water pixel. Later, each pixel value was accumulated to calculate the total cumulative volume of the raster. This process was repeated for each SWOT waster mask raster timesteps, which resulted in the volume variation timeseries above the DEM from the SWOT water mask raster product. This volume variation timeseries was plotted together with volume variation timeseries calculated from satellite observations to evaluate the SWOT product's performance in volume estimation.

6.2. Results

6.2.1. SWOT products based water extent maps

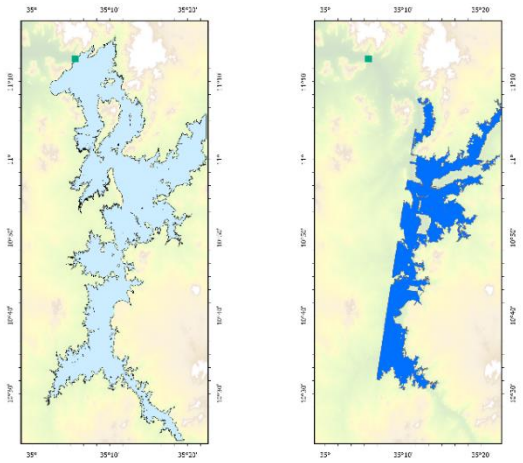

Intersection Area	405,942,972 m²
Union Area	1,203,051,025 m²
Intersection over Union (IOU)	**0.3373**

Figure 6-3. The validation of the product Planet and SWOT data. (left) Planet polygonised reservoir extent, (right) SWOT_lake_SP polygon

The Planet data was first converted into a polygon to create this validation product. The SWOT product was then compared with this polygon using the Intersection over Union (IOU) metric. The comparison, as shown in the figure, indicates that the SWOT product does not perform well and fails to capture the entire reservoir area accurately.

Table 6-3. Table of Mean Accuracy Assessment Metrics

Product	Overall Accuracy	Precision	Recall	F1 Score	IOU
SWOT L2 Lake Sigle Pass	-	-	-	-	0.3373
SWOT L2 Raster Mask	0.889008	0.715048	0.947426	0.814975	-
SWOT L2 Pix Cloud	0.78381	0.844581	0.865415	0.854861	-

Based on the accuracy assessment metrics, it is evident that the IOU metric for the SWOT L2 Lake Single Pass is 0.3373, indicating poor performance due to its low value. In contrast, the other two products, L2 Raster Mask and L2 Pix Cloud, show much better overall accuracy with values of 0.889 and 0.783, respectively. These high values indicate a high number of correctly detected water pixels and a low number of misclassifications. When examining precision, which measures the ratio of true water pixel classifications, SWOT L2 Pix Cloud outperforms SWOT L2 Raster Mask. The lower precision of the L2 Raster Mask can be attributed to a slight offset in the northwestern region, which leads to misclassifications in that area.

Table 6-3 displays the accuracy assessment of three SWOT product: the validation product from Planet data, the SWOT pixel cloud-based classification of water and non-water pixels, and the performance of the classification results, indicating commission, omission, true negative, and true positive values. This classification was run 50 times, resulting in an overall accuracy between 0.78 and 0.79, which is quite a good range and demonstrates that the overall classification performs well. The other metrics are - precision between 0.82 and 0.87, recall between 0.86 and 0.87, and an F1 score between 0.85 and 0.86. Precision, which is the ratio of true positives to the sum of true positives and false positives, indicates the model's accuracy in identifying water pixels while minimizing false positives. Recall, or sensitivity, which measures the ability to identify actual positives, indicates the model's effectiveness in detecting true water pixels. The F1 score, the harmonic mean of precision and recall, provides a balanced measure of the model's accuracy by combining precision and recall into a single metric.
Although the classification performs quite well statistically, it shows some wrong classifications when visually comparing both validation sets (Figures 6-4 and 6-5). They both show offset in the northwestern region; therefore, some commission errors are visible in this region. Besides, the areas near the land-water edge of the reservoir were not classified very well.

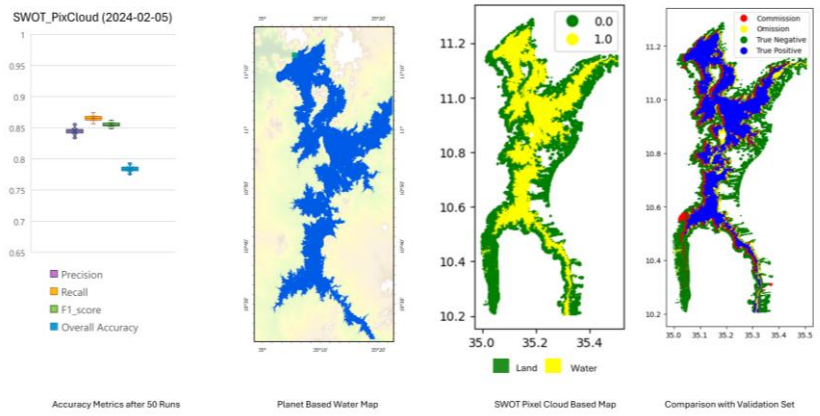

Figure 6-5. SWOT Pixel Cloud Product comparison with SVM based Planet water map

6.2.2. SWOT product based volume estimation considering single water level

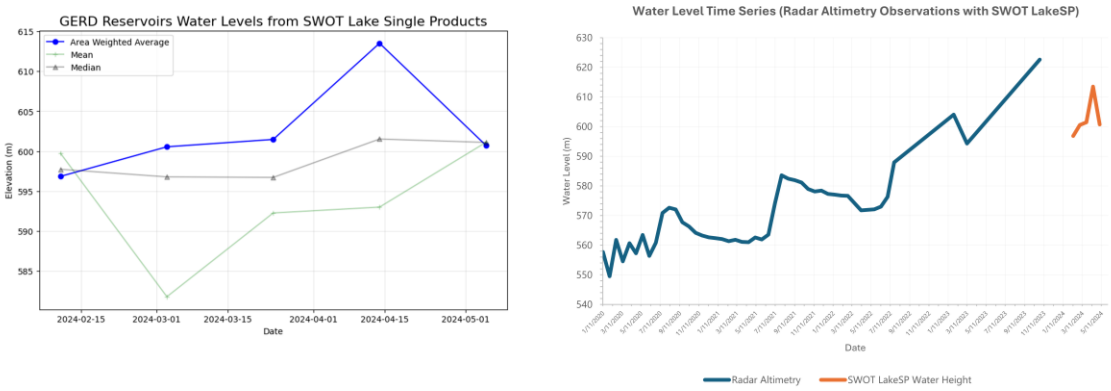

Figure 6-6. GERD Reservoirs water level from SWOT Lake Single Products (Left) and Water Level Time series Comparison between Lake SP and Radar Altimetry (right)

The graph (figure 6-6) shows the plot of the area-weighted average, while the second graph compares this data with the radar altimetry-based area time series. However, due to the lack of sufficient observations and the absence of simultaneous observations, making a direct comparison is quite hard. An upward trend is evident from the radar altimetry time series, with a noticeable drop from November to March. This trend rises again in March and April before dropping once more. This rise in March and April is also observed in the area-weighted average time series.

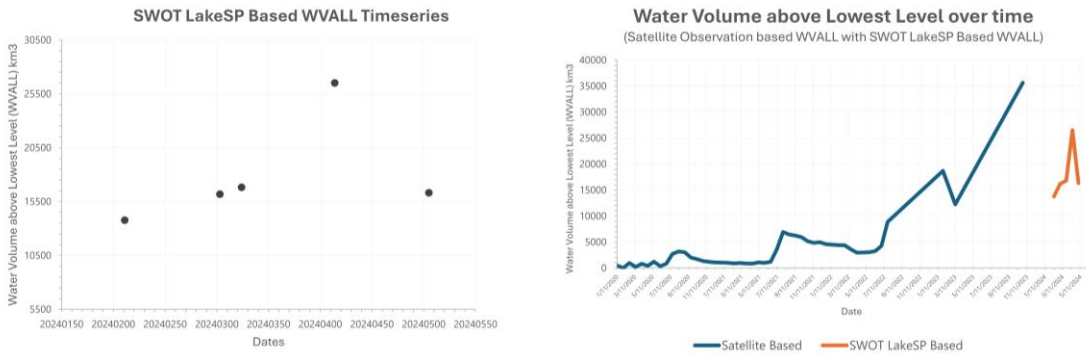

Figure 6-7. SWOT lakeSP based WVALL Timeseries (left) and Water Volume above lowest level over time (right)

The graph (figure 6-7) displays the water volume variation derived from the SWOT Lake Single product. This was obtained by applying the height estimates from the SWOT Lake Single product to the satellite based WVALL and WLALL relationship equation. The subsequent graph compares these results with a satellite-based time series. However, interpreting this comparison is quite challenging due to the lack of simultaneous observations. The satellite-based time series exhibits clear seasonality, with distinct patterns that repeat annually.

6.2.3. SWOT product-based volume estimation considering the water slopes

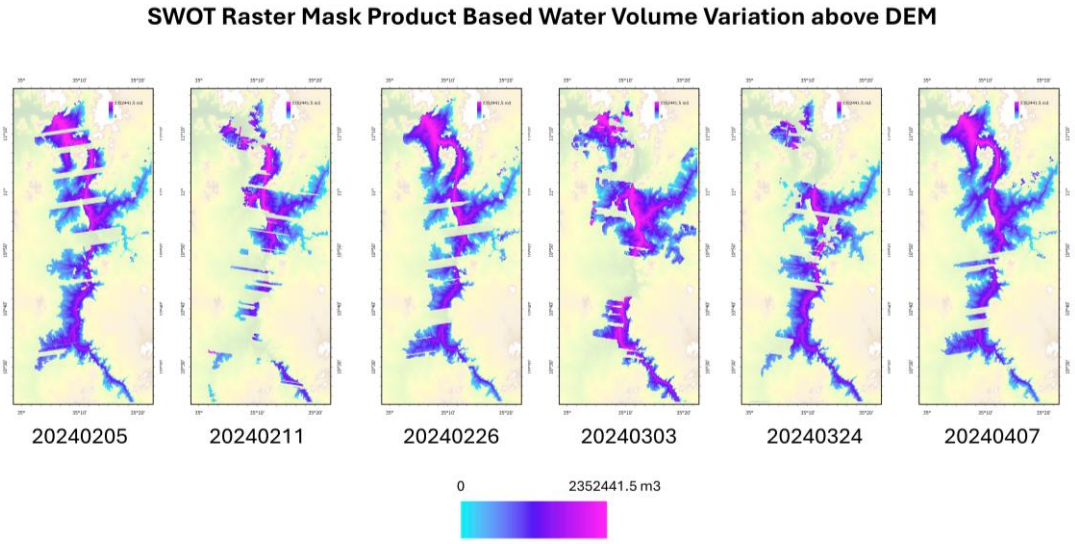

Figure 6-8. SWOT water mask raster product based water volume variation above DEM

The SWOT water mask raster product identified water elevation from each reservoir pixel. By utilizing this data, it was possible to determine which portion of the dam contributes the most to the total accumulated volume. After addressing the data discrepancies mentioned in the discussion section, the processed SWOT water mask raster product was used for volume calculations. The difference between the Copernicus DEM and the SWOT water mask raster estimated the water level above the DEM, resulting in a map of water level variation across the GERD reservoir. Each variation was multiplied by the pixel area to estimate volume changes at the pixel level, as shown in Figure 6-8.

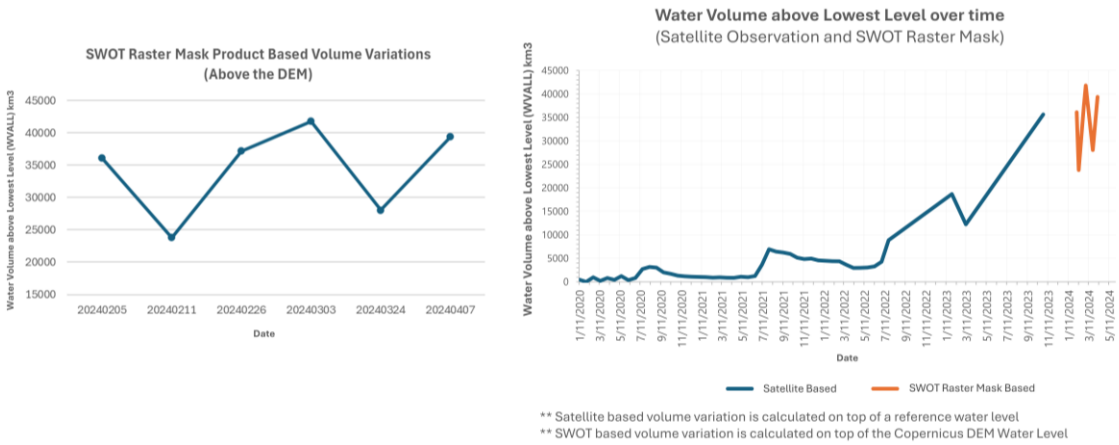

Figure 6-9. SWOT water mask raster product based volume variations (above DEM) time series and comparison with Satellite based timeseries

Despite losing some observations during quality filtering, the overall volume variation timeseries map indicates that the downstream section near the dam significantly contributes to the cumulative volume, while upstream regions and land-water transitional zones contribute less. Despite higher water levels, the northeastern part occupies less volume due to its terrain. The total reservoir volume variation was calculated by summing pixel estimates, resulting in the timeseries plot in Figure 6-9. This was compared with the satellite based WVALL. No clear trend is visible, but the SWOT water mask raster-based volume variation rises after January, which is unusual compared to the 2020-2024 WVALL timeseries. Higher estimates in the SWOT water mask raster-based variation are due to different reference levels: it uses the DEM, while WVALL uses the lowest water level. The DEM, produced before the dam's operation, had lower water levels than the February 2020 altimetry data, making higher SWOT volume variations acceptable.

7. DISCUSSION AND CONCLUSION

This chapter provides an interpretation and relevance of the results presented in chapters 4 – 6. The results are evaluated with previous research, and the possible causes of the unsatisfactory results are investigated. The limitations of this research are also discussed in detail.

7.1. Water Extent And Water Level Variation Over Time

7.1.1. How does Edge Otsu Algorithm based water detection method perform in this study?

This study determined water extent using Sentinel-1 data, demonstrating good performance in mapping the reservoir's water extent. However, while visually investigating the water maps throughout the timeseries, it was observed that the classification results were less accurate during the pre-dam operation period. The reservoir was fragmented into different sections. During this period, the raster histogram was highly imbalanced, with more non-water pixels than water pixels. The edge Otsu method classification technique classifies data based on thresholding the given raster's histogram. This method was affected by the availability of fewer water pixels in the raster dataset, which led to less accurate results and a fragmented reservoir area.

A significant finding of this study is that the edge Otsu method, which determines the threshold for classification based on the histogram of pixel intensities, was less effective in water detection when the raster dataset has fewer available water pixels than non-water regions. The imbalance in the raster dataset resulted in skewness in the pixel intensity histogram, on which edge the Otsu method detected threshold can not result in a fine separation between water and nonwater pixel intensity values. As a result, misclassification of pixels takes place. Therefore, fragmented reservoir regions were developed in the final map.

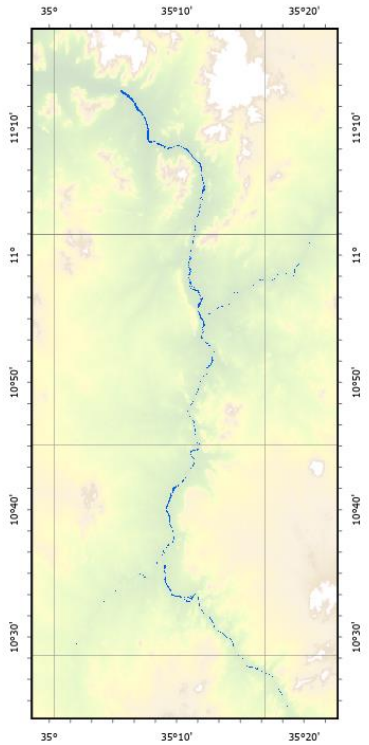

Figure 7-1. Fragmented Sentinel 1-based Map of pre dam operation period

7.1.2. How did water levels at virtual station observations change before and after the dam began operations?

Initially, before the dam operations, data from virtual stations indicated a significant difference in water levels. Specifically, the Hydroweb 7837 station, situated downstream, consistently reported lower water levels compared to upstream DAHITI stations. However, following the first operational phase of the dam, Hydroweb 7837 water levels rose close to upstream DAHITI and G-REALM virtual stations observations, while observations in upstream virtual stations did not rise much in this period. During the second filling phase, water levels rose significantly for all the available observations, correlating with the reservoir's water extent expansion. From this, it can be concluded that the height difference throughout different reservoir sections tends to diminish with the filling operation. Unfortunately, continuous data from these sources was unavailable during the third and fourth dam operational phases in 2022 and 2023. As a result, it was not possible to determine if this trend continued in the subsequent filling phases.

7.1.3. What factors validate the highest water level observed in late 2023, according to ICESat-2 data?

The segmented observations from ICEsat-2 indicated higher water levels in mid and late 2023. Moreover, the most recent radar altimetry-based height estimation, derived from ICESat-2, depicts the highest water level observed among all other datasets. This observation is consistent with independent satellite-based water extent data, which showed the largest area coverage during the same period. Moreover, abundant rainfall in this period likely contributed to the dam's filling, which resulted in the highest reservoir extent and water level observed. Therefore, despite the absence of similar water level observations during that period, these factors support the high water levels from ICEsat-2 seem feasible.

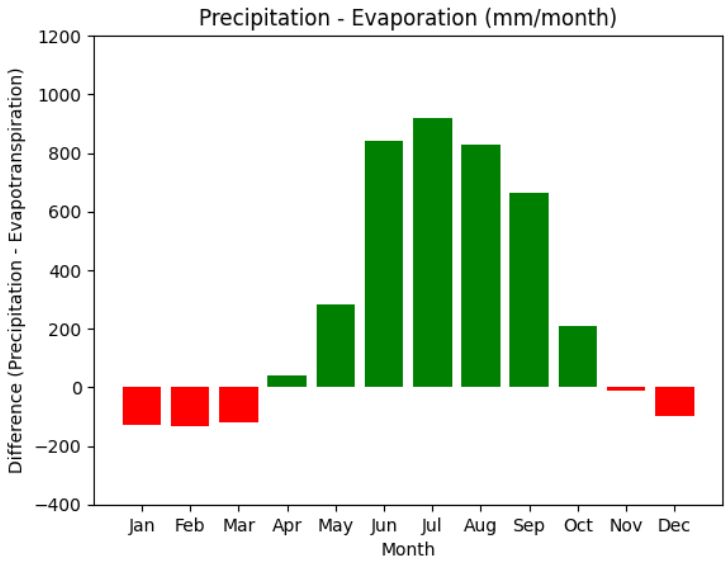

Figure 7-2. Monthly average precipitation – Evapotranspiration for the year 2023. Precipitation data was collected from CHIRPS (Climate Hazards InfraRed Precipitation with Station) and Evapotranspiration data was collected from WAPOR (Water Productivity Open Access Portal) for the reservoir region.

7.2. Water Volume Dynamics Over Time

7.2.1. Why is there a notable difference between DEM-based and satellite-based volume estimations?

This study estimated the volume variation from DEM and satellite-based observations. This volume was estimated using the Area–Elevation relationship developed from this source. DEM-based area–elevation relationship agreed well with existing studies on the GER dam reservoir (Eldardiry & Hossain, 2021). However, no existing studies are still available where this relationship was developed through satellite-based observations. The computed volume from these two sources, DEM based and satellite-observation-based, show good alignment between the estimations, but differences in values are evident, as indicated by an RMSE of 2736.35 km^3. This discrepancy might have arisen from an unnoticed scaling error during volume variation computation.

Another potential reason for the discrepancy is the noticeable slope of the reservoir, where water levels vary across different parts of the reservoir. A single water level used for volume estimation does not capture this gradient effectively. Unlike DEM-based contouring, which assumes uniform flooding across similar elevations, satellite-based observations depict the actual variation in water extent. While comparing visually, it was found that the DEM contouring based water extent was significantly greater than the actual extent. This overestimation in reservoir extent was carried onto cumulative volume computation, potentially contributing to the discrepancies in volume variation estimates between these two methods. A significant find from this study is that for water bodies in topographical settings with evident elevation variations, DEM contouring method-based area–volume estimates might result in erroneous output, which might not represent reality.

7.2.2. Why did the modified DEM-based volume estimation not work well?

Water elevation variances in different reservoir portions made it difficult to estimate the water volume precisely using a single water level. Therefore, this study attempted to correct the slope of the DEM to minimize the difference in water height.

The study experimented with a simplified method involving two points for the correction – one located upstream and one located downstream. However, this method proved inadequate for capturing the full complexity of the reservoir's topography. Due to the oversimplification of the reservoir topography, the final volume computation resulted in an overestimation of aerial extent in elevation bands and, consequently, higher cumulative volume estimates. The reservoir has some island mountains, which are located in proximity to the downstream selected point. Due to two point-based corrections, the elevation of this high land parts also got corrected and flooded in minimum water elevation. Those landforms flooded during the 3rd and 4th dam operation phases. DEM correction considering multiple points can be experimented for a more accurate representation of reality. Unfortunately, the limitation of using only two points introduced significant errors for this complex-shaped water body, highlighting the need for a different approach in future studies.

7.3. Comparison of SWOT based Products with Other Satellite Observations

7.3.1. How does SWOT product based water extent detection perform in this study?

This study examined three SWOT products for water extent detection. Among these three, the SWOT Lake single product performed worst with a 0.33 IOU value. It happened mostly because this product could not capture the entire view of the reservoir due to its narrow swath, which led it to delineate only a portion of the reservoir.

Although the SWOT pixel cloud product and SWOT water mask raster swath had the capacity to cover the entire reservoir, when compared with Planet-based water maps, they reported moderate overall accuracy

ranging from 0.78 to 0.89. Both products reported less accuracy than Sentinel 1-based water maps. However, while visually examining, it was found that SWOT based products exhibited higher false positives in the land-water transitional regions. This happened particularly due to their slight spatial distortion in the north-western area. Similar distortions effects of SWOT Lake Single Products were reported in a study (Hamoudzadeh et al., 2024c). The authors reported notable anomalies in detected water bodies in higher altitude regions. This also seems feasible for this study as the GER dam reservoir is situated in a region with a similar altitude.

7.3.2. Why does the SWOT water mask raster-based volume estimation tend to fluctuate more than the satellite observation based estimations?

SWOT water mask raster was used to derive volume considering the slope of the GER dam reservoir. However, while comparing these estimates with satellite based volume estimates, it was found that SWOT-based volume estimates showed more fluctuations. This happened because of the difference in the water extent in SWOT based calculations. The quality filter operation performed on the SWOT water mask raster product reduced the actual extent of the water bodies. Therefore, the final volume was only calculated for the available water elevation pixels, which resulted in lower volume variation than expected.
Additionally, in SWOT water mask raster-based estimations, the water volume was calculated above the DEM, where the water elevation was significantly lower than the reference water level used for volume variation estimation with satellite based observations. Therefore, the SWOT water mask raster based volume variation is supposed to be higher than satellite-based. Although several water-masked regions were excluded, the resulting volume variation remains within a similar range to the volume variation estimates derived from satellite-observed height and extent.

7.4. Uncertainty of Using Products From Multiple Satellites For Estimations

This study utilized data from various satellites and sources, which led to inherent uncertainties in the final results. These uncertainties arise from several key areas: water level estimates, water extent calculations, the polynomial approximation of the area-elevation relationship, and the approximation of a single water level for the GERD reservoir. Water level estimates can vary due to differences in measurement techniques of radar altimetry and its instrument precision, while water extent calculations can be affected by different speckle filtering, terrain correction, and shadow layover correction techniques. The polynomial equation used to approximate the area-elevation relationship depends on the quality and number of data points, and using a single water level for the entire reservoir introduces simplifications that might be distant from reality and lead to errors. Similar sources of uncertainty have been reported in previous studies (S. Zhang et al., 2014), where they calculated uncertainties from ICESat storage estimation errors, which resulted in less than 10% uncertainty. Additionally, preprocessing steps for SWOT data, including outlier removal techniques, height offset approximation, spatial offset approximations, etc., could contribute to the final estimation uncertainty. The author is aware of these uncertainties in the final estimation, but statistical evaluation of these uncertainties was not carried out due to limited time constraints.

7.5. Conclusion and Limitations of the Study

This study attempted to estimate the GER dam reservoir water extent, water level, and water volume variation in different operational phases using a combination of satellite products. Reservoir extent variation was mapped with Sentinel 1 data using an unsupervised method called the edge otsu algorithm. The output maps were in good agreement with the validation sets consisting of Planet and Sentinel 2 based water maps. The study utilized different SWOT satellite based products to estimate the reservoir extent as well. Among these products, SWOT Lake Single Product performed worst, while SWOT waster mask raster and SWOT pixel cloud product based reservoir extent were quite representative and moderately agreed with the

validation products. Subsequently, the volume variation in different dam operation phases was estimated using satellite-based observations and the DEM contouring-based method. Estimates from these two methods showed higher correlation but had significant differences in value. A DEM slope correction method was utilized to minimize the effect of the water slope present in the GER dam reservoir. However, as it was corrected based on only two points, the estimated volume was not representative. SWOT satellite products showed promising results in estimating the volume variation. SWOT Lake single product based height estimates were used to determine volume from a single water level, while SWOT water mask raster was used to compute volume variation considering the water slope. Though there were no temporally collocated data with SWOT observation to validate the volume estimate, the volume variation estimates from SWOT products seemed promising, showing almost the same trend as the volume variation estimates from satellite-based observations. Despite these results, this study has several limitations that need to be addressed. Which are:

7.5.1. In-situ Gauge Data Unavailability

The Grand Ethiopian Renaissance (GER) Dam reservoir is a geopolitically sensitive water body due to its strategic importance and the potential for regional impacts on water resources. As a result, reservoir monitoring gauge estimates, which provide critical data on water levels, are not publicly available. Therefore, radar altimetry-based estimated water levels could not be validated. The inability to validate radar altimetry and SWOT based water level data with in-situ measurements reduce confidence in the satellite observations. Potential errors in the satellite based estimates might have gone undetected, leading to uncertainties in the estimated water level and volume variation time series.

7.5.2. Temporal Discontinuation of Altimetry Based Water Height Databases

For this study, most radar altimetry observations were collected from altimetry based water heights databases (dahiti, hydroweb, G-REALM). Unfortunately, the water height observations for the GER dam reservoir were unavailable throughout the study phase. Almost all the stations discontinued observations from mid-2022 onwards. Therefore, it was not possible to develop water level variation timeseries for all the GER dam reservoir filling phases. Moreover, if the data for the whole time series were available, the developed polynomial relationship might report fewer errors than the current one.

7.5.3. Unavailability of Optical Images in Dam Filling Periods

Planet and Sentinel 1 data, used as validation sets in this study, were a monthly median composite of the designated months. As the dam-filling months are mostly rainy season-oriented and these months have the most cloud presence in the satellite scenes, the cloud-free best monthly composite was the best approach to obtaining observations from these sources. These monthly composites were compared against single-day observations from Sentinel 1 and SWOT. This might have resulted in unwanted bias in the accuracy assessment metrics.

7.5.4. Delayed of SWOT Satellite Products Publishing

SWOT Science orbit-based data products were supposed to be available from August 2023. However, all the data products for the study area were available only from February 2024 onwards. Data from August 2023 to January 2024 is still unavailable in the study area. Therefore, the SWOT estimates did not have a temporal match with any other radar altimetry observations, and it was not possible to validate the results of SWOT products directly.

7.5.5. GER Dam Reservoir Extent

Grand Ethiopian Renaissance Dam reservoir extent is not universally defined, which creates variability and subjectivity in its delineation. The dam reservoir is expanding with different filling operation phases in the upstream regions of the north-eastern and southern sections. Therefore, the boundaries in these regions can be subjective. Having different boundaries from other studies might result in differences in results.

7.5.6. Temporally Co-located Water Extent and Water Level

This study matched Sentinel 1-based water extents with a 21-day mean of radar altimetry based water level timeseries based on the temporal nearest neighbor method. Due to a lack of temporal revisits of radar altimetry based observations and discontinuation of observations, exact data-wise matching with water extent timeseries was not possible. However, the water body is very dynamic, and its extent and height could change quickly. Though this method resulted in a workable solution to match the extent and water level temporally, it has also introduced potential inaccuracies that might differ from reality.

8. ETHICAL CONSIDERATIONS

This study aimed to estimate the volume variation in the GER Dam Reservoir by utilizing freely available global data sources. It is essential to mention that this research did not involve any primary human involvement in data collection. Instead, it heavily relied on gathering information from various freely accessible sources to analyze and understand the changes in the dam reservoir volume. For instance, all the satellite imageries used in this study were collected from the Google Earth Engine platform. The associated scripts to download these data products are submitted to ITC and will be available upon request. Besides, the altimetry-based products were downloaded from the NASA PODAAC data server using Python API. The timeseries of water elevation datasets were retrieved from the databases of Hydroweb and DAHITI. Therefore, this study does not have any privacy concerns.

The downloaded raw datasets went through several processing and transformation stages to ensure data harmonization in terms of spatial and temporal context. All the processing was also done through Python to be easily reproducible. I understand the geopolitical sensitivity of this study. Therefore, reproducibility was given utmost importance for every possible output of this study. Any interested parties can reproduce the outputs from this study using the Python scripts provided.

Disclaimer About AI Usage

During the entire period of my thesis, I used *ChatGPT* to understand challenging topics and took assistance in developing Python code snippets for data processing. I also used the Grammarly tool to refine my spelling, grammar, sentence structure and paraphrasing throughout the writing process.

LIST OF REFERENCES

Alsdorf, D. E., Rodríguez, E., & Lettenmaier, D. P. (2007). Measuring surface water from space. *Reviews of Geophysics*, *45*(2). https://doi.org/10.1029/2006RG000197

Aus der Beek, T., Voß, F., & Flörke, M. (2011). Modelling the impact of Global Change on the hydrological system of the Aral Sea basin. *Physics and Chemistry of the Earth, Parts A/B/C*, *36*(13), 684–695. https://doi.org/10.1016/J.PCE.2011.03.004

Awange, J. (2021). Lake Victoria Monitored from Space. *Lake Victoria Monitored from Space*. https://doi.org/10.1007/978-3-030-60551-3

Bartsch, A., Pathe, C., Scipal, K., & Wagner, W. (2008). Detection of permanent open water surfaces in central Siberia with ENVISAT ASAR wide swath data with special emphasis on the estimation of methane fluxes from tundra wetlands. *Hydrology Research*, *39*(2), 89–100. https://doi.org/10.2166/nh.2008.041

Bhatt, C. M., Rao, G. S., & Jangam, S. (2020). Detection of urban flood inundation using RISAT-1 SAR images: a case study of Srinagar, Jammu and Kashmir (North India) floods of September 2014. *Modeling Earth Systems and Environment*, *6*(1), 429–438. https://doi.org/10.1007/S40808-019-00690-Z/FIGURES/7

Biancamaria, S., Lettenmaier, D. P., & Pavelsky, T. M. (2016). The SWOT Mission and Its Capabilities for Land Hydrology. In *Surveys in Geophysics* (Vol. 37, Issue 2, pp. 307–337). Springer Netherlands. https://doi.org/10.1007/s10712-015-9346-y

Binh, P. D., & Son, T. S. (2021). Monitoring spatial temporal dynamics of small lakes based on SAR Sentinel-1 Observations. *Vietnam Journal of Earth Sciences*, 1–17.

Bose, I., Jayasinghe, S., Chinaporn Meechaiya, ;, Ahmad, S. K., Biswas, N., & Hossain, F. (2021). *River Bathymetry and Time-Varying Height for 4 Chindwin River in Myanmar Using SRTM and Landsat Chindwin River*. https://doi.org/10.1061/17

Crétaux, J. F., Abarca-del-Río, R., Bergé-Nguyen, M., Arsen, A., Drolon, V., Clos, G., & Maisongrande, P. (2016). Lake Volume Monitoring from Space. *Surveys in Geophysics 2016 37:2*, *37*(2), 269–305. https://doi.org/10.1007/S10712-016-9362-6

Cretaux, J. F., Letolle, R., & Bergé-Nguyen, M. (2013). History of Aral Sea level variability and current scientific debates. *Global and Planetary Change*, *110*, 99–113. https://doi.org/10.1016/J.GLOPLACHA.2013.05.006

Dandabathula, G., & Srinivasa Rao, S. (2020). Validation of ICESat-2 Surface Water Level Product ATL13 with Near Real Time Gauge Data. *Hydrology*, *8*(2), 19. https://doi.org/10.11648/j.hyd.20200802.11

Donchyts, G., Schellekens, J., Winsemius, H., Eisemann, E., & van de Giesen, N. (2016). A 30 m Resolution Surface Water Mask Including Estimation of Positional and Thematic Differences Using Landsat 8, SRTM and OpenStreetMap: A Case Study in the Murray-Darling Basin, Australia. *Remote Sensing 2016, Vol. 8, Page 386*, *8*(5), 386. https://doi.org/10.3390/RS8050386

Druce, D., Tong, X., Lei, X., Guo, T., Kittel, C. M. M., Grogan, K., & Tottrup, C. (2021). An optical and SAR based fusion approach for mapping surface water dynamics over mainland China. *Remote Sensing*, *13*(9). https://doi.org/10.3390/rs13091663

Duan, Z., & Bastiaanssen, W. G. M. (2013). *Estimating water volume variations in lakes and reservoirs from four operational satellite altimetry databases and satellite imagery data*. https://doi.org/10.1016/j.rse.2013.03.010

Eldardiry, H., & Hossain, F. (2021). Evaluating the hydropower potential of the Grand Ethiopian Renaissance Dam. *Journal of Renewable and Sustainable Energy*, *13*(2), 24501. https://doi.org/10.1063/5.0028037/15707032/024501_1_ACCEPTED_MANUSCRIPT.PDF

Elmer, N. J., Hain, C., Hossain, F., Desroches, D., & Pottier, C. (2020). Generating Proxy SWOT Water Surface Elevations Using WRF-Hydro and the CNES SWOT Hydrology Simulator. *Water Resources Research*, *56*(8). https://doi.org/10.1029/2020WR027464

Gao, H. (2015a). Satellite remote sensing of large lakes and reservoirs: from elevation and area to storage. *WIREs Water*, *2*, 147–157. https://doi.org/10.1002/wat2.1065

Gao, H. (2015b). Satellite remote sensing of large lakes and reservoirs: from elevation and area to storage. *Wiley Interdisciplinary Reviews: Water*, *2*(2), 147–157. https://doi.org/10.1002/WAT2.1065

Grippa, M., Rouzies, C., Biancamaria, S., Blumstein, D., Cretaux, J. F., Gal, L., Robert, E., Gosset, M., & Kergoat, L. (2019). Potential of SWOT for Monitoring Water Volumes in Sahelian Ponds and Lakes. *IEEE Journal of Selected Topics in Applied Earth Observations and Remote Sensing*, *12*(7), 2541–2549. https://doi.org/10.1109/JSTARS.2019.2901434

Hamoudzadeh, A., Ravanelli, R., & Crespi, M. (2024a). SWOT Level 2 Lake Single-Pass Product: The L2_HR_LakeSP Data Preliminary Analysis for Water Level Monitoring. *Remote Sensing*, *16*(7). https://doi.org/10.3390/rs16071244

Hamoudzadeh, A., Ravanelli, R., & Crespi, M. (2024b). SWOT Level 2 Lake Single-Pass Product: The L2_HR_LakeSP Data Preliminary Analysis for Water Level Monitoring. *Remote Sensing*, *16*(7). https://doi.org/10.3390/rs16071244

Hamoudzadeh, A., Ravanelli, R., & Crespi, M. (2024c). SWOT Level 2 Lake Single-Pass Product: The L2_HR_LakeSP Data Preliminary Analysis for Water Level Monitoring. *Remote Sensing 2024, Vol. 16, Page 1244*, *16*(7), 1244. https://doi.org/10.3390/RS16071244

Hannoun, D., & Tietjen, T. (2023). Lake management under severe drought: Lake Mead, Nevada/Arizona. *JAWRA Journal of the American Water Resources Association*, *59*(2), 416–428. https://doi.org/10.1111/1752-1688.13090

Huang, C., Chen, Y., Zhang, S., & Wu, J. (2018a). Detecting, Extracting, and Monitoring Surface Water From Space Using Optical Sensors: A Review. *Reviews of Geophysics*, *56*(2), 333–360. https://doi.org/10.1029/2018RG000598

Huang, C., Chen, Y., Zhang, S., & Wu, J. (2018b). Detecting, Extracting, and Monitoring Surface Water From Space Using Optical Sensors: A Review. *Reviews of Geophysics*, *56*(2), 333–360. https://doi.org/10.1029/2018RG000598

Irwin, K., Beaulne, D., Braun, A., & Fotopoulos, G. (2017). Fusion of SAR, optical imagery and airborne LiDAR for surface water detection. *Remote Sensing*, *9*(9). https://doi.org/10.3390/rs9090890

JPL D-109532. (2024). *SWOT Science Data Products User Handbook*. https://epdm.jpl.nasa.gov

Kang, S., Xu, Y., You, Q., Flügel, W. A., Pepin, N., & Yao, T. (2010). Review of climate and cryospheric change in the Tibetan Plateau. *Environmental Research Letters*, *5*(1), 015101. https://doi.org/10.1088/1748-9326/5/1/015101

Kostianoy, A. G., Lebedev, S. A., Kostianaia, E. A., & Prokofiev, Y. A. (2022). Interannual Variability of Water Level in Two Largest Lakes of Europe. *Remote Sensing*, *14*(3). https://doi.org/10.3390/rs14030659

Lei, Y., Yang, K., Wang, B., Sheng, Y., Bird, B. W., Zhang, G., & Tian, L. (2014). Response of inland lake dynamics over the Tibetan Plateau to climate change. *Climatic Change*, *125*(2), 281–290. https://doi.org/10.1007/S10584-014-1175-3/FIGURES/5

Li, J., Ma, R., Cao, Z., Xue, K., Xiong, J., Hu, M., & Feng, X. (2022). Satellite Detection of Surface Water Extent: A Review of Methodology. In *Water (Switzerland)* (Vol. 14, Issue 7). MDPI. https://doi.org/10.3390/w14071148

Li, Y., Gao, H., Allen, G. H., & Zhang, Z. (2021). Constructing reservoir area-volume-elevation curve from TanDEM-X DEM data. *IEEE Journal of Selected Topics in Applied Earth Observations and Remote Sensing*, *14*, 2249–2257. https://doi.org/10.1109/JSTARS.2021.3051103

Li, Y., Niu, Z., Xu, Z., & Yan, X. (2020). Construction of high spatial-temporal water body dataset in China based on Sentinel-1 archives and GEE. *Remote Sensing*, *12*(15). https://doi.org/10.3390/RS12152413

Liu, Q., Huang, C., Shi, Z., & Zhang, S. (2020). Probabilistic river water mapping from Landsat-8 using the support vector machine method. *Remote Sensing*, *12*(9). https://doi.org/10.3390/RS12091374

Markert, K. N., Markert, A. M., Mayer, T., Nauman, C., Haag, A., Poortinga, A., Bhandari, B., Thwal, N. S., Kunlamai, T., Chishtie, F., Kwant, M., Phongsapan, K., Clinton, N., Towashiraporn, P., & Saah, D. (2020a). Comparing Sentinel-1 Surface Water Mapping Algorithms and Radiometric Terrain Correction Processing in Southeast Asia Utilizing Google Earth Engine. *Remote Sensing 2020, Vol. 12, Page 2469*, *12*(15), 2469. https://doi.org/10.3390/RS12152469

Markert, K. N., Markert, A. M., Mayer, T., Nauman, C., Haag, A., Poortinga, A., Bhandari, B., Thwal, N. S., Kunlamai, T., Chishtie, F., Kwant, M., Phongsapan, K., Clinton, N., Towashiraporn, P., & Saah, D. (2020b). Comparing Sentinel-1 surface water mapping algorithms and radiometric terrain correction processing in southeast Asia utilizing Google Earth Engine. *Remote Sensing*, *12*(15). https://doi.org/10.3390/RS12152469

Martinis, S., Kuenzer, C., Wendleder, A., Huth, J., Twele, A., Roth, A., & Dech, S. (2015). Comparing four operational SAR-based water and flood detection approaches. *International Journal of Remote Sensing*, *36*(13), 3519–3543. https://doi.org/10.1080/01431161.2015.1060647

McFeeters, S. K. (1996). The use of the Normalized Difference Water Index (NDWI) in the delineation of open water features. *International Journal of Remote Sensing*, *17*(7), 1425–1432. https://doi.org/10.1080/01431169608948714

Musa, Z. N., Popescu, I., & Mynett, A. (2015). A review of applications of satellite SAR, optical, altimetry and DEM data for surface water modelling, mapping and parameter estimation. In *Hydrology and Earth System Sciences* (Vol. 19, Issue 9, pp. 3755–3769). Copernicus GmbH. https://doi.org/10.5194/hess-19-3755-2015

Nagai, H., Abe, T., & Ohki, M. (2021). SAR-based flood monitoring for flatland with frequently fluctuating water surfaces: Proposal for the normalized backscatter amplitude difference index (NoBADI). *Remote Sensing*, *13*(20), 4136. https://doi.org/10.3390/RS13204136/S1

Nair, A. S., Kumar, N., Indu, J., & Vivek, B. (2021). Monitoring Lake Levels From Space: Preliminary Analysis With SWOT. *Frontiers in Water*, *3*. https://doi.org/10.3389/frwa.2021.717852

Ngo, T. T., Mazet, V., Collet, C., & De Fraipont, P. (2017). Shape-Based Building Detection in Visible Band Images Using Shadow Information. *IEEE Journal of Selected Topics in Applied Earth Observations and Remote Sensing*, *10*(3), 920–932. https://doi.org/10.1109/JSTARS.2016.2598856

Nicholson, S. E., & Yin, X. (2002). *Mesoscale Patterns of Rainfall, Cloudiness and Evaporation over the Great Lakes of East Africa*. 93–119. https://doi.org/10.1007/0-306-48201-0_3

O'Loughlin, F. E., Neal, J., Yamazaki, D., & Bates, P. D. (2016). ICESat-derived inland water surface spot heights. *Water Resources Research*, *52*(4), 3276–3284. https://doi.org/10.1002/2015WR018237

Pekel, J. F., Cottam, A., Gorelick, N., & Belward, A. S. (2016). High-resolution mapping of global surface water and its long-term changes. *Nature*, *540*(7633), 418–422. https://doi.org/10.1038/nature20584

Pickens, A. H., Hansen, M. C., Hancher, M., Stehman, S. V., Tyukavina, A., Potapov, P., Marroquin, B., & Sherani, Z. (2020). Mapping and sampling to characterize global inland water dynamics from 1999 to 2018 with full Landsat time-series. *Remote Sensing of Environment*, *243*. https://doi.org/10.1016/j.rse.2020.111792

Roberts, D. R., Bahn, V., Ciuti, S., Boyce, M. S., Elith, J., Guillera-Arroita, G., Hauenstein, S., Lahoz-Monfort, J. J., Schröder, B., Thuiller, W., Warton, D. I., Wintle, B. A., Hartig, F., & Dormann, C. F. (2017). Cross-validation strategies for data with temporal, spatial, hierarchical, or phylogenetic structure. *Ecography*, *40*(8), 913–929. https://doi.org/10.1111/ECOG.02881

Rosenqvist, Å., & Birkett, C. M. (2002). Evaluation of JERS-1 SAR mosaics for hydrological applications in the Congo river basin. *International Journal of Remote Sensing*, *23*(7), 1283–1302. https://doi.org/10.1080/01431160110092902

Schwatke, C., Dettmering, D., Bosch, W., & Seitz, F. (2015). DAHITI - An innovative approach for estimating water level time series over inland waters using multi-mission satellite altimetry. *Hydrology and Earth System Sciences*, *19*(10), 4345–4364. https://doi.org/10.5194/hess-19-4345-2015

Shen, X., Wang, D., Mao, K., Anagnostou, E., & Hong, Y. (2019). Inundation extent mapping by synthetic aperture radar: A review. *Remote Sensing*, *11*(7). https://doi.org/10.3390/RS11070879

Sheng, Y., Song, C., Wang, J., Lyons, E. A., Knox, B. R., Cox, J. S., & Gao, F. (2016). Representative lake water extent mapping at continental scales using multi-temporal Landsat-8 imagery. *Remote Sensing of Environment*, *185*, 129–141. https://doi.org/10.1016/j.rse.2015.12.041

Singh, A., Seitz, F., & Schwatke, C. (2012). Inter-annual water storage changes in the Aral Sea from multi-mission satellite altimetry, optical remote sensing, and GRACE satellite gravimetry. *Remote Sensing of Environment*, *123*, 187–195. https://doi.org/10.1016/j.rse.2012.01.001

Tierney, J. E., Smerdon, J. E., Anchukaitis, K. J., & Seager, R. (2013). Multidecadal variability in East African hydroclimate controlled by the Indian Ocean. *Nature 2013 493:7432*, *493*(7432), 389–392. https://doi.org/10.1038/nature11785

Tourian, M. J., Elmi, O., Shafaghi, Y., Behnia, S., Saemian, P., Schlesinger, R., & Sneeuw, N. (2021). *HydroSat: a repository of global water cycle products from spaceborne geodetic sensors*. https://doi.org/10.5194/essd-2021-174

Vapnik, V. N. (1995). *The Nature of Statistical Learning Theory* (Second). University of Minnesota. https://books.google.nl/books?hl=en&lr=&id=sna9BaxVbj8C&oi=fnd&pg=PR7&dq=Vapnik,+V.N.+The+Nature+of+Statistical+Learning+Theory%3B+The+Nature+of+Statistical+Learning+Theory%3B+University+of+Minnesota:+Minneapolis,+MN,+USA,+1995.&ots=oqPgLSqngc&sig=ytThKe6ttbwHU6ZJQw20FYsc6fU&redir_esc=y#v=onepage&q&f=false

Vollrath, A., Mullissa, A., & Reiche, J. (2020). Angular-based radiometric slope correction for Sentinel-1 on google earth engine. *Remote Sensing*, *12*(11). https://doi.org/10.3390/rs12111867

Wu, W., Li, Q., Zhang, Y., Du, X., & Wang, H. (2018). Two-Step Urban Water Index (TSUWI): A New Technique for High-Resolution Mapping of Urban Surface Water. *Remote Sensing 2018, Vol. 10, Page 1704*, *10*(11), 1704. https://doi.org/10.3390/RS10111704

Xi, J., & Zhang, J. Z. (2012). Edge Detection from Remote Sensing Images Based on Canny Operator and Hough Transform. *Advances in Intelligent and Soft Computing*, *141 AISC*, 807–814. https://doi.org/10.1007/978-3-642-27948-5_108

Xu, H. (2006). Modification of normalised difference water index (NDWI) to enhance open water features in remotely sensed imagery. *International Journal of Remote Sensing*, *27*(14), 3025–3033. https://doi.org/10.1080/01431160600589179

Yamazaki, D., Ikeshima, D., Tawatari, R., Yamaguchi, T., O'Loughlin, F., Neal, J. C., Sampson, C. C., Kanae, S., & Bates, P. D. (2017). A high-accuracy map of global terrain elevations. *Geophysical Research Letters*, *44*(11), 5844–5853. https://doi.org/10.1002/2017GL072874

Zhang, G., Xie, H., Kang, S., Yi, D., & Ackley, S. F. (2011). Monitoring lake level changes on the Tibetan Plateau using ICESat altimetry data (2003–2009). *Remote Sensing of Environment*, *115*(7), 1733–1742. https://doi.org/10.1016/J.RSE.2011.03.005

Zhang, S., Gao, H., & Naz, B. S. (2014). Monitoring reservoir storage in South Asia from multisatellite remote sensing. *Water Resources Research*, *50*(11), 8927–8943. https://doi.org/10.1002/2014WR015829

APPENDICES

The figures with maps are added in this section with larger size and better quality for better understanding of the users.

SVM Model Train testing details

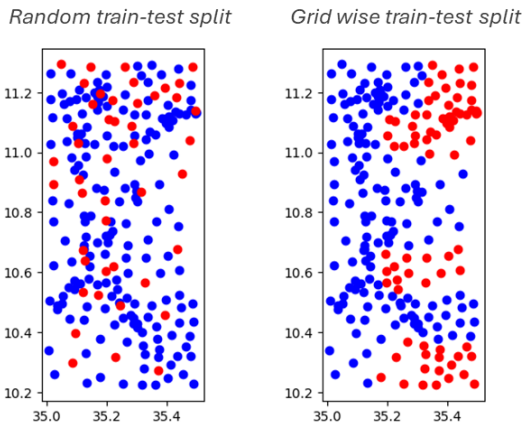

(a)

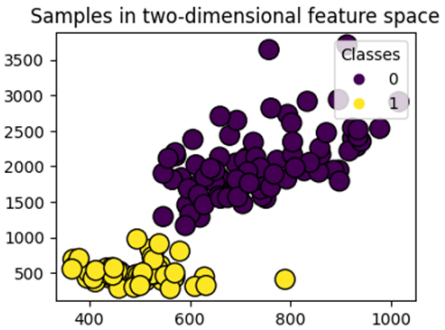

(b)

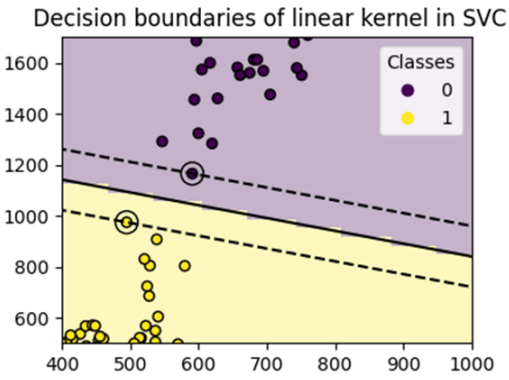

(c)

SVM Model Details	
Used Features	(i) Green (ii) NIR
Kernel Type	Linear
Grid Search of C	50 values ranging from 0.001 to 10
Best C Value	0.001
Number of SV	2
Overall Accuracy	0.986

(d)

Same Location Multiple Virtual Stations

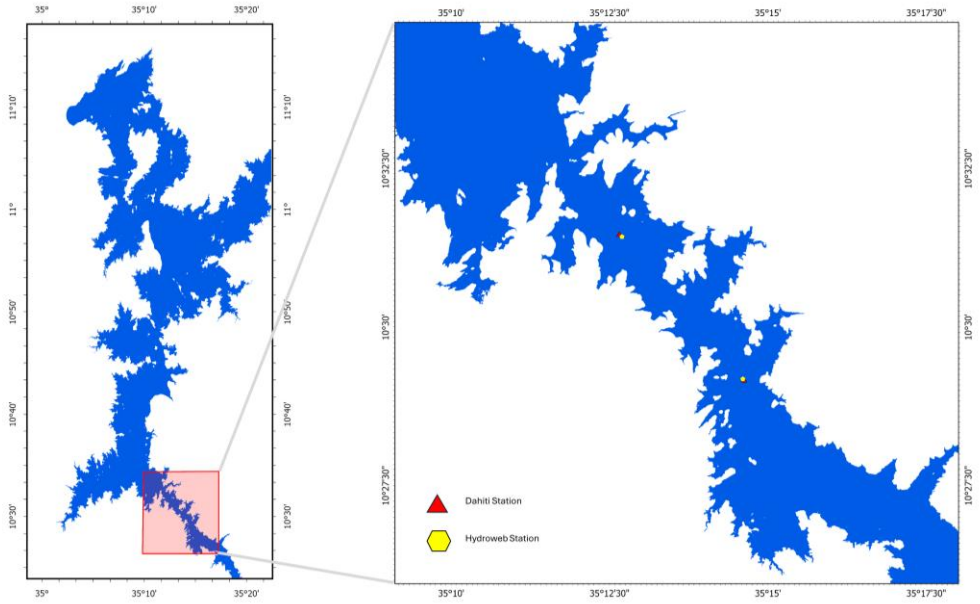

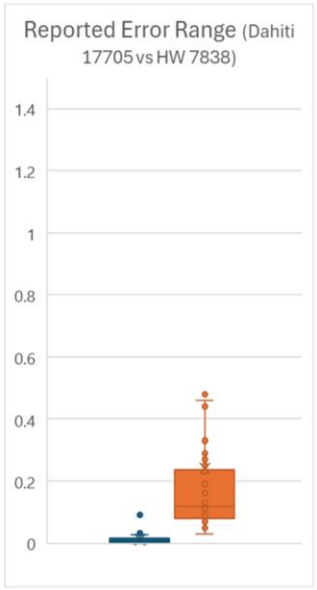

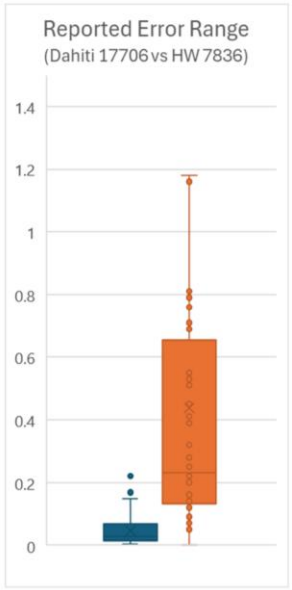

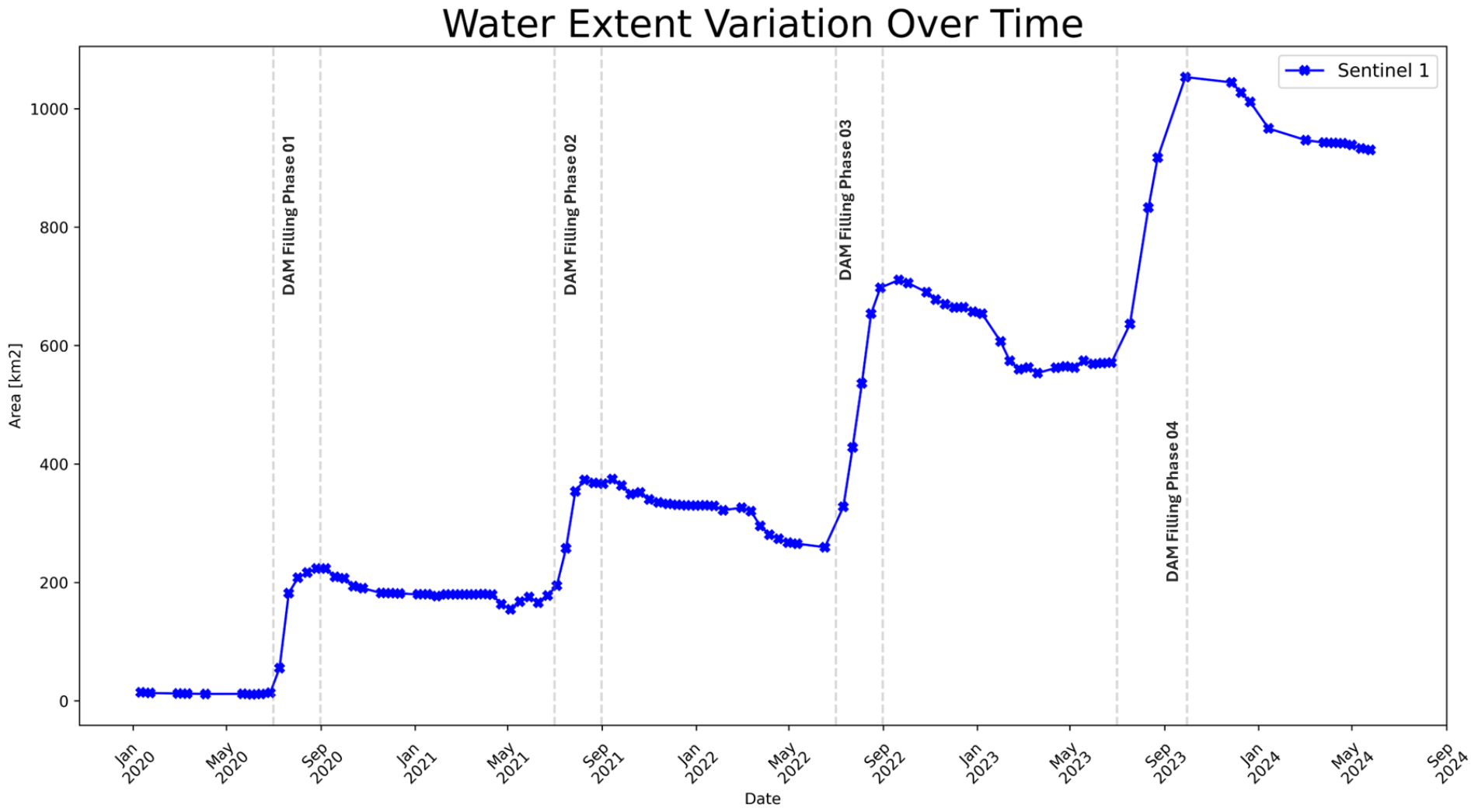
Water Extent Variation Over Time
Sentinel 1
DAM Filling Phase 01
DAM Filling Phase 02
DAM Filling Phase 03
DAM Filling Phase 04
Area [km2]
0
200
400
600
800
1000
Jan 2020
May 2020
Sep 2020
Jan 2021
May 2021
Sep 2021
Jan 2022
May 2022
Sep 2022
Jan 2023
May 2023
Sep 2023
Jan 2024
May 2024
Sep 2024
Date

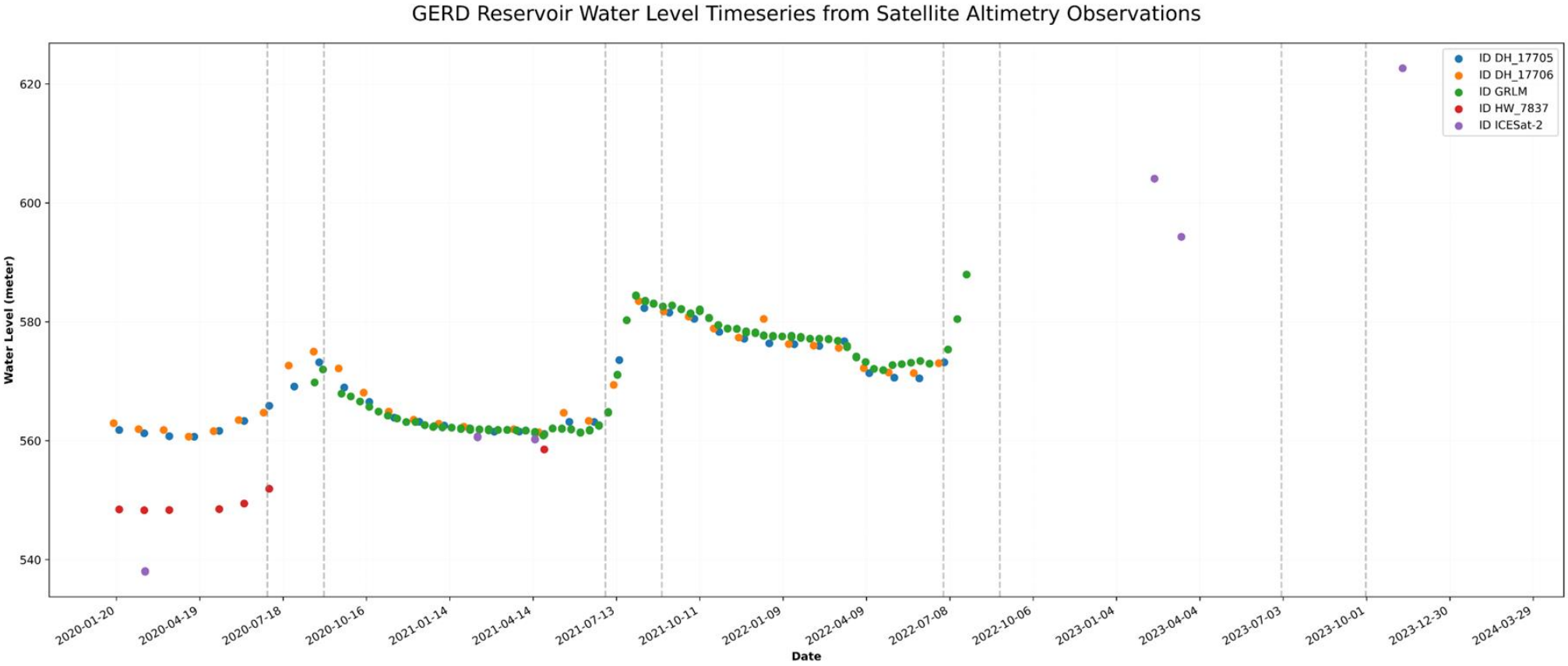
GERD Reservoir Water Level Timeseries from Satellite Altimetry Observations
ID DH_17705
ID DH_17706
ID GRLM
ID HW_7837
ID ICESat-2
Water Level (meter)
620
600
580
560
540
2020-01-20
2020-04-19
2020-07-18
2020-10-16
2021-01-14
2021-04-14
2021-07-13
2021-10-11
2022-01-09
2022-04-09
2022-07-08
2022-10-06
2023-01-04
2023-04-04
2023-07-03
2023-10-01
2023-12-30
2024-03-29
Date

Sentinel 1 Comparison with Planet Water Map

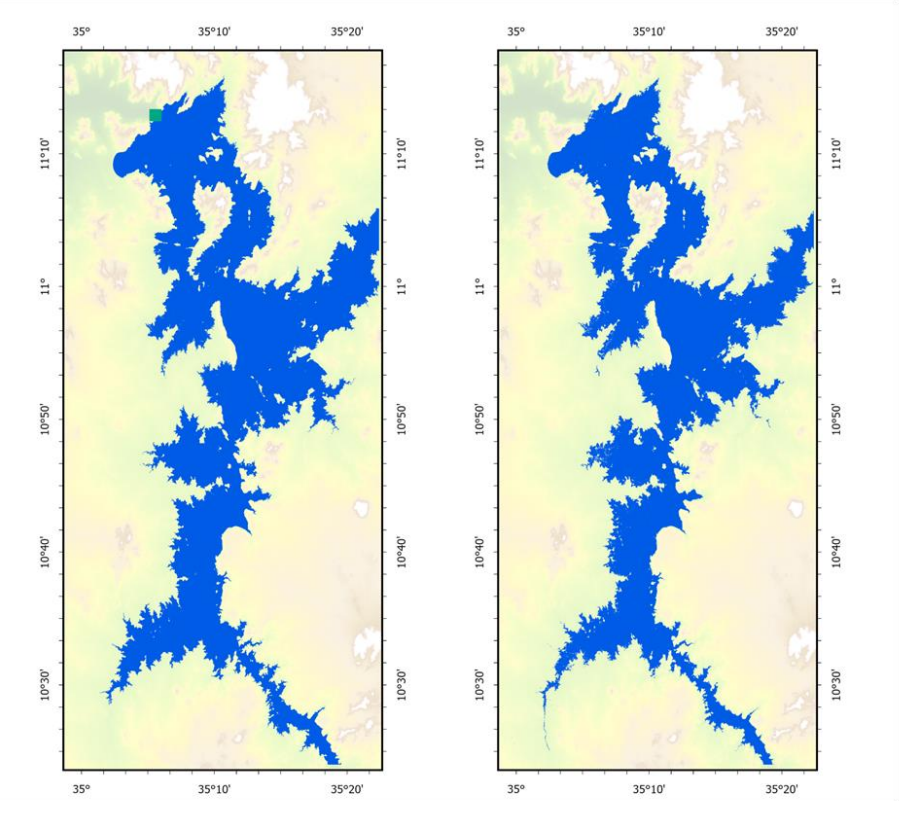

Planet Based Water Map

S1 Based Water Map

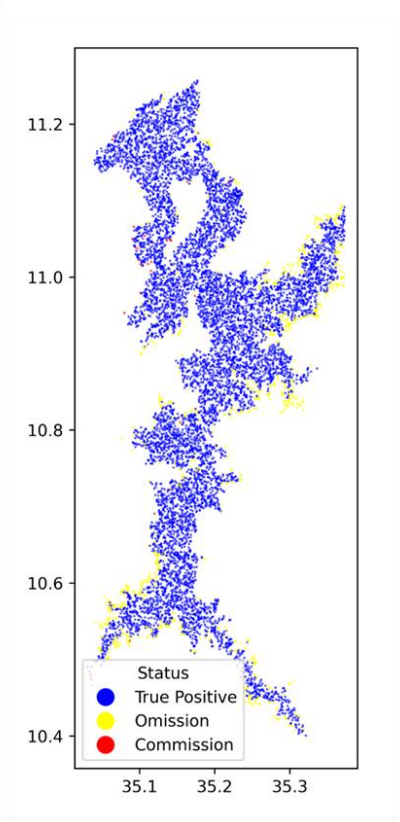

Comparison with Validation Set

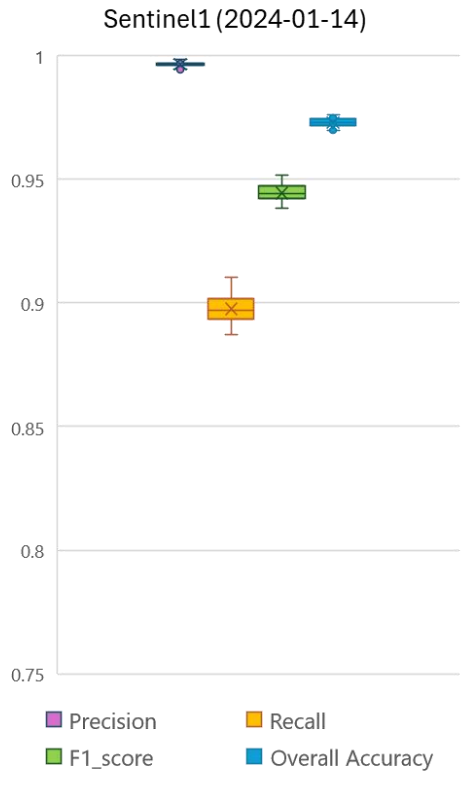

Accuracy Metrics after 50 Runs

Sentinel 1 Comparison with Planet Water Map

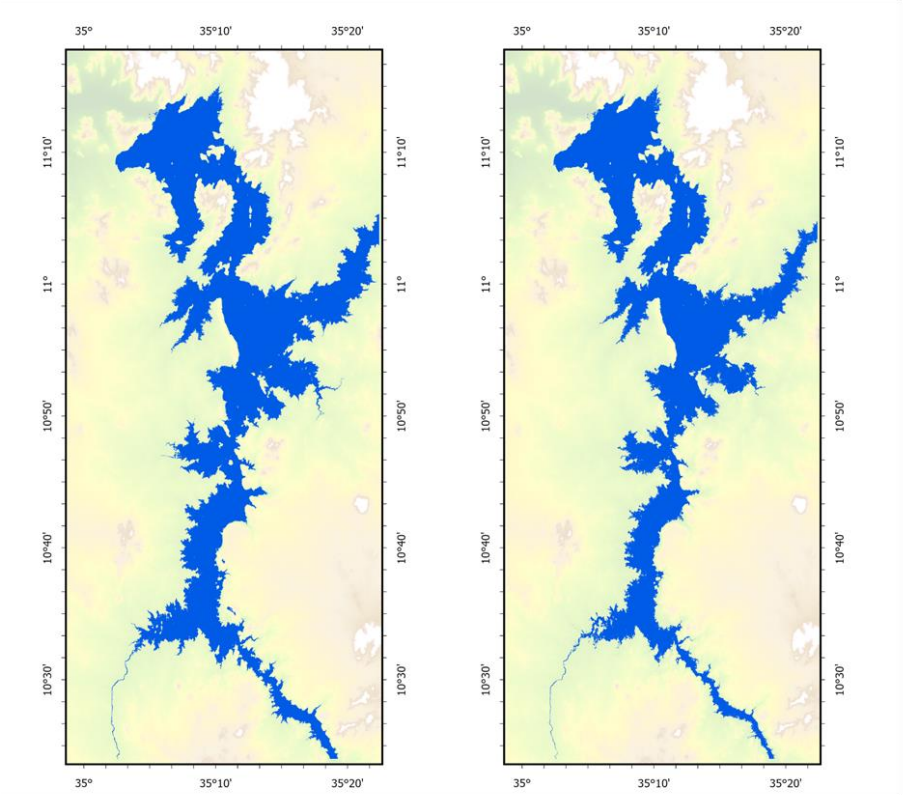

Planet Based Water Map

S1 Based Water Map

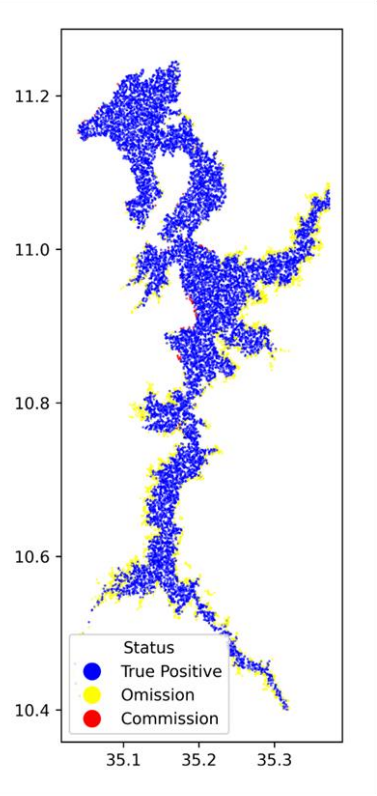

Comparison with Validation Set

Accuracy Metrics after 50 Runs

Sentinel 1 Comparison with Sentinel 2 Water Map

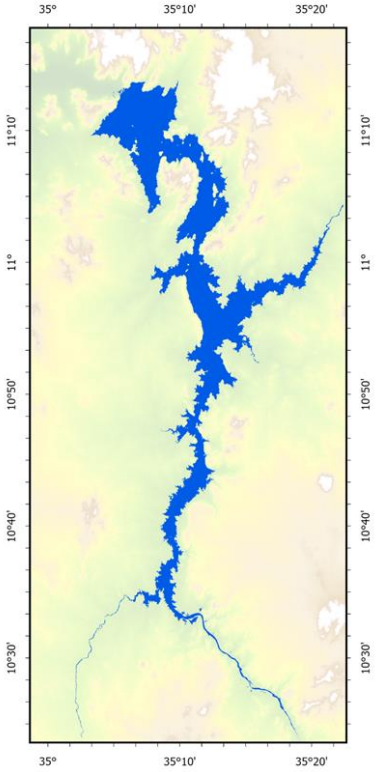

S2 Based Water Map

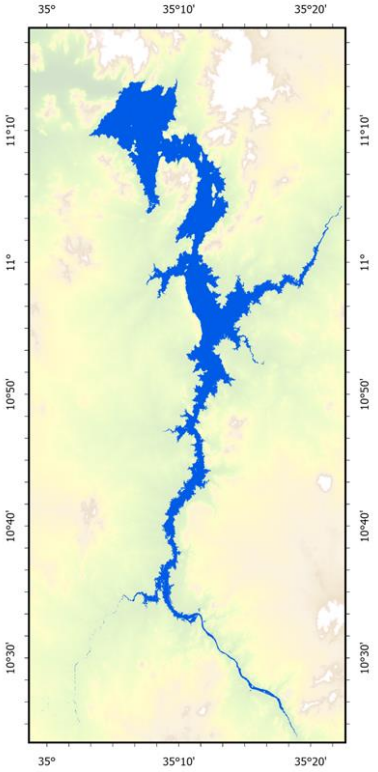

S1 Based Water Map

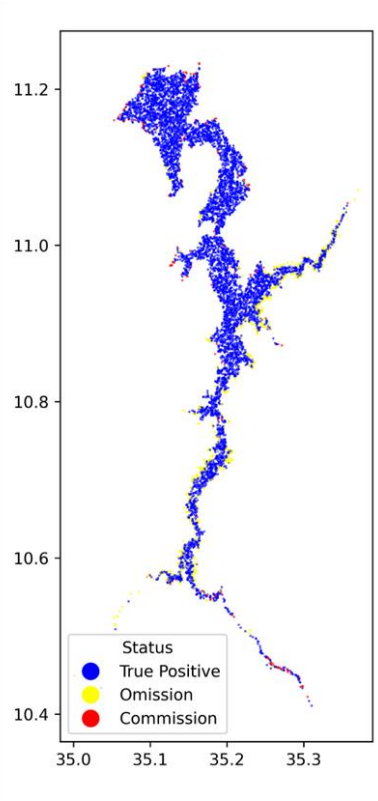

Comparison with Validation Set

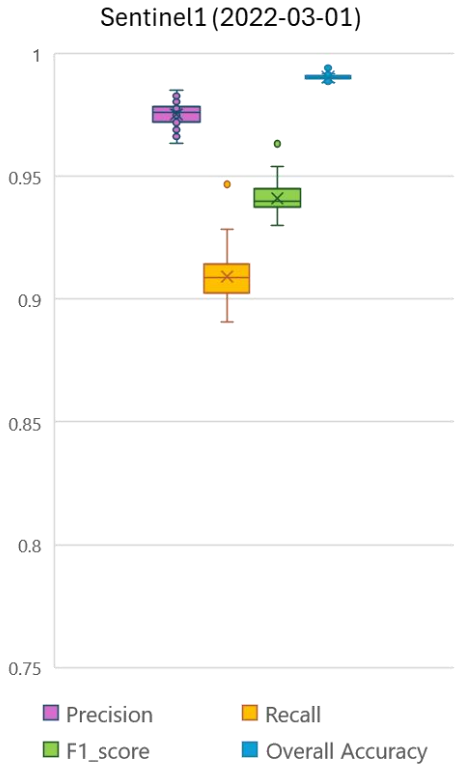

Accuracy Metrics after 50 Runs

Sentinel 1 Comparison with Sentinel 2 Water Map

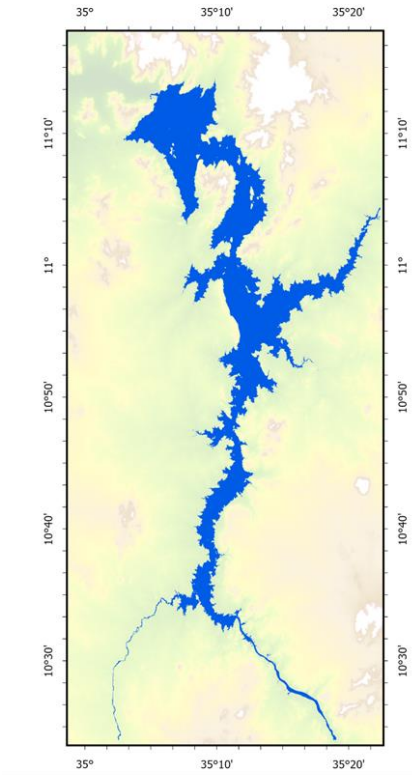

S2 Based Water Map

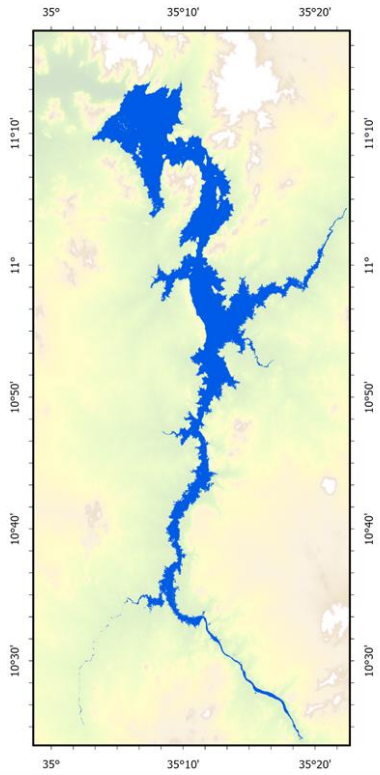

S1 Based Water Map

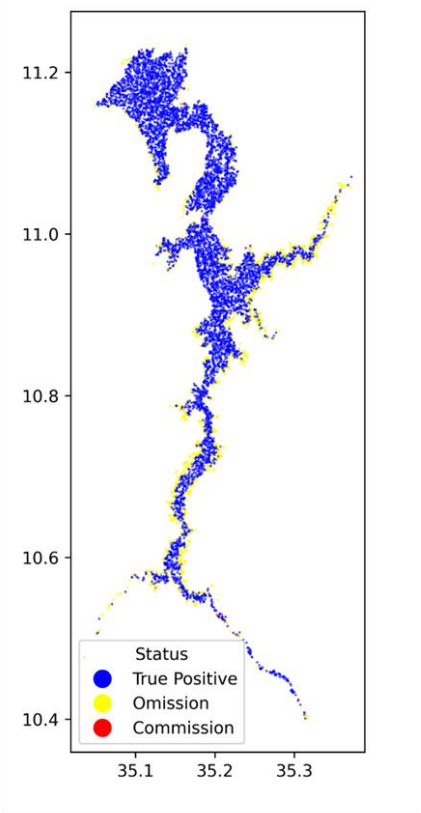

Comparison with Validation Set

Accuracy Metrics after 50 Runs

Sentinel 1 Comparison with Sentinel 2 Water Map

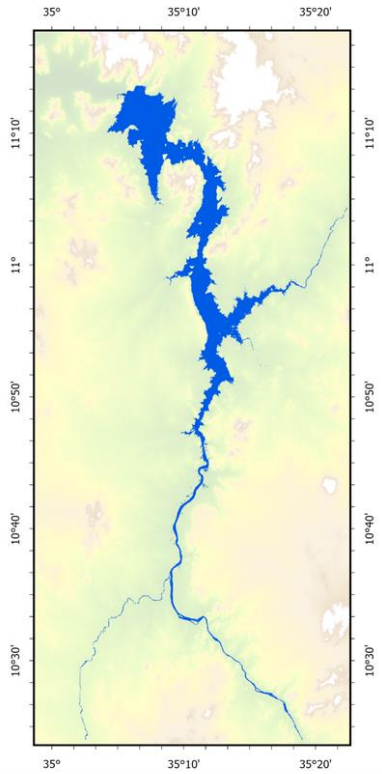

S2 Based Water Map

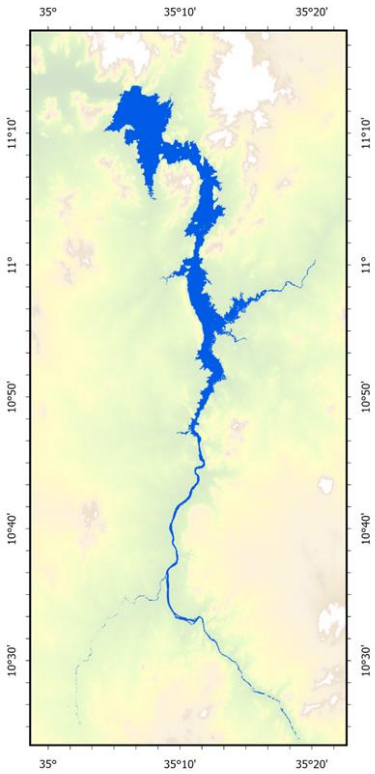

S1 Based Water Map

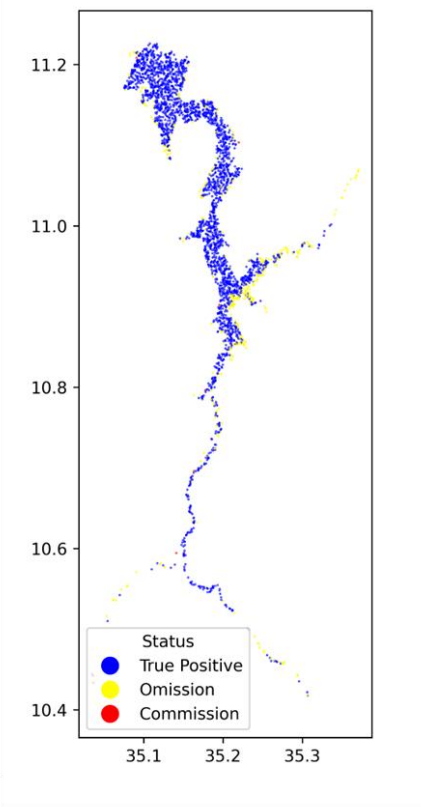

Comparison with Validation Set

Accuracy Metrics after 50 Runs

SWOT Water Mask Raster Comparison with Planet Based Water Map

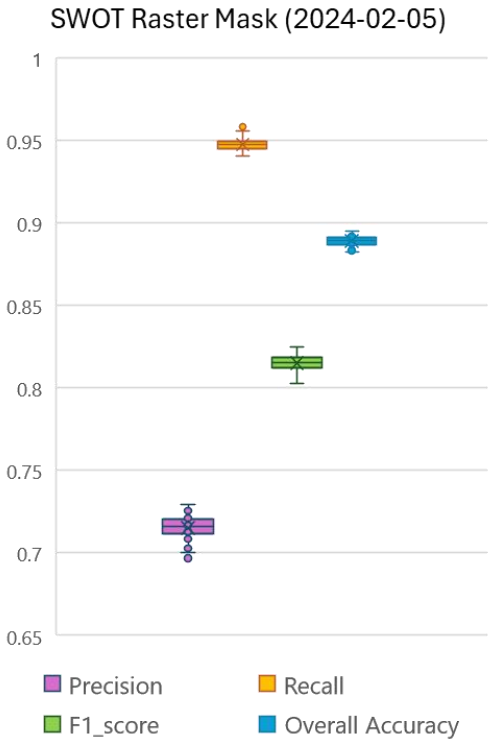

Accuracy Metrics after 50 Runs

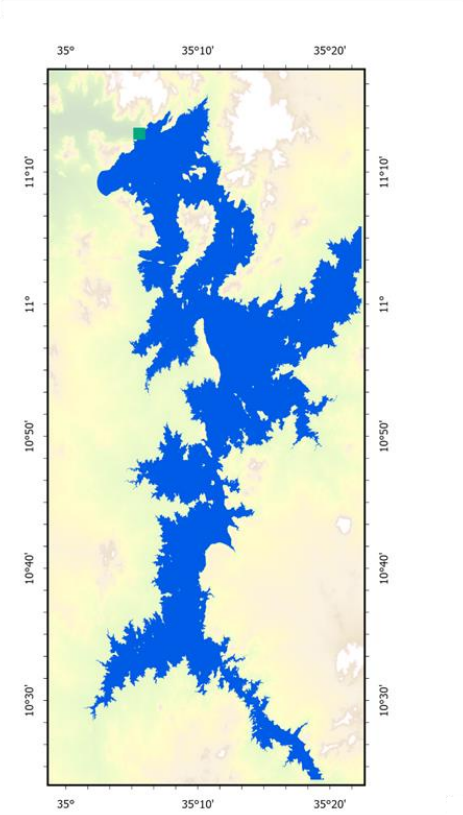

Planet Based Water Map

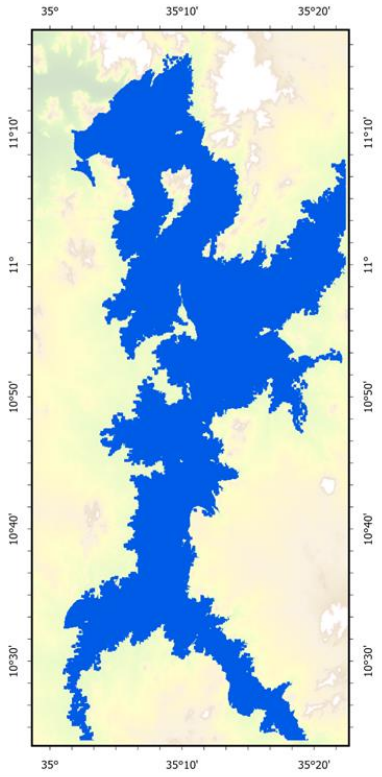

SWOT Raster Mask Based Map

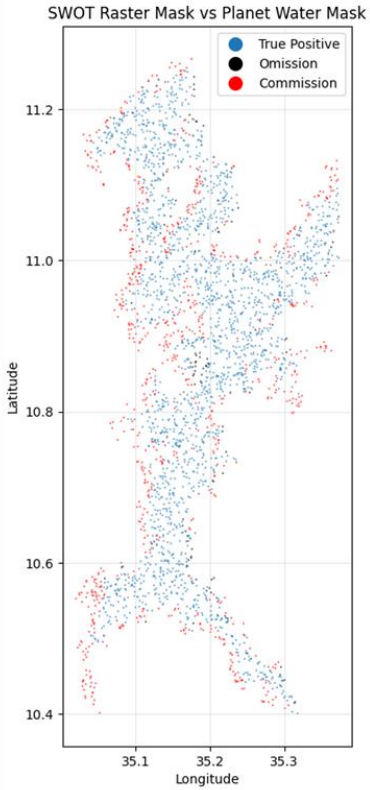

Comparison with Validation Set

SWOT Pixel Cloud Product Comparison with Planet Based Water Map

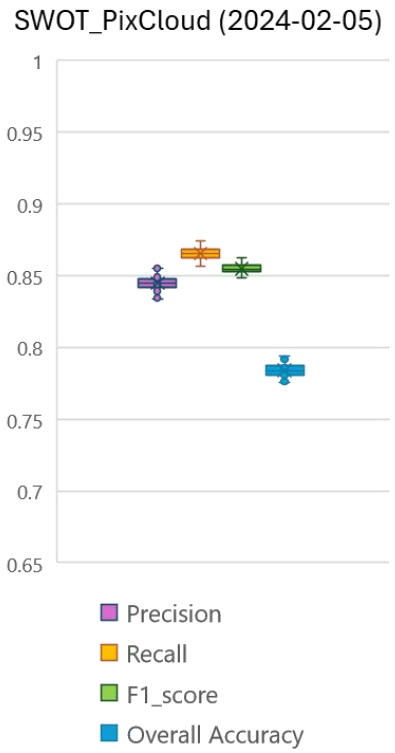

Accuracy Metrics after 50 Runs

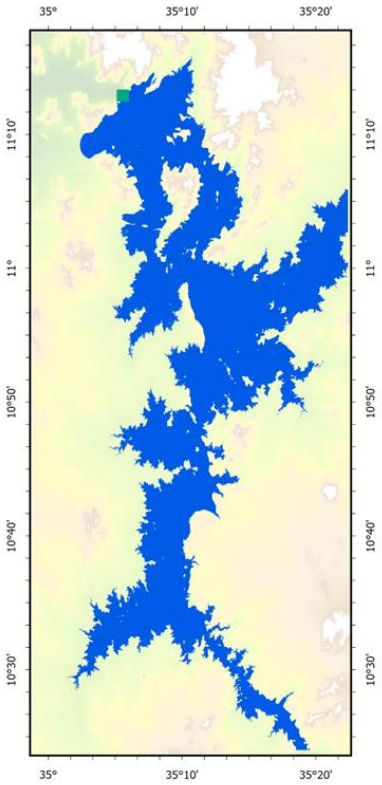

Planet Based Water Map

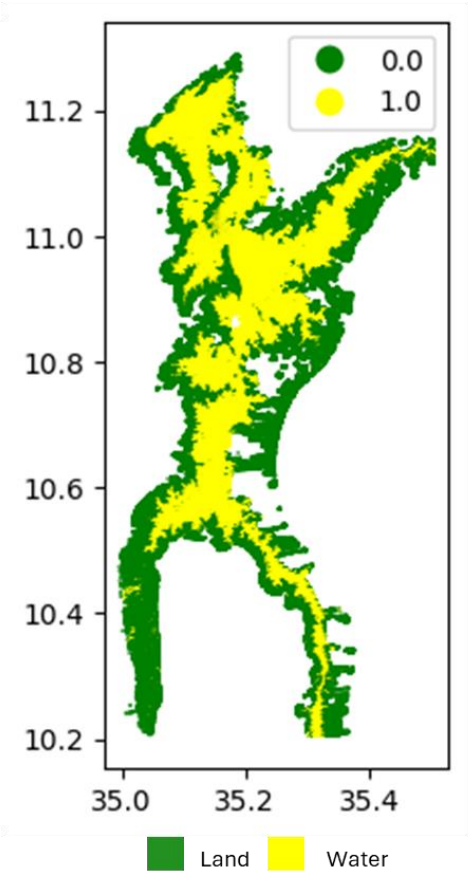

SWOT Pixel Cloud Based Map

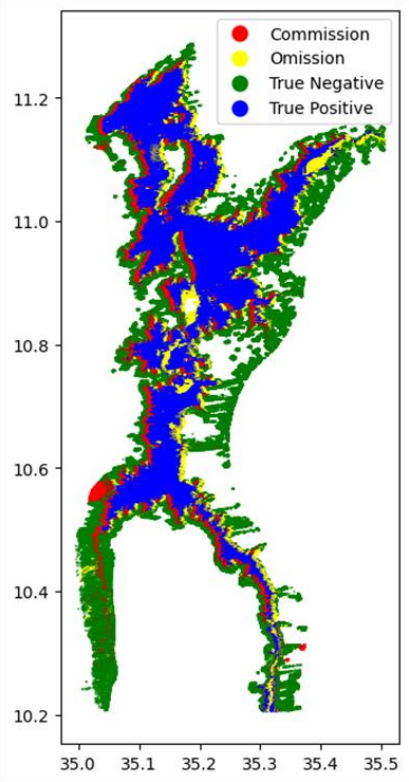

Comparison with Validation Set

SWOT Lake Single Pass Product Comparison with Polygonised Planet Reservoir Boundary

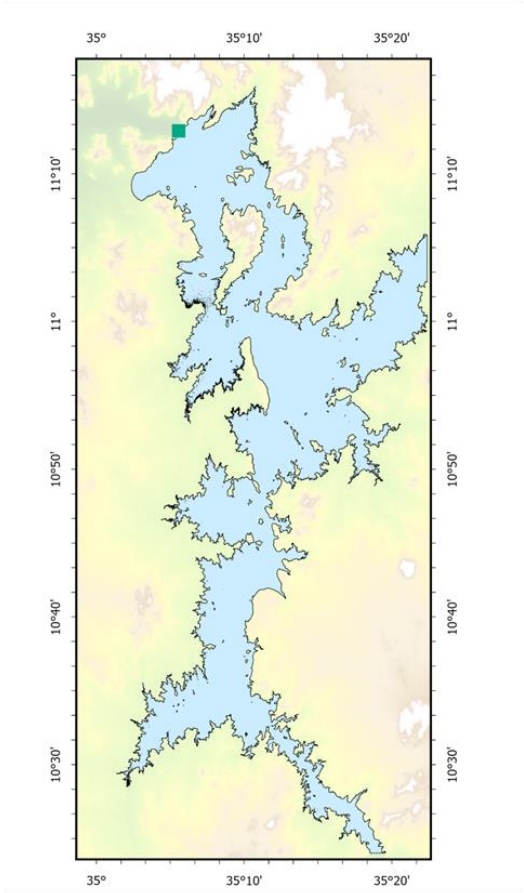

Planet Based Water Map

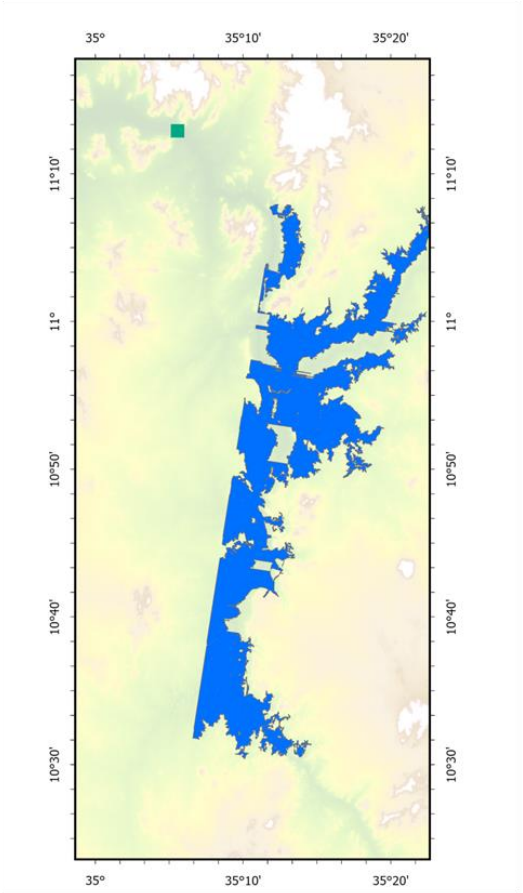

SWOT Lake Single Product based Water Map

Intersection Area	405,942,972 m²
Union Area	1,203,051,025 m²
Intersection over Union (IOU)	**0.3373**

SWOT Raster Mask Product Based Water Volume Variation above DEM

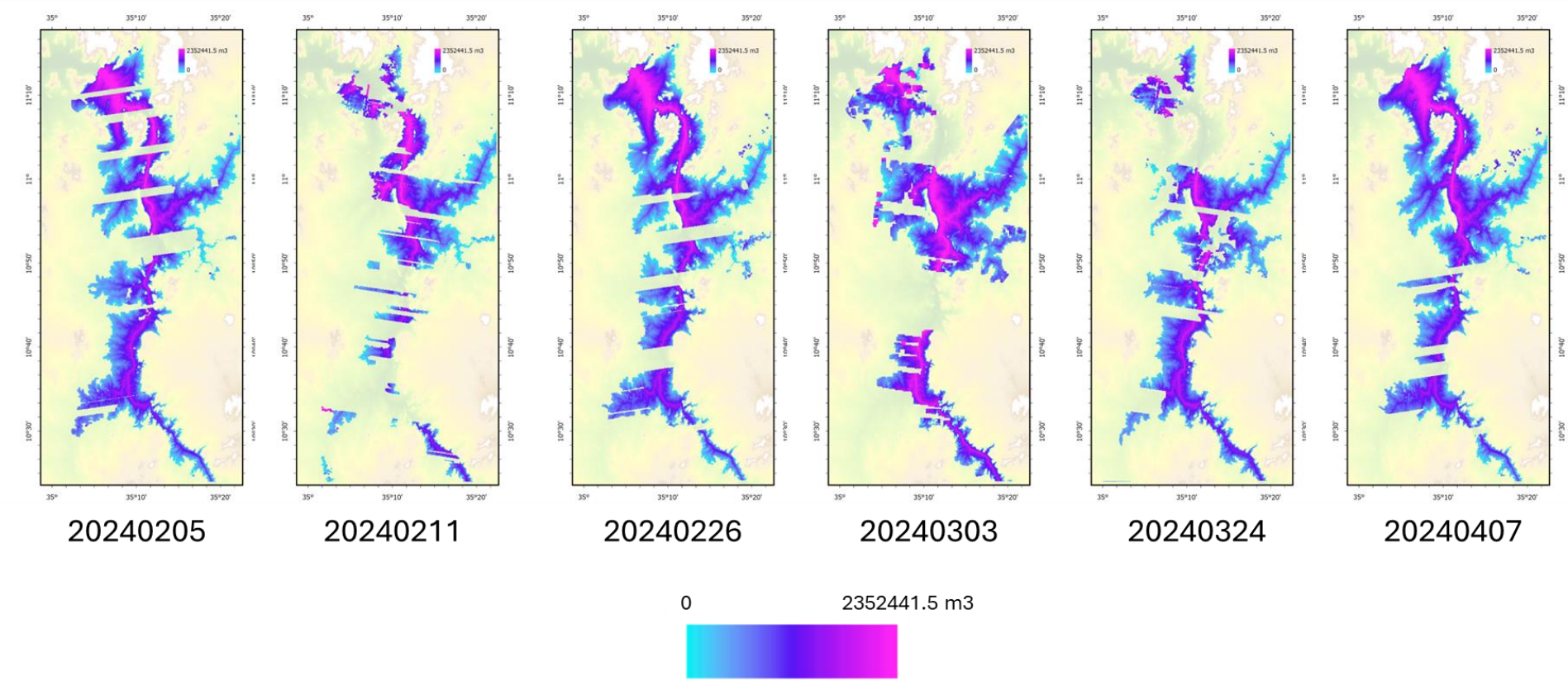

SWOT Pixel Cloud Data Products Quality Flags

Decimal	Classification_qual	Meaning
1	no_coherent_gain	The coherent gain from the coherent power computation is less than 1
2	power_close_to_noise_floor	The coherent power is near the estimated noise (low SNR)
4	detected_water_but_no_prior_water	Water was detected but the prior water probability is low
8	detected_water_but_bright_land	Water was detected, but the prior bright-land flag was nonzero
16	water_false_detection_rate_suspect	Water was detected, but both the estimated false detection rate is high, and the prior water probability is low
2048	coherent_power_suspect	At least one rare power value used to compute the coherent power is marked suspect, or the coherent gain is less than 1.
8192	tvp_suspect	At least some of the ephemeris or attitude information used for processing is marked suspect
16384	sc_event_suspect	A spacecraft event such as a maneuver, eclipse transition, etc. may affect the interferogram quality.
32768	small_karin_gap	There is a small gap in the raw KaRIn HR data; a measurement is still computed, but it may have lower quality

262144	in_air_pixel_degraded	The pixel/range-bin does not intersect the Earth's surface for the corresponding range (hence it is in the air)
524288	specular_ringing_degraded	The interferogram quality is degraded due to range point-target-response side-lobe ringing from a bright target near nadir.
134217728	coherent_power_bad	Both rare power values used to compute the coherent power are marked bad, or the coherent power fails sanity checks.
268435456		
536870912	tvp_bad	At least some of the ephemeris or attitude information needed for processing is marked bad
1073741824	sc_event_bad	A spacecraft event such as a maneuver, eclipse transition, etc. likely makes the interferogram quality poor
2147483648	large_karin_gap	There is a large gap in the raw KaRIn HR data, or there is no KaRIn HR data at all; a measurement is not computed.